AD NUMBER

AD824227

NEW LIMITATION CHANGE

TO

Approved for public release, distribution unlimited

FROM

Distribution authorized to U.S. Gov't. agencies and their contractors; Critical Technology; OCT 1967. Other requests shall be referred to Air Force Materials Lab., Wright-Patterson AFB, OH 45433.

AUTHORITY

USAFSC ltr, 26 May 1972

AFML-TR-67-327
Volume II

DEVELOPMENT OF THE MANUFACTURING CAPABILITIES OF THE HYDROSTATIC EXTRUSION PROCESS

Volume II

R. J. Fiorentino
J. C. Gerdeen
B. D. Richardson
A. M. Sabroff
F. W. Boulger

BATTELLE MEMORIAL INSTITUTE
COLUMBUS LABORATORIES

TECHNICAL REPORT AFML-TR-67-327, VOLUME II
October, 1967

METALLURGICAL PROCESSING BRANCH
MANUFACTURING TECHNOLOGY DIVISION
AIR FORCE MATERIALS LABORATORY
RESEARCH AND TECHNOLOGY DIVISION
AIR FORCE SYSTEMS COMMAND
WRIGHT-PATTERSON AIR FORCE BASE, OHIO

NOTICES

When U. S. Government drawings, specifications, or other data are used for any purpose other than in connection with a definitely related Government procurement operation, the United States Government thereby incurs no responsibility nor any obligation whatsoever; and the fact that the Government may have formulated, furnished, or in any way supplied the said drawings, specifications, or other data, is not to be regarded by implication or otherwise as in any manner licensing the holder or any other person or corporation, or conveying any rights or permission to manufacture, use, or sell any patented invention that may in any way be related thereto.

DDC RELEASE TO OTS NOT AUTHORIZED.

Qualified requesters may obtain copies of this report from DDC, Defense Document Service Center, Cameron Station, Alexandria, Virginia, 22134. Orders will be expedited if placed through the librarian or other person designated to request documents from DDC.

Copies of this report should not be returned to the Research Technology Division unless return is required by security considerations, contractual obligations, or notice on a specific document.

This document is subject to special export controls and each transmittal to foreign governments or foreign nationals may be made only with prior approval to the Manufacturing Technology Division.

DISCLAIMER NOTICE

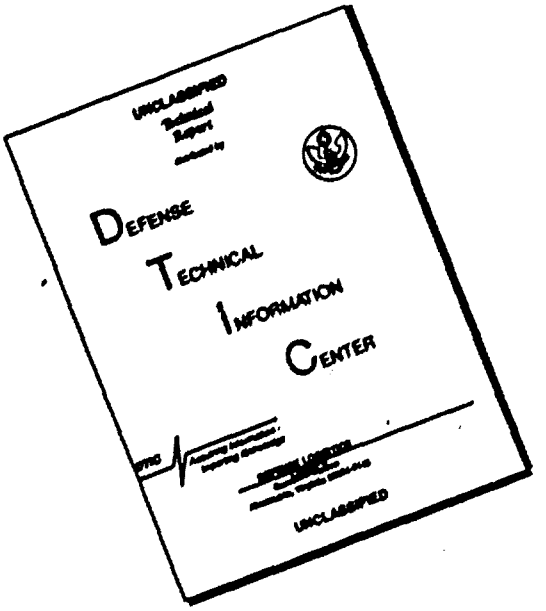

THIS DOCUMENT IS BEST QUALITY AVAILABLE. THE COPY FURNISHED TO DTIC CONTAINED A SIGNIFICANT NUMBER OF PAGES WHICH DO NOT REPRODUCE LEGIBLY.

DEVELOPMENT OF THE MANUFACTURING CAPABILITIES OF THE HYDROSTATIC EXTRUSION PROCESS

VOLUME II

R. J. Fiorentino
J. C. Gerdeen
B. D. Richardson
A. M. Sabroff
F. W. Boulger

FOREWORD

This final technical report in two volumes covers the work performed under Contract AF 33(615)-3190 from 1 December 1964 through 8 July 1967. Volume I covers the results of the experimental work in hydrostatic extrusion and Volume II contains the work relative to design and construction of high-pressure hydrostatic extrusion containers. The manuscript was released by the authors on 29 September 1967 for publication as an AFML technical report.

This contract with Battelle Memorial Institute of Columbus, Ohio, was initiated under Manufacturing Methods Project No. 8-198, "Development of the Manufacturing Capabilities of the Hydrostatic-Extrusion Process". It was administered under the technical direction of Mr. Charles S. Cook until September 1965 and then by Mr. Gerald A. Gegel of the Metallurgical Processing Br. (MATB), Manufacturing Technology Division, Air Force Materials Laboratory, Patterson Air Force Base, Ohio.

The program was conducted at Battelle with the prime responsibility assigned to the Metalworking Research Division and with Mr. R. J. Fiorentino, Associate Chief, as Project Engineer. Others contributing to the program were Mr. B. D. Richardson, Research Metallurgical Engineer, Mr. G. E. Meyer, Research Metallurgical Engineer, Mr. F. W. Fawn, Technician, Mr. A. M. Sabroff, Division Chief, and Mr. F. W. Boulger, Senior Technical Advisor. The late Mr. W. R. Hansen, Research Metallurgist, made a significant contribution to the program up to the time of his death in August, 1966. Mr. R. L. Jentgen, Associate Chief in the Structural Physics Division, assisted in the fluid and lubrication studies of the program. Dr. J. C. Gerdeen, Senior Research Mechanical Engineer in the Advanced Solid Mechanics Division, conducted the stress analysis for the high-pressure-container-design study. Mr. E. C. Rodabaugh, Mr. M. Vagins, Senior Mechanical Engineers, and Mr. T. J. Atterbury, Chief of the Applied Solid Mechanics Division, also assisted in this study. Mr. R. E. Mesloh, Research Mechanical Engineer of the Applied Solid Mechanics Division, designed an instrument for measuring fluid pressure at elevated temperatures. Data from which this report has been prepared are contained in Battelle Laboratory Record Books Nos. 21799, 21990, 23065, 23287, 23585, 23791, 23836, and 24446.

This project has been accomplished as a part of the Air Force Manufacturing Methods program, the primary object of which is to develop, on a timely basis, manufacturing processes, techniques, and equipment for use in economical production of USAF materials and components. The program encompasses the following technical areas:

Metallurgy – Rolling, Forging, Extruding, Casting, Fiber, Powder.
Chemical – Propellant, Coating, Ceramic, Graphite, Nonmetallics.
Fabrication – Forming, Material Removal, Joining, Components.
Electronics – Solid State, Materials and Special Techniques, Thermionics.

Suggestions concerning additional Manufacturing Methods development required on this or other subjects will be appreciated.

H. A. Johnson

H. A. JOHNSON, Chief
Metallurgical Processing Branch
Manufacturing Technology Division

ABSTRACT

The purpose of the program was to develop the manufacturing capabilities of the hydrostatic-extrusion process. Specific applications studied were fabrication of wire, tubing, and shapes from relatively difficult-to-work materials such as refractory-metal alloys, high-strength steels, aluminum alloys, titanium alloys, beryllium, and other selected materials. Phase I was concerned with process optimization and Phase II with direct process application.

As part of Phase I, the effects of critical process variables on pressure requirements and product quality were studied for wrought and powder materials ranging from relatively high-strength easy to work materials such as aluminum alloys and steels to the relatively more difficult-to-work materials such as Ti-6Al-4V titanium alloy and superalloys. With these materials, fluids and lubricants tended to be the factor controlling pressure requirements and product quality. With almost every material extruded the limit in extrusion ratio was set by the design pressure capacity of the container except for the aluminum alloys where the limit was set more by the efficiency of the lubrication system.

In the hydrostatic extrusion of brittle materials, die design proved to be the most significant factor controlling the production of sound, good quality extrusions. New die-design concepts have opened up new fields for the application of hydrostatic extrusion to brittle materials.

Except for the aluminum alloys, the hydrostatic extrudability of the above range of materials was also investigated at 400 and 500 F. Again, fluids and lubricants were developed to enable the production of good quality extrusions. Of particular interest here was the wide range of lubricants that operated successfully at this temperature level.

As part of Phase II of the program, tubing, mill shapes and wire were produced from a variety of materials. For tubing, the floating-mandrel arrangement enabled higher extrusion-ratio capabilities than those for solid rounds. An analysis of the beneficial effects of the floating-mandrel arrangement is given.

T-sections were extruded from round billets and were re-extruded into smaller T-sections. Materials evaluated here were 7075-0 aluminum, AISI 4340 steel, Ti-6Al-4V alloy and Cb752 columbium alloy. The problem of sealing against leaks between the T-billet and die in the re-extrusion of shapes was overcome to some extent following the evaluation of several methods of sealing.

In the reduction of T-sections and wire, a technique of hydrostatic-extrusion drawing developed at Battelle was used. This method, called the HYDRAW technique, was used to reduce wire of Ti-6Al-4V alloy, beryllium, and TZM molybdenum alloy wire at single pass reductions of up to 60 percent. That reduction appeared to be by no means the limit of single-pass reduction achievable with these materials.

During the experimental program, a study of high-pressure container designs was made. Several design concepts that were analyzed are presented in detail in this report. The most promising concept for containing fluid pressures up to 450,000 psi in large-bore containers was that of using pressurized-fluid support as in the ring-fluid-ring design. This and other designs were analyzed on the basis of fatigue-strength criterion, which is believed to be a new and more sound basis for the design of high-pressure containers.

VOLUME II

TABLE OF CONTENTS

TABLE OF CONTENTS
(Continued)

LIST OF ILLUSTRATIONS

LIST OF ILLUSTRATIONS
(Continued)

LIST OF ILLUSTRATIONS
(Continued)

LIST OF TABLES

LIST OF TABLES
(Continued)

LIST OF SYMBOLS SECTION 3

A_n, B_n = coefficients of materials in fatigue relations

N = the total number of components in a container; N also denotes the outermost component

n = a specific component when numbered from inside out; i.e., n = 1, 2, ..., N

r_n = outside radius of component n, inches

r_{n-1} = inside radius of component n, inches

r_o = bore radius of container, inches (inside radius of liner)

r_N = outer radius of container, inches

k_n = wall ratio of component n, $k_n = r_n/r_{n-1}$

K = over-all wall ratio of container, $K = r_N/r_o = k_1k_2 \ldots k_N$

K' = wall ratio of inner part of ring-fluid-segment container, $K' = r_3/r_o$

E_n = modulus of elasticity of component n, psi

p_n = pressure acting on component n at r_n when $p \neq 0$, psi

p_{n-1} = pressure acting on component n at r_{n-1} when $p \neq 0$, psi

p = bore pressure, psi, $p_o = p$ (internal pressure acting on the liner)

q_n = residual interface pressure acting on component n at r_n when $p = 0$, psi

q_r = residual interface pressure required at room temperature for a container designed for use at elevated temperature

q_{n-1} = residual interface pressure acting on component n at r_{n-1} when $p = 0$, psi

S = shear stress, psi

S_r = semirange in shear stress for a cycle of bore pressure, psi

S_m = mean shear stress for a cycle of bore pressure, psi

S_{min} = minimum shear stress during a cycle of bore pressure, psi

S_{max} = maximum shear stress during a cycle of bore pressure, psi

σ = design tensile stress of ductile steel, psi ($\sigma \leq$ ultimate tensile strength)

σ_1 = design tensile stress of high-strength steel, psi ($\sigma_1 \leq$ ultimate tensile strength)

$(\sigma)_r$ = semirange in tensile stress for a cycle of bore pressure, psi

LIST OF SYMBOLS SECTION 3
(Continued)

$(\sigma)_m$ = mean tensile stress for a cycle of bore pressure, psi

σ_y = yield tensile stress, psi

σ_u = ultimate tensile stress, psi

$(\sigma)_{min}$ = minimum tensile stress during a cycle of bore pressure, psi

$(\sigma)_{max}$ = maximum tensile stress during a cycle of bore pressure, psi

σ_r = radial stress, psi

σ_θ = circumferential stress, psi

σ_z = axial (longitudinal) stress, psi

α_r = semirange stress parameter for high-strength steel, $\alpha_r = (\sigma)_r/\sigma_1$

α_m = mean stress parameter for a high-strength steel, $\alpha_m = (\sigma)_m/\sigma_1$

M_1 = bending moment on ring segment

M_2 = bending moment on pin segment

u = radial displacement, inches

v = circumferential displacement, inches

ν = Poisson's ratio

r, θ, z = cylindrical coordinates for radial, circumferential, and axial directions, respectively

Δ_n = interference required (as manufactured) between cylinder, n, and cylinder, n + 1, inches

Δ_{12} = interference required (as manufactured) between the liner, segments, and cylinder, 3, of the ring-segment and ring-fluid-segment containers, inches

α_1, α_2 = coefficient of thermal expansion of material comprising rings 1 and 2

XXI

INTRODUCTION

The purpose of this program was to develop the manufacturing capabilities of the hydrostatic-extrusion process. The program was divided into two phases with the following general objectives:

Phase I. Process-Development Studies

Part 1. (a) To study the effect of critical process variables on pressure requirements and surface quality in hydrostatic extrusion of AISI 4340 steel, Ti-6Al-4V titanium alloy, and 7075 aluminum alloy.

(b) To correlate all available hydrostatic-extrusion-pressure data with material properties wherever possible in order to assist direction of the experimental effort and maximize the information developed on the present program.

Part 2. To explore the hydrostatic extrudability of TZM molybdenum alloy, beryllium, A286 iron-base superalloy, Alloy 718 nickel-base superalloy, powder compacts, and other selected materials.

Part 3. To conduct a design study for high-temperature, high-pressure hydrostatic-extrusion tooling based on (1) estimated pressure requirements for high-ratio extrusion of materials of interest to the Air Force, (2) latest high-pressure-vessel technology, and (3) latest tooling materials available.

Part 4. To conduct a process economic study on the construction, installation, and operation of equipment with the same operational and size requirements as the tooling developed in the previous program on Contract No. AF 33(600)-43328.

Phase II. Process-Application Studies

Part 1. To evaluate the application of the hydrostatic-extrusion process for sizing and finishing conventionally hot-extruded (or rolled) structural shapes by various combinations of drawing and extruding. Primary emphasis was to be on AISI 4340 steel, although some effort was to be devoted to Ti-6Al-4V, 7075-0 aluminum, and selected refractory metals.

Part 2. To determine the feasibility of producing wire and filaments from beryllium, TZM molybdenum alloy, and Ti-6Al-4V titanium alloy by combinations of hydrostatic extrusion and drawing.

Part 3. To develop tooling and define process parameters necessary for the reduction of tube blanks to finish tubing from AISI 4340 steel, 7075-0 aluminum, and Ti-6Al-4V titanium.

The results of the experimental and analytical work connected with Phases I and II were covered in Interim Engineering Progress Reports I through IX.

This, the Final Technical Report in two volumes, contains the results of the program in their entirety. Volume I contains Section 1, "A Study of the Critical Process Variables in the Hydrostatic Extrusion of Several Materials" and Section 2, "Production Aspects of Hydrostatic Extrusion". Volume II contains Section 3, "Analysis of Several High-Pressure Container-Design Concepts" and Section 4, "Hydrostatic-Extrusion Containers Designed and Constructed in the Program". The experimental program started December 1, 1964, and was completed on July 8, 1967.

XXII

SUMMARY OF VOLUME II

The experimental work conducted in this program has taken the technology of the hydrostatic-extrusion process from the experimental stage to the threshold of its application in a production operation. Commercial exploitation of the process is possible without any further major experimentation and it is believed that this report gives the guidelines that will enable these steps to be taken immediately. What remains now is the complete design of production hydrostatic-extrusion equipment that will be competitive with conventional-extrusion equipment. At the time of this writing, a program is underway at Battelle-Columbus Laboratories in which such equipment is being designed. The program, "Design Study of Production Press for Ultrahigh-pressure Hydrostatic-Extrusion Equipment", is sponsored by the Metallurgical Processing Branch, Manufacturing Technology Division at Wright-Patterson Air Force Base, Ohio, on Contract No. AF 33(615)-67-C-1434.

One of the most important aspects of the aforementioned design study is the design of the high-pressure container. Section 3 of this report contains a thorough analysis of several concepts of high-pressure containers. This analysis will be drawn on heavily in the design study. Section 4 describes the development of three containers designed and constructed in this program.

Both Sections 3 and 4 are complete in themselves and each contains its own summary.

SECTION 3

ANALYSIS OF SEVERAL HIGH-PRESSURE CONTAINER DESIGN CONCEPTS

SECTION 3

ANALYSIS OF SEVERAL HIGH-PRESSURE CONTAINER DESIGN CONCEPTS

XXIII

SUMMARY FOR SECTION 3

Five types of pressure-vessel designs were analyzed in detail: a multiring container, a ring-segment container, a ring-fluid-segment container, a pin-segment container and a ring-fluid-ring container. (These are illustrated in Figures 39 and 40 of the text.) The multiring container is made up of cylindrical ring components. The ring-segment container is like the multiring container except that the second ring, adjacent to the liner, is a segmented ring. The ring-fluid-segment container is a combination of a ring-segment container on the inside with a multiring container on the outside, and with a fluid support pressure in between. In the ring-fluid-ring container, the inner ring is of single or multiring construction. The pin-segment container has a cylindrical inner liner supported by a pinned segment-plate arrangement. A wire-wrapped (strip-wound) vessel and a controlled fluid-fill vessel were also considered but in less detail.

The four types of pressure vessel designs shown in Figure 39 were analyzed and reported in Interim Reports III, IV and V.[20, 21, 22] These analyses are described in detail in this section. Though the concept of the ring-fluid-ring design was reported in Interim Report IV, its complete analysis is reported for the first time in this section.

The operating cycle of high-pressure containers for hydrostatic extrusion and forming consists of application of the pressure needed, followed by a decrease in the pressure to zero. Such highly cyclic conditions coupled with extreme operating pressures can be expected to cause fatigue failures of the containers. A fatigue strength criterion was selected as the basis of the study because a high-pressure container for commercial application should, of course, be capable of repeated use without frequent failure.

To achieve the desired high pressure it was found necessary to use high-strength liner materials. For the high-strength steels (ultimate tensile strengths of 250,000 psi and greater) a maximum-tensile-stress criterion of fatigue was assumed and available uniaxial fatigue data from the literature were used in design evaluations. However, the fatigue behavior was left arbitrary in the analysis by formulating the analysis in terms of α_r and α_m, semirange and mean tensile stress parameters. The outer rings of the containers were assumed to be of more ductile materials in order to avoid catastrophic failures. A maximum shear criterion of fatigue was used for the ductile outer rings and the Goodman relation was used to relate the semirange and mean shear stresses.

For the analysis, equations were derived that relate the interface and the radial deformations between components. Elasticity solutions for stress and deformations were used together with fatigue relations to determine formulas for maximum bore pressures. Stresses due to the bore pressure and shrink-fit assembly were analyzed. The effect of temperature change (from operating temperature to room temperature) upon the prestresses (residual stresses) was included. The analyses for maximum pressure capability, residual stresses, and required shrink-fit interferences were programmed for calculation on Battelle's CDC 3400 and CDC 6400 computers.

Theoretically, large pressures (up to 1,000,000 psi in the ring-fluid-segment design) were found to be possible in the containers. However, designs based on the theoretical pressures were not always considered practicable because of manufacturing and assembly limitations. For example, a ring-fluid-segment container designed to a theoretical maximum pressure capability of 450,000 psi requires outside diameters of 88.0 inches and 218.0 inches for 6- and 15-inch-diameter bore designs, respectively. Such large-diameter cylinders would present problems in producibility, heat-treating, and transportation. This container design also requires a shrink-fit interference of 0.0128 in./in., which is difficult, if not impossible, to achieve in assembly. This large interference requirement is necessary to overcome excessive deformation of segments. Also, relatively larger outside diameters are required for segmented containers because segments offer no hoop support to the liner. These are distinct disadvantages of containers using segments.

Because of the practicable design limitations, the designs were evaluated for outside diameters limited to 72 inches and interferences limited to 0.007 in./in. maximum. High-strength liner materials of 300,000 psi ultimate tensile strength were assumed for which some fatigue data were available. A fatigue life of 10^4-10^5 cycles was selected for ideal conditions, i.e., no stress concentrations or material flaws in the liner. On this basis, the predictions of maximum pressure capability for 6-inch-diameter bore designs, for example, are as follows:

Container	Outside Diameter, inches	Maximum Pressure, p_i psi
Multiring	51.0	300,000
Ring-segment	60.0	290,000
Ring-fluid-segment	72.0	286,000
Pin-segment	72.0	195,000

These pressure capabilities apply at room or elevated temperatures, provided the ultimate strength of the liner is 300,000 psi at temperature. Higher maximum pressures are theoretically possible with higher strength materials. For example, a maximum pressure of 450,000 psi would be predicted for a multiring container with a 450,000 psi ultimate strength liner material, if such a material could be found that had the same proportionate increase in its fatigue strength.

Residual stress limitations were also found for containers designed for high-temperature use. If the coefficient of thermal expansion of the liner is smaller than that of the outer components, then a decrease in temperature from operating temperature to room temperature may cause excessive residual stresses in the liner. Therefore, a higher coefficient of thermal expansion would be recommended for the liner.

There are other possible material limitations. The design evaluations conducted herein were based necessarily on the uniaxial fatigue data available for the liner materials, although a biaxial or triaxial state of stress exists in a pressure container. Also, a compressive mean stress on the liner was assumed beneficial. However, fatigue behavior of high-strength steels under combined stresses and compressive mean stress is unknown. In addition to fabrication and transportation difficulties, heat treatment of large cylindrical forgings may also present problems. In this respect a pin-segment-plate arrangement or a strip-wound layer offers advantages as a replacement of cylindrical rings for outer support members.

A material study is proposed to determine data on the important properties of high-strength materials for high-pressure-container applications.

Based on the design study of the four containers listed above, the ring-fluid-ring design was suggested. This design makes use of the benefits of fluid-support pressure and prestress from shrink fit. It avoids the difficulties associated with the segmented containers. It is shown in this analysis that a ring-fluid-ring container having a bore of 6-inch diameter could withstand a pressure level of 450,000 psi with an outer unit diameter of 60 inches. The fatigue life of this container would be 10^4-10^5 cycles.

Additional details of analysis are included in the appendices of this report. Bending deformations and stresses within segments, and derivations of shrink-fit interferences are some of the items included. Computer programs used for calculations are also briefly described.

XXIV

SCOPE OF ANALYSIS

The purpose of this study was to determine the maximum pressure capability of several designs of vessels for containing fluids at the pressures encountered in hydrostatic extrusion and other hydrostatic-forming processes. Containment of bore-fluid pressures up to 450,000 psi at room temperature and at temperatures of 500 F and 1000 F is considered.

The operating cycle of these high-pressure containers consists of application of the pressure needed for extrusion or forming, followed by a decrease in the pressure to zero. To be useful in production, the high-pressure containers must withstand a large number of such operating cycles. Therefore, fatigue strength of component materials must be an important design consideration. However, consideration of fatigue strength appears to be lacking in design analyses heretofore. The general method of design analysis has been to use a safety factor on the yield pressure. As the design pressures have been steadily increased, material limitations have necessitated lower factors of safety, sometimes less than 1:1. Consequently, fatigue failures are being experienced. Because of the extreme operating pressures being considered for hydrostatic extrusion and other forming operations (up to about 450,000 psi), it was essential that the various container-design concepts be analyzed and compared on the basis of a fatigue criterion.

In order to estimate the pressure capability of each container, stress analyses are conducted. Only stresses due to the bore pressure and shrink-fit assembly are analyzed; no thermal gradients are assumed present. However, the effect of temperature change (from operating temperature to room temperature) upon the prestress (residual stresses) is included in the analyses. Excessive residual stresses may result because of differences in thermal expansion of the component parts of each container.

Four types of pressure vessel designs were analyzed in detail. These are:

(1) Multiring container
(2) Ring-segment container
(3) Ring-fluid-segment container
(4) Pin-segment container.

The four concepts for cylindrical containers are shown in Figure 39. A wire-wrapped (strip-wound) vessel and a controlled fluid-fill, cylindrical-layered container also were considered, but only briefly.

As a result of these analyses, a further refinement of the ring-fluid-segment container was conceived in which the segments were replaced by a shrink-ring assembly as shown in Figure 40. An extended analysis of this advanced container design has been completed recently and is described for the first time in this report. A rigorous analysis of the advanced concept together with a more general formulation of fatigue criteria for multiring containers are reported separately at the end of this section.

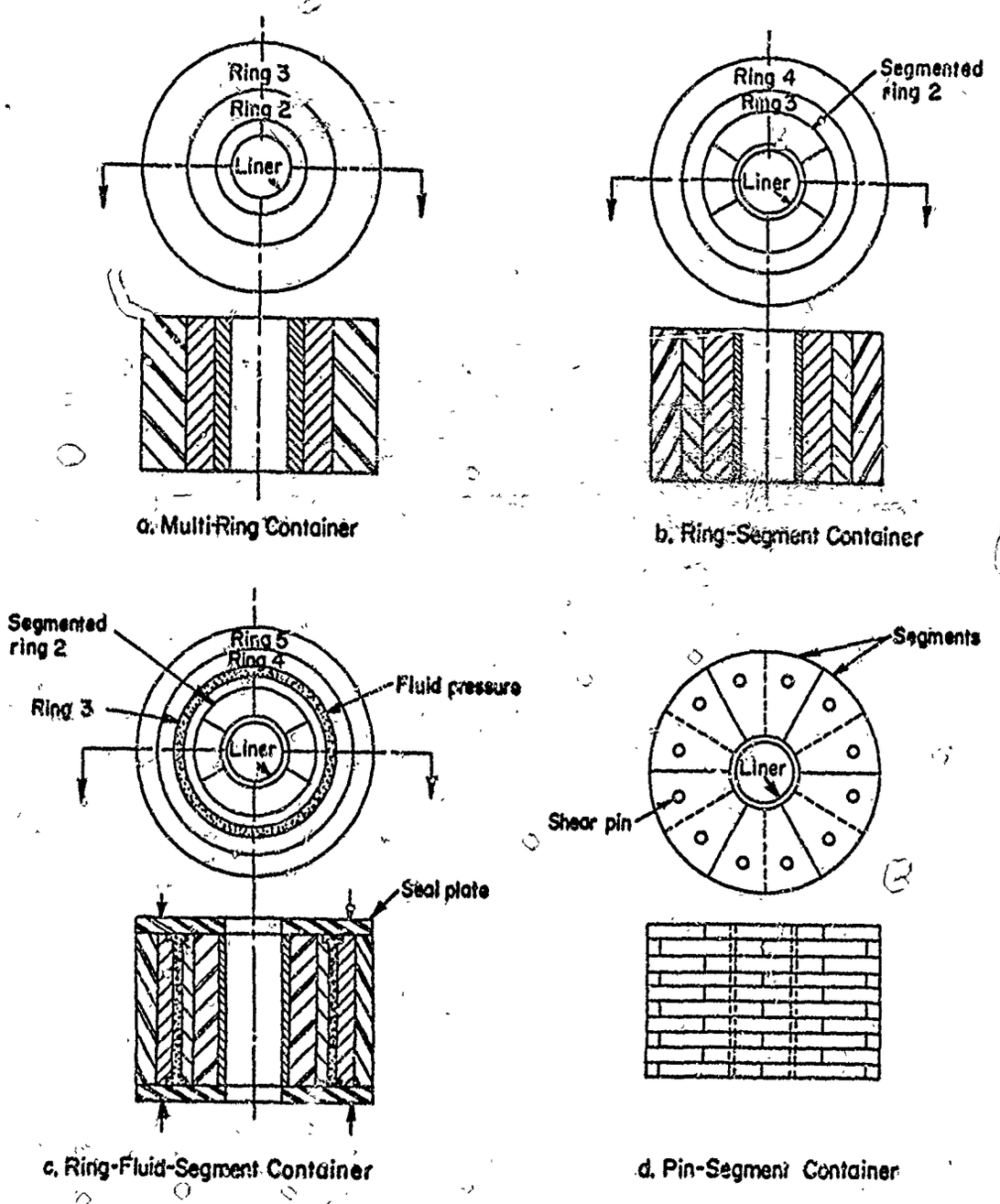

FIGURE 39. SCHEMATIC OF HIGH-PRESSURE-CONTAINER DESIGN CONCEPTS ANALYZED IN THE PRESENT STUDY

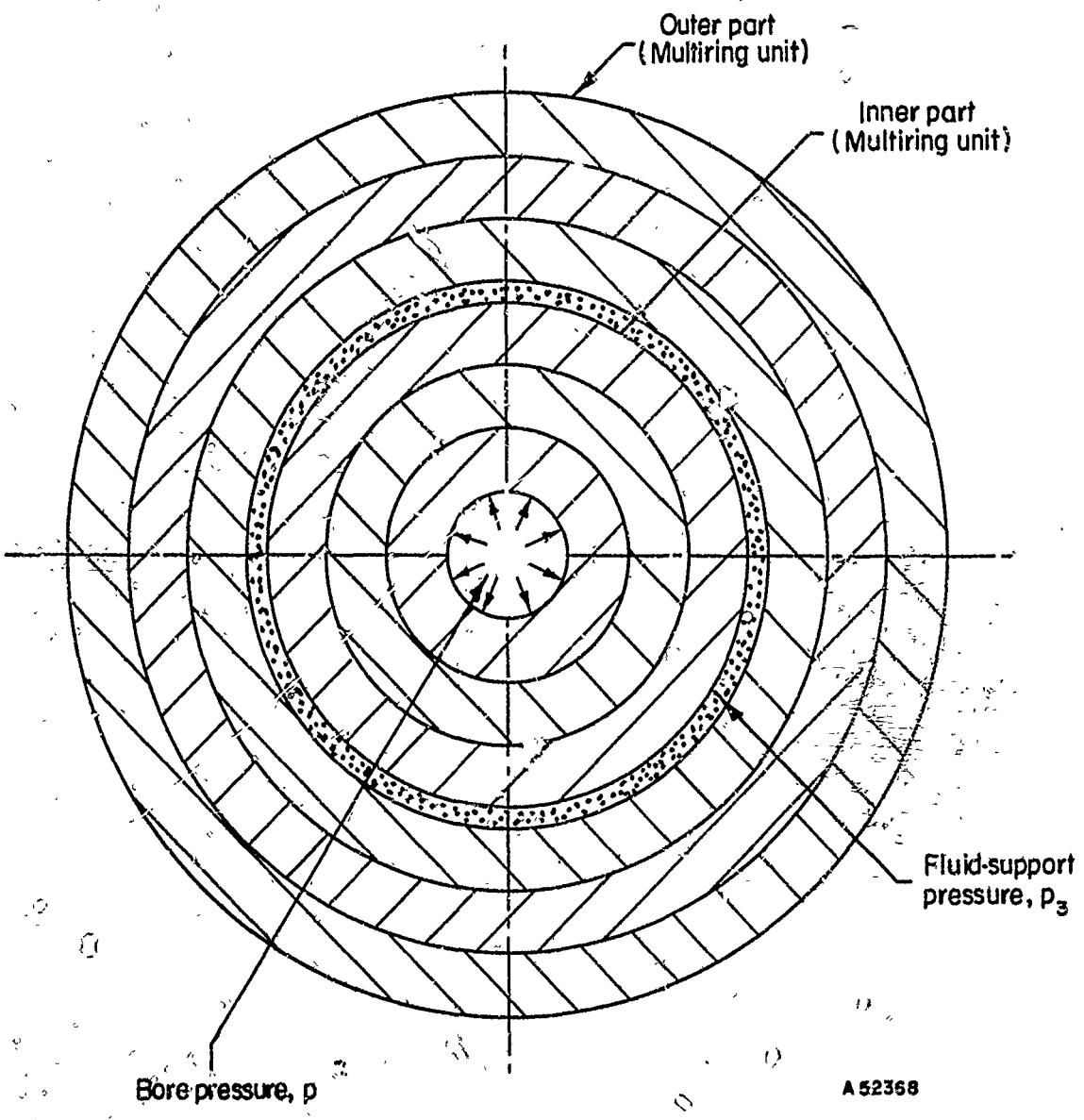

FIGURE 40. RING-FLUID-RING CONTAINER FOR HIGH P[illegible]ESS[illegible]

The design involves the combined use of interference fit multi-ring construction with fluid-pressure sup

The multiring container was one of the first design modifications of the monoblock, thick-walled cylinder*. An initial compressive stress at the bore is achieved by shrink-fit assembly of successive cylinders each manufactured to provide an interference fit with its mating cylinder. The multiring container has been analyzed on the basis of static shear strength by Manning[23, 24, 25].

The ring-segment container with one outer ring was patented by Poulter in 1951.[26] One intent of this design is to reduce the pressure acting upon the outer ring by using a segmented cylinder to redistribute the pressure at a larger diameter. However, the inner cylinder is always subject to the bore pressure. The external diameter of the vessel necessarily increases with increasing segment size.

The ring-fluid-segment container makes use of the fluid-pressure support principle. This container is essentially constructed of two parts. The inner part is a ring-segment-type container with one outer ring, but with a fluid support pressure, p_3, as shown in Figure 41. The outer part is a multiring container subject to an internal pressure, p_3, the support pressure for the inner part. The advantage of this design is that the fluid pressure (p_3) provides a compressive hoop stress at the bore which counteracts the tensile hoop stress resulting from the bore pressure, p. Theoretically, p_3 can be changed in proportion to the change in bore pressure in order to reduce the bore stress over an entire cycle of bore pressure. This variation of p_3 with the bore pressure is assumed in the analysis.

The origin of the ring-fluid-segment concept is not clear. Ballhausen patented an approach of this sort in 1963.[27] Another application of the same principle was patented by G. Gerard and J. Brayman, also in 1963.[28] A similar design, but with additional features, was reported by F. J. Fuchs in 1965.[29]

The pin-segment design is an approach proposed by Zeitlin, Brayman, and Boggio.[30] Like the ring-segment container this vessel also uses segments to reduce the pressure that must be carried by the external support. Unlike the ring-segment container, the pin-segment container has segmented disks (thin plates) rather than segmented cylinders. Also, the external supporting members in this case are pins rather than an external ring. The pins carry the reaction to the bore pressure predominantly in shear.

The ring-fluid-ring container shown in Figure 40, like the ring-fluid-segment design, makes use of the fluid pressure support principle. The use of an inner multiring unit, however, avoids the numerous difficulties encountered in segmental design. Since suggestion of the design, description of similar designs have been noted in the literature.[31, 32, 33] Thus, the design is not new, but the analytical-design basis described toward the end of this section is. It is believed that this program is the first to incorporate the fatigue-strength design of high-pressure containers on a rigorous basis.

All five containers have one thing in common: the liner is subject to the full bore pressure. The five containers differ in the manner and in the amount they constrain the liner.

*The monoblock, thick-wall cylinder is the simplest type of pressure container. However, for the very high pressure levels considered in this study it is a relatively inefficient design.

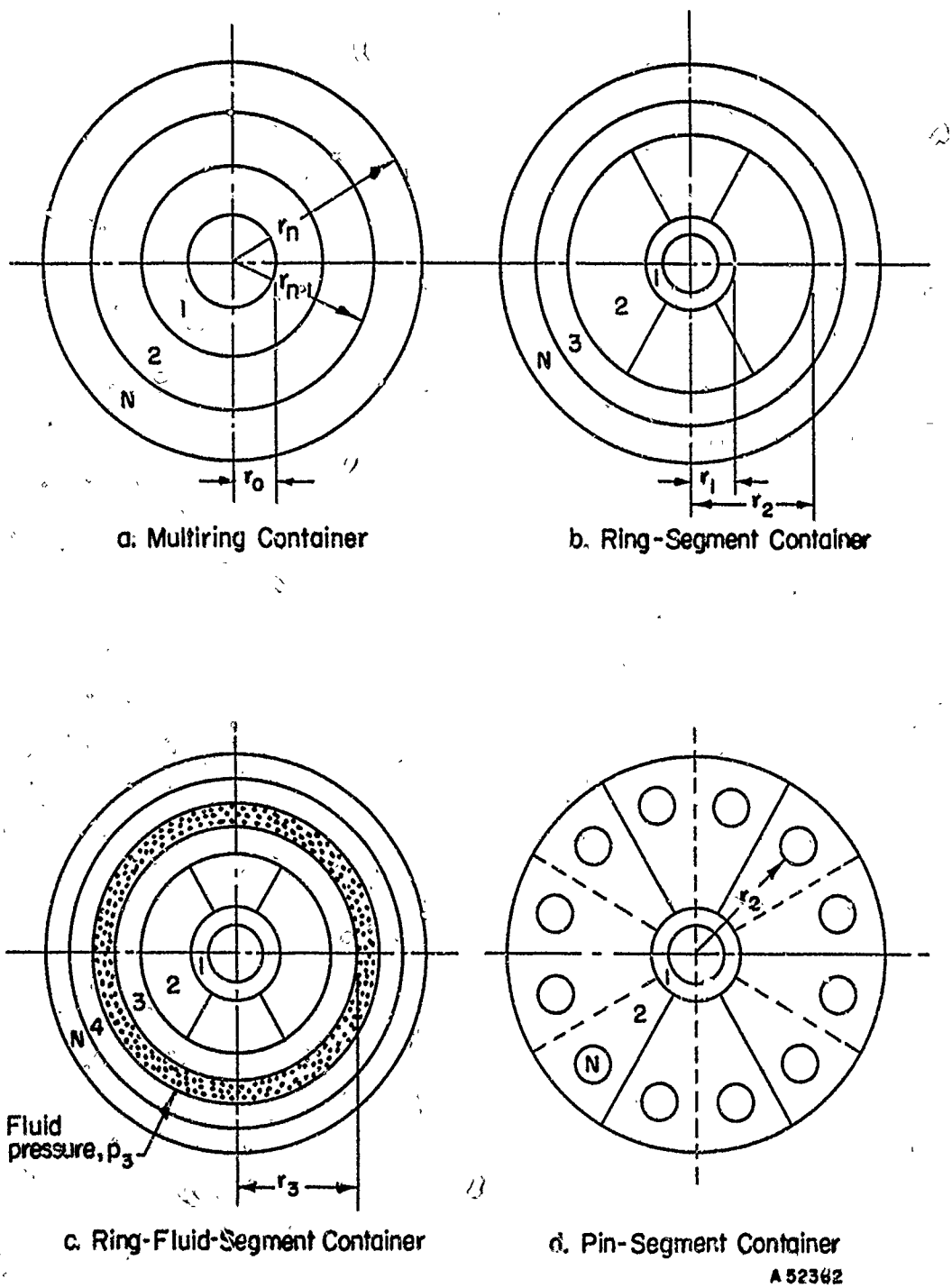

FIGURE 41. NOTATIONS USED FOR ANALYSIS OF CONTAINER-DESIGN CONCEPTS

XXV

BASIS AND METHOD OF ANALYSIS

In this study the four design concepts for high-pressure containers are evaluated on the basis of a selected strength criterion for the component materials. Different strength criteria could be chosen, each of which could lead to different predictions of maximum pressure capability. If rupture under static load is the strength criterion then a burst pressure can be predicted. This pressure would be higher than the yield pressure predicted on the basis of static yield strength. However, a vessel subject to a great number of pressure cycles at less than the yield pressure could fail by fatigue. A high-pressure container for commercial hydrostatic extrusion should, of course, be capable of repeated use without frequent failure. Therefore, it was considered essential that a fatigue strength criterion be used as the basis of evaluation in this study.

It also has to be ascertained what kind of stress and strain analysis is needed – elastic, plastic, or elastic-plastic. This is determined from the fatigue life desired. Manson and Hirschberg have shown that for most materials, failure by low-cycle fatigue (life less than about 1000 cycles) involves almost entirely plastic strain.(34) Above about 1000 cycles life the amount of plastic strain is appreciably smaller, and above 100,000 cycles life the plastic strain is negligible. For the relatively high-strength materials, however, the strain at fracture is predominantly elastic for lifetimes as low as 100 cycles. Because lifetimes greater than 1000 cycles are desirable in commercial applications, and since high pressures require use of high-strength materials, elasticity theory rather than plastic or elastic-plastic analysis is used. Use of elastic theory rather than elastic-plastic theory also aids the study because elasticity solutions are easier to formulate and can be superimposed.

For the analysis, equations are derived that relate the interface pressures and the radial deformations between components. Elasticity solutions for stresses and deformations are used together with fatigue relations to determine formulas for maximum bore pressures.

XXVI

METHOD OF PARAMETER NOTATION

The components of each design are identified from the inside out by the numbers 1, 2, 3, ..., N. N refers to the outermost component. Figure 41 shows the use of radii r_{n-1} and r_n to denote the inner and outer radii of component number n.

For the multiring container all the components are circular hollow cylinders. For the ring-segment and ring-fluid-segment containers, Component 2 refers to the segments. The only exception to the notation on the radii occurs in the pin-segment design where the segment is divided for analysis into two parts and where r_2 is the radius to the inside of the pins as shown in Figure 41.

The operating pressures and the residual pressures are identified by q_n and p_n* respectively. Because the outer radius of each container refers to a free surface, the pressure there is zero,

$$p_N = 0 \quad , \qquad q_N = 0 \tag{4a, b}$$

The definition of the q_n gives

$$q_0 = 0 \tag{5}$$

The wall ratio for component n is denoted by k_n. The overall diameter ratio of the container is denoted as K, where

$$k_n = \frac{r_n}{r_{n-1}}$$

and

$$K = \frac{r_N}{r_o} \quad .$$

*See list of symbols for definitions.

XXVII

FATIGUE CRITERIA

Two fatigue criteria are formulated here in order that both relatively low-strength ductile materials and high-strength, more brittle materials may be used in one design. The intention is to use high-strength steels as liner materials and lower strength ductile steels for the outer cylinders in order to prevent catastrophic brittle failure.

Fatigue Criterion for Ductile Outer Cylinders

From both torsion and triaxial fatigue tests on low-strength steels (120 to 150 ksi ultimate strength) conducted by Morrison, Crossland, and Parry[35] it is concluded that a shear criterion applies. Therefore, a shear theory of failure is assumed for outer rings made of ductile steel.

To formulate a fatigue relation, the semirange in shear stress and the mean shear stress are needed. These stresses are defined as

$$S_r = \frac{S_{max} - S_{min}}{2}$$

$$S_m = \frac{S_{max} + S_{min}}{2} \qquad (6a, b)$$

respectively.

A linear fatigue relation in terms of shear stresses is assumed. This relation is

$$\frac{S_r}{S_e} + \frac{S_m}{S_u} = 1, \text{ for } S_m \geqq 0 \quad ,$$

where S_e is the endurance limit in shear and S_u is the ultimate shear stress. For $S_u = 1/2\ \sigma_u$, where σ_u is the ultimate tensile stress, this relation can be rewritten as:

$$\frac{S_r}{S_e} + \frac{2S_m}{\sigma_u} = 1, \ S_m \geqq 0 \qquad (7)$$

The stresses S_r and S_m given by Equations (6a, b) can be calculated from elasticity solutions. In order to employ the fatigue relation (7) for general use, it is assumed that S_e can be related to S_u. This is a valid assumption as shown by Morrison, et al[35]. Referring to Reference (35), the ratio S_e/S_u can be established. Table XLI lists some fatigue data and results of calculation of S_e from Equation (7).

From Table XLI is is evident that fluid pressure contacting the material surface has a detrimental effect on fatigue strength; the endurance limit S_e for unprotected triaxial fatigue specimens is lower than that for torsional specimens. However, protection of the bore of triaxial specimens increases S_e under triaxial fatigue to a value equal

that for torsional fatigue. Since in the high-pressure containers, outer cylinders are subject to interference contact pressures and not to fluid pressures, it is assumed that the data for a protected bore in Table XLI are applicable in the present analysis. Therefore, the following relation between S_e and σ_u is assumed:

$$S_e = \frac{1}{3}\sigma_u \tag{8}$$

Substitution of Relation (8) into (7) gives

$$3S_r + 2S_m = \sigma, \text{ where } \sigma \leqq \sigma_u \tag{9}$$

Equation (9) now has a factor of safety, σ_u/σ, and can be expected to predict lifetimes of 10^6 cycles and greater for ductile steels based upon the linear fatigue relation and available fatigue data. (Of course, stress concentration factors due to geometrical discontinuities or material flaws would reduce the expected lifetime.)

TABLE XLI. TORSIONAL AND TRIAXIAL FATIGUE DATA ON VIBRAC STEEL[a]

Test	Stresses, psi				
	σ_u	S_r	S_m	S_e	S_e/σ_u
Torsion	126,000	43,700	0	43,700	0.347
	149,000	52,900	0	52,900	0.354
Triaxial (unprotected bore)	126,000	20,900	20,900	31,300[c]	0.248
	149,000	26,300	26,300	40,600	0.273
Triaxial[b] (protected bore)	126,000	26,500	26,500	45,900	0.363

(a) From Reference (35). Composition of this steel in weight percent is 0.29 to 0.3 C, 0.14 to 0.17 Si, 0.64 to 0.69 Mn, 0.015 S, 0.013 P, 2.53 to 2.58 Ni, 0.57 to 0.60 Cr, 0.57 to 0.60 Mo.

(b) The bore of the cylindrical specimens was protected with a neoprene covering.

(c) S_e for the triaxial tests is calculated from Equation (7).

Fatigue Criterion for High-Strength Liner

Triaxial fatigue data on high-strength steels ($\sigma_u \geqq 250$ ksi) are not available. Fatigue data in general are very limited. Therefore, a fatigue criterion for high-strength steels under triaxial fatigue cannot be as well established as it was for the lower strength steels. The high-strength steels are expected to fail in a brittle manner. Accordingly, a maximum tensile stress criterion of fatigue failure is postulated.

Because fatigue data are limited while tensile data are available the tensile stresses $(\sigma)_r$ and $(\sigma)_m$ are related to the ultimate tensile strength by introduction of two parameters α_r and α_m. These are defined as follows:

$$\alpha_r = \frac{(\sigma)_r}{\sigma_1}, \qquad \alpha_m = \frac{(\sigma)_m}{\sigma_1} \tag{10a, b}$$

where $(\sigma)_r$ is the semirange in stress, $(\sigma)_m$ is the mean stress*, and σ_1 is less than or equal to the ultimate tensile strength depending upon the factor of safety desired. In order to get some estimations of what values α_r and α_m may be, some data from the literature are tabulated in Tables XLII, XLIII, and XLIV. These data are for rotating-beam and push-pull tests.

The fatigue life again is found to depend on the range in stress and the mean stress, and upon the temperature. This dependence is illustrated in Figure 42 for 10^4 to 10^5 cycles life in terms of the parameters α_r and α_m. (Points (α_r, α_m) above the curves in Figure 42 would correspond to $<10^4$-10^5 cycles life and points below the curves would correspond to $>10^4$-10^5 cycles life.) The 1000 F temperature data are for Vascojet 1000. Although α_r increases with temperature for this steel, the ultimate tensile strength decreases and the fatigue strength at 10^4 to 10^5 cycles for $\alpha_m = 0$ remains nearly constant over the temperature range of 75 F to 1000 F.

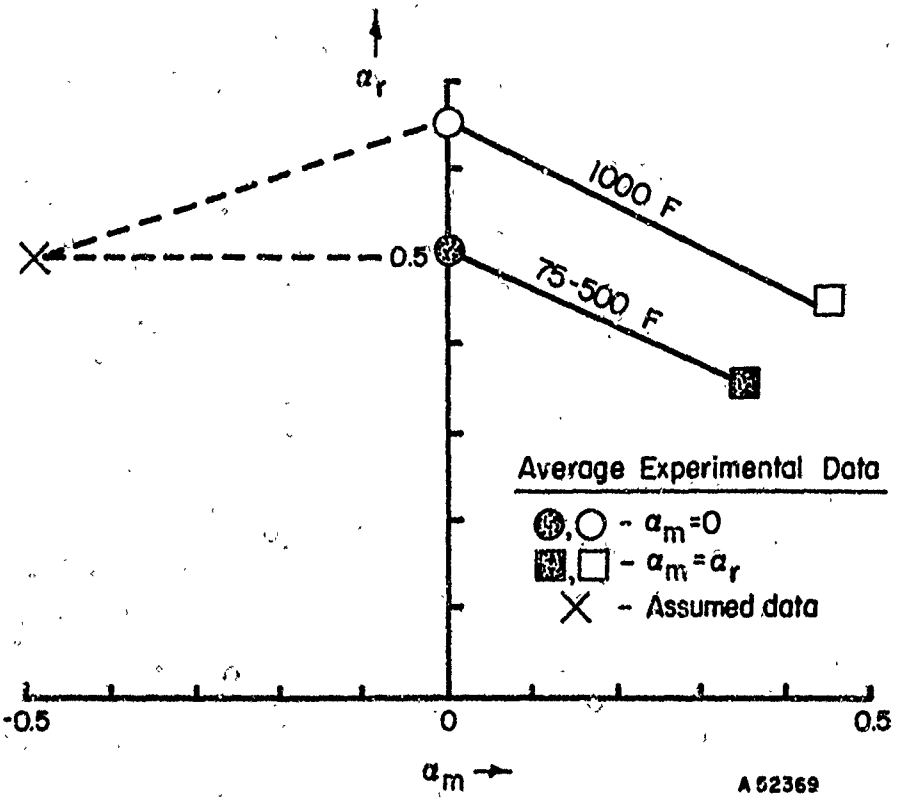

FIGURE 42. FATIGUE DIAGRAM FOR 10^4-10^5 CYCLES LIFE FOR HIGH-STRENGTH STEELS AT TEMPERATURES OF 75 F TO 1000 F

α_r and α_m are defined by Equations (10a, b)

*$(\sigma)_r$ and $(\sigma)_m$ are defined by expressions similar to Equations (9a, b) for S_r and S_m.

TABLE XLII. FATIGUE STRENGTHS OF HIGH-STRENGTH STEELS FROM ROOM-TEMPERATURE ROTATING-BEAM TESTS, $\alpha_m = 0$

Material	Reference	Ultimate Tensile Strength, ksi	Yield Tensile Strength, ksi	α_r, Stress Range Parameter[a], for Cycles 10^4	10^5	10^6	10^7
18% Ni maraging steel	(36)	300	280		0.49	0.43	0.41
	(37)	300	285		0.33	0.31	0.30[b]
	(38)	295	285	0.68	0.44	0.38	0.36
		270	265	0.74	0.43	0.37	0.37
H-11 (CEVM)	(38)	250-280	210-230	0.75	0.57	0.54	0.54
D6AC	(39)[c]	270	237	0.66	0.41	0.37	0.37
Vascojet 1000	(39)[c]	309	251		0.45	0.29	0.29

(a) $\alpha_r \equiv (\sigma)_r/\sigma_u$, $\alpha_m \equiv (\sigma)_m/\sigma_u$, where $(\sigma)_r$, $(\sigma)_m$, σ_u are the semirange, mean, and ultimate tensile stresses, respectively.
(b) These are stated to be 90 percent probability data.
(c) Tests in Reference (39) were push-pull tests with, $\alpha_m = 0$.

TABLE XLIII. FATIGUE STRENGTHS OF HIGH-STRENGTH STEELS FROM ROOM-TEMPERATURE PUSH-PULL TESTS, $\alpha_m = \alpha_r$

Material	Reference	Ultimate Tensile Strength, ksi	Yield Tensile Strength, ksi	α_r, Stress Range Parameter[a], for Cycles 10^4	10^5	10^6	10^7
18% Ni maraging steel	(38)	295	285	0.40	0.25	0.22	0.22
		270	265	0.43	0.28	0.25	0.24
H-11 (CEVM)	(38)	280-300		0.38	0.31	0.29	0.29
D6AC	(39)	270	237	0.44	0.33	0.28	0.28
Vascojet 1000	(39)	309	251		0.33	0.27	0.25

(a) $\alpha_r \equiv (\sigma)_r/\sigma_u$, $\alpha_m \equiv (\sigma)_m/\sigma_u$, where $(\sigma)_r$, $(\sigma)_m$, σ_u are the semirange, mean, and ultimate tensile stresses, respectively.

TABLE XLIV. FATIGUE STRENGTHS OF HIGH-STRENGTH STEELS FROM PUSH-PULL TESTS AT ELEVATED TEMPERATURES[a]

Material	Test Temp., F	Ultimate Tensile Strength, ksi	Yield Tensile Strength, ksi	Test Conditions[c]	α_r, Stress Range Parameter[b], for Cycles 10^4	10^5	10^6	10^7
D6AC	450	260	175	$\alpha_m = 0$	0.56[d]	0.48	0.40	0.31
				$\alpha_m = \alpha_r$	0.41	0.35	0.31	0.26
	550	230	160	$\alpha_m = 0$	0.65	0.52	0.41	0.33
				$\alpha_m = \alpha_r$	0.44	0.38	0.34	0.29
Vascojet 1000	800	260	200	$\alpha_m = 0$	0.69	0.56	0.42	0.31
				$\alpha_m = \alpha_r$		0.40	0.32	0.23
	1000	230	176	$\alpha_m = 0$	0.75[d]	0.61	0.43	0.26
				$\alpha_m = \alpha_r$		0.39	0.27	0.21

(a) Data are taken from Reference (33).
(b) $\alpha_r \equiv (\sigma)_r/\sigma_u$, $\sigma_m \equiv (\sigma)_m/\sigma_u$, where $(\sigma)_r$, $(\sigma)_m$, σ_u are the semirange, mean, and ultimate tensile stresses, respectively, at temperature.
(c) The cycle rate was 3100 cps.
(d) S-N curve extrapolated to 10^4 cycles.

The fatigue data available are only for positive and zero mean stresses. However, there is evidence that compressive mean stress may significantly increase the fatigue strength[35,40]. The reasons for this are thought to be that compression may reduce the detrimental effect of fluid pressure entering minute cracks or voids in the material and the compression may restrain such flaws from growing. Since the liner of a high-pressure container can be precompressed by shrink-fit assembly, an important factor in triaxial fatigue may be the prestress that can be initially provided. Therefore, for 10^4 to 10^5 cycles triaxial fatigue life, α_r and α_m are assumed to be

$$\alpha_r = 0.5, \quad \alpha_m = -0.5 \tag{11a, b}$$

as indicated in Figure 42. With $\alpha_m = -\alpha_r$ the maximum tensile stress at the bore would be zero.

In order to approximate a life of one cycle, it is assumed that

$$\alpha_r = 1.0, \quad \alpha_m = 0, \quad \text{for one cycle} \tag{12a, b}$$

which represents a cycle between $\pm\sigma_u$, the ultimate strength.

XXVIII

ELASTICITY SOLUTIONS

Cylindrical polar coordinates (r, θ, z) are used in the analysis. Axial symmetry is assumed; the stresses are independent of the angle θ. End effects are not considered*; the stresses found are independent of the axial coordinate z.

Elasticity Solutions for a Cylinder

The two-dimensional solutions for a cylinder loaded by uniform inner and outer pressures is given by Timoshenko and Goodier(41). The expressions for stresses and displacement in cylinder n are

$$\sigma_r = \frac{1}{k_n^2-1}\left[p_{n-1} - p_n k_n^2 - (p_{n-1} - p_n)\left(\frac{r_n}{r}\right)^2\right]$$

$$\sigma_\theta = \frac{1}{k_n^2-1}\left[p_{n-1} - p_n k_n^2 + (p_{n-1} - p_n)\left(\frac{r_n}{r}\right)^2\right] \qquad (13a\text{-}c)$$

$$\tau_{r\theta} = 0$$

$$\frac{u}{r} = \frac{1}{E_n(k_n^2-1)}\left[(1-\nu)(p_{n-1} - p_n k_n^2) + (1+\nu)(p_{n-1} - p_n)\left(\frac{r_n}{r}\right)^2\right] \qquad (14a, b)$$

$$v = 0$$

where σ_r, σ_θ, and $\tau_{r\theta}$ are the radial stress, hoop stress, and shear stress, respectively, and where u and v are the radial and circumferential displacements, respectively. (The radii r_n, the pressures p_n, and the wall ratios k_n have been defined previously.) Equation (13a-c) also gives the residual stresses if the operating pressures p_n are replaced by the residual pressures q_n.

For a fatigue analysis of a cylinder of ductile material the range and mean shear stresses are needed. The greatest range in the shear stress in a cylinder occurs at the bore on a plane oriented at 45 degrees to the r and θ axes. The shear stress there is given by

$$S = \frac{\sigma_\theta - \sigma_r}{2} \qquad (15)$$

*It may be important to consider end effects depending upon the method of end closure in the design. These effects and possible axial stresses resulting from large shrink fits may not be negligible.

Formulating the range in stress from the Definition (6a), we get

$$S_r = \frac{1}{2}\left[\frac{\sigma_\theta(p_n, p_{n-1}) - \sigma_r(p_n, p_{n-1})}{2} - \frac{\sigma_\theta(q_n, q_{n-1}) - \sigma_r(q_n, q_{n-1})}{2}\right] \text{ at } r = r_{n-1}$$

hence,

$$S_r = \frac{k_n^2}{2(k_n^2-1)}\left[(p_{n-1} - p_n) - (q_{n-1} - q_n)\right], \text{ at } r = r_{n-1} \tag{16}$$

The mean shear stress at the same location on the same plane is

$$S_m = \frac{k_n^2}{2(k_n^2-1)}[(p_{n-1} - p_n) + (q_{n-1} - q_n)], \text{ at } r = r_{n-1} \tag{17}$$

Elasticity Solutions for Segmented Components

Elasticity solutions for the segments were derived. The derivations are outlined in Appendix I and only the results are given here. There are two types of segments. The ring segment is loaded by p_1 at r_1 and by p_2 at r_2. The pin segment is loaded by p_1 at r_1 but by more complex loading at r_2.

Ring Segment

The results for the ring segment are:

$$\sigma_r = (\sigma_r)_c + \frac{4M_1p_1}{\beta_1} f_1(r)$$

$$\sigma_\theta = (\sigma_\theta)_c + \frac{4M_1p_1}{\beta_1} f_2(r) \tag{18a-c}$$

$$\tau_{r\theta} = 0$$

$$\frac{u}{r} = (u)_c + \frac{M_1p_1}{E_2\beta_1} f_3(r) + \frac{G_1p_1}{r}\cos\theta$$

$$\frac{v}{r} = \frac{8M_1p_1}{E_2\beta_1}(k_2^2-1)\theta - \frac{G_1p_1}{r}\sin\theta \tag{19a, b}$$

where:

$$f_1(r) = \left(\frac{r_2}{r}\right)^2 \log k_2 + k_2^2 \log\left(\frac{r}{r_2}\right) + \log\left(\frac{r_1}{r}\right)$$

$$f_2(r) = -\left(\frac{r_2}{r}\right) \log k_2 + k_2^2 \log\left(\frac{r}{r_2}\right) + \log\left(\frac{r_1}{r}\right) + k_2^2 - 1$$

$$f_3(r) = -4(1+\nu)\left(\frac{r_2}{r}\right) \log k_2 + 4(1-\nu)\left[k_2^2 \log\left(\frac{r}{r_2}\right) - \log\left(\frac{r}{r_1}\right)\right] - 4(k_2^2 - 1) \qquad (20a\text{-}c)$$

and where $(\sigma_r)_c$, $(\sigma_\theta)_c$, and $(u)_c$ are given by Equations (13a-c) and (14a, b) for $k_n = k_2$, $p_{n-1} = p_1$, $p_n = p_2$, and $E_n = E_2$. For a ring segment p_1 and p_2 are related for equilibrium as follows:

$$p_2 = p_1/k_2 \qquad (21)$$

Formulas for the constants β_1, G_1, and M_1 (functions of k_2) are given in Appendix I. M_1 represents a bending moment that causes a bending displacement v as shown in Equation (19b).

Pin Segment

The solution for the pin segment is more complicated due to the pin loading at r_2. The resulting expressions are:

$$\sigma_r = (\sigma_r)_c + \frac{4M_2p_1}{\beta_1} f_1(r) + g_{m1}(r) \cos m\theta$$

$$\sigma_\theta = (\sigma_\theta)_c + \frac{4M_2p_1}{\beta_1} f_2(r) + g_{m2}(r) \cos m\theta \qquad (22a\text{-}c)$$

$$\tau_{r\theta} = g_{m3}(r) \sin m\theta$$

$$\frac{u}{r} = (u)_c + \frac{M_2p_1}{E_2\beta_1} f_3(r) + \frac{G_2p_1}{r} \cos\theta + \frac{1}{E_2} g_{m4}(r) \cos m\theta \qquad (23a, b)$$

$$\frac{v}{r} = \frac{8M_2p_1}{E_2\beta_1}(k_2^2 - 1)\theta - \frac{G_2p_1}{r} \sin\theta + \frac{1}{E_2} g_{m5}(r) \sin m\theta$$

where $(\sigma_r)_c$, $(\sigma_\theta)_c$, and $(u)_c$ are again given by Equations (13a-c) and (14a, b) for $k_n = k_2$, $p_{n-1} = p_1$, $p_n = p_2$, and $E_n = E_2$. For a pin segment p_2 is related to p_1 as follows:

$$p_2 = \frac{(m^2-1)(1 + 2\cos\pi/m)}{2(m^2-2)(1 + \cos\pi/m)} \left(\frac{p_1}{k_2}\right) \tag{24}$$

where m defined as

$$m = 2N_s \tag{25}$$

and where N_s is the number of segments per disc.

The functions $f_1(r)$, $f_2(r)$, and $f_3(r)$ are again given by Equations (20a-c) and β_1, G_2, M_2, g_{m1}, ..., $g_{m5}(r)$ are given in Appendix I.

The elasticity solutions now can be used to determine formulas for maximum pressure capability from the fatigue relations. This is done in the next section.

XXIX

NONDIMENSIONAL PARAMETER ANALYSIS

The maximum pressure a container will withstand is a function of the material fatigue strength, the amount of prestress, the number of components N, and the wall ratios k_n. To determine the function dependence on these variables and to determine the best designs, a nondimensional analysis is now presented. The calculations for the analysis of each design were programmed on Battelle's CDC 3400 computer.

Multiring Container

Static Shear Strength Analysis

Although a fatigue criterion of failure has been chosen it is illustrative to review an analysis based upon static shear strength for ductile materials first conducted by Manning[23]. The method outlined here differs from that of Manning and is more straightforward. In this analysis the optimum design is found such that each component of the same material has the same value of maximum shear stress S under the pressure load p. The given information is $p_o = p$, $p_N = 0$, and K. The unknowns are the interface pressures p_n, (N-1) in number; the k_n, N in number and S. The total unknowns are 2N. There are N equations resulting from Equation (15) and having the form

$$S = (p_{n-1} - p_n)\frac{k_n^2}{k_n^2-1}, \quad n = 1, 2, \ldots, N \tag{26}$$

There is the equation, $K = k_1 k_2 \ldots k_n$, that relates the k_n and K. Also N-1 equations can be formulated from the requirement that S be a minimum, i.e.,

$$\frac{\partial S}{\partial k_n} = 0, \quad n = 1, 2, \ldots, N-1 \tag{27}$$

(There are not N equations in the Form (27) because there is one equation relating the k_n.) Thus, there are also 2N equations which can be solved for the 2N unknowns. The solution gives

$$p_n = p_{n-1} - \frac{(k_n^2-1)}{k_n^2} S, \quad n = 1, 2, \ldots, N-1 \tag{28}$$

$$k_1 = k_2 = \ldots = k_N \tag{29}$$

$$S = \frac{p}{N}\frac{K^{2/N}}{(K^{2/N}-1)} \tag{30}$$

The residual pressures q_n and the required interferences for the shrink-fit assembly have yet to be found. The radial stress σ_{rn} at the radius r_n resulting from the bore pressure p is given by Equation (13a) with K replacing k_n, p replacing p_{n-1}, r_N replacing r_n, r_n replacing r, and $p_n = p_N = 0$. σ_{rn} becomes:

$$\sigma_{rn} = \frac{p}{K^2-1}\left(1 - k_{n+1}^2\, k_{n+2}^2 \ldots k_N^2\right) \tag{31}$$

The pressure p_n is the sum of q_n and $(-\sigma_{rn})$. Therefore,

$$q_n = p_n - (-\sigma_{rn}) \tag{32}$$

The interference as manufactured, Δ_n at r_n, is given by

$$\frac{\Delta_n}{r_n} = \frac{-u_n(r_n)}{r_n} + \frac{u_{n+1}(r_n)}{r_n} \tag{33}$$

where

$u_n(r_n)$ = radial deformation at r_n of cylinder N due to the residual pressure q_n at r_n and the residual pressure q_{n-1} at r_{n-1}.

and

$u_{n+1}(r_n)$ = radial deformation at r_n of cylinder n+1 due to the residual pressure q_n at r_n and the residual pressure q_{n+1} at r_{n+1}.

Substituting the Expressions (32) for q_n into Expressions (14a) for the u_n and substituting the results into Equation (33), we find that Δ_n/r_n reduces to:

$$\frac{\Delta_n}{r_n} = \frac{2p}{NE} \tag{34}$$

The result p/2S given by Equation (34) is plotted in Figure 43 for various N. The limit curve is given by

$$\left(\frac{p}{2S}\right)_{limit} = \frac{K^2-1}{K^2} \tag{35}$$

at which limit the minimum shear stress becomes equal to -S at the bore in the inner cylinder.

Figure 43 has been obtained under the assumption that $\frac{\sigma_\theta - \sigma_r}{2}$ always gives the maximum shear stress. As pointed out by Berman, the maximum shear stress in a closed-end container* is given by $\frac{\sigma_z - \sigma_r}{2}$ when $\sigma_z > \sigma_\theta$.(42) Therefore, it is important to know the limit to $\frac{p}{2S}$ for which σ_z becomes equal to σ_θ. σ_z is given by

*Containers for hydrostatic extrusion generally are not closed-end containers. The effect of axial stress is included here for completeness.

$$\sigma_z = \frac{p}{K^2-1}$$

σ_θ is given by Equation (13b). Equating σ_θ at r_o to σ_z, we get the surprising result that the limit to $\frac{p}{2S}$ in this case is also given by Equation (35). Thus, the limit curve in Figure 43 has two meanings: it is the limit at which the minimum of the shear stress $\frac{\sigma_\theta - \sigma_r}{2}$ from residual pressures becomes equal to -S at the bore, and it is also the limit at which the bore shear stresses $\frac{\sigma_\theta - \sigma_r}{2}$ and $\frac{\sigma_z - \sigma_r}{2}$ become equal under the bore pressure p.

From the limit curve in Figure 43 and from Equation (35) it is found that

$$\lim_{K \to \infty} \left(\frac{p}{2S}\right) = 1 \qquad (36)$$

Thus, the maximum possible pressure in a multiring container designed on the basis of static shear strength using ductile materials is p = 2S. For a ductile material with a tensile yield strength of 2S = 180,000 psi, this means that the maximum pressure is limited to 180,000 psi.

Fatigue Shear Strength Analysis

The optimum design of a multiring container having all rings of the same material and based on fatigue shear strength is found by an analysis similar to that conducted on the basis of static shear strength. Instead of minimizing S in Equation (27), σ given by the fatigue relation, Equation (9) is minimized, i.e.,

$$\frac{\partial \sigma}{\partial k_n} = 0, \quad n = 1, 2, \ldots, N-1 \qquad (37)$$

The stresses S_r and S_m needed in expressing σ in Equation (9) are given by Equations (16) and (17).

The results of carrying out the analysis are:

$$p_n = p_{n-1} + \frac{p(k_n^2-1)}{4(K^2-1)}\, k_{n+1}^2\, k_{n+2}^2 \cdots k_N^2 - \frac{\sigma(k_n^2-1)}{2k_n^2}, \quad n = 1, 2, \ldots, N-1 \qquad (38)$$

$$k_1 = k_2 \ldots = k_N \qquad (39)$$

$$\sigma = \frac{5}{2N}\, p\, \frac{K^{2/N}}{K^{2/N}-1} \qquad (40)$$

The q_n are again given by Equation (32) and the resulting interference required is

$$\frac{\Delta_n}{r_n} = \frac{5p}{2NE} \tag{41}$$

The result p/σ is plotted in Figure 44. The limit curve is for $S_{rn} = 0$ in the inner cylinder and is given by

$$\lim_{K \to \infty} \left(\frac{p}{\sigma}\right) = \lim_{K \to \infty} \left(\frac{2}{3}\frac{K^2-1}{K^2}\right) = \frac{2}{3} \tag{42}$$

If a ductile material has an ultimate tensile strength of 210,000 psi, then Equation (42) gives a maximum pressure of 140,000 psi based upon the shear fatigue criterion.

These results on ductile materials show that higher strength materials will have to be used in order to reach the high pressures desired. Accordingly, an analysis of a multiring container with a high-strength liner is now described.

High-Strength Liner Analysis

The hoop stress σ_θ at the bore of the liner undergoes the greatest range in stress during a cycle of pressure. Therefore, the tensile fatigue criterion is applied to the σ_θ stress. The range in the σ_θ stress at the bore of a multi-ring container depends only upon the over-all ratio K and the bore pressure p and is independent of the number of rings, i.e.,

$$(\sigma_\theta)_r = \frac{p}{2}\frac{K^2+1}{K^2-1} \tag{43}$$

[Equation (43) is found from Equation (13b) for $r = r_o$, $r_n = r_N$, and $k_n = K$.]

In the formulation of the tensile fatigue criterion the parameter α_r has been defined by Equation (10a). Thus, from Equations (10a) and (43) it is found that

$$\frac{p}{\sigma_1} = 2\alpha_r \frac{K^2-1}{K^2+1}, \quad \sigma_1 \leqq \sigma_u \tag{44}$$

where σ_u is the ultimate tensile stress of the liner. The ratio p/σ_1 is plotted in Figure 45 for various K and α_r.

The fatigue data at room temperature of high-strength steels ($\sigma_u \leqq 300,000$ psi) listed previously in Tables XLII, XLIII, and XLIV are generally for $\alpha_r \geqq 0.5$ for lifetimes of 10^4 and greater. Hence, it is concluded that the maximum repeated pressure possible in a multiring container with a liner of $\sigma_u = 300,000$ psi is approximately 300,000 psi if appreciable fatigue life is required. This conclusion presupposes that the outer components can also be designed to withstand the required interface pressure and that sufficient precompression can be provided in the liner so that $\alpha_r = 0.5$ can be expected to give up to 10^4 cycles life. This is investigated next.

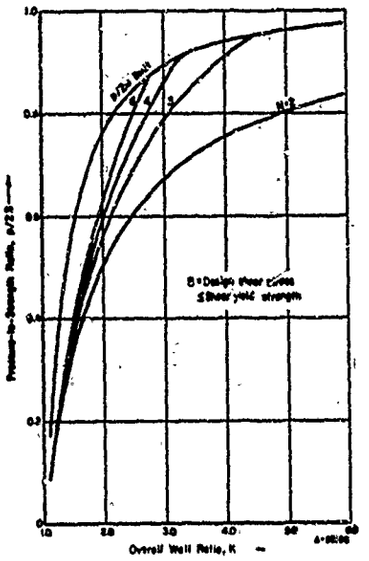

FIGURE 43. MAXIMUM PRESSURE-TO-STRENGTH RATIO, p/2S, IN MULTIRING CONTAINER DESIGNED ON BASIS OF STATIC SHEAR STRENGTH

Each ring is assumed to be of the same ductile material.

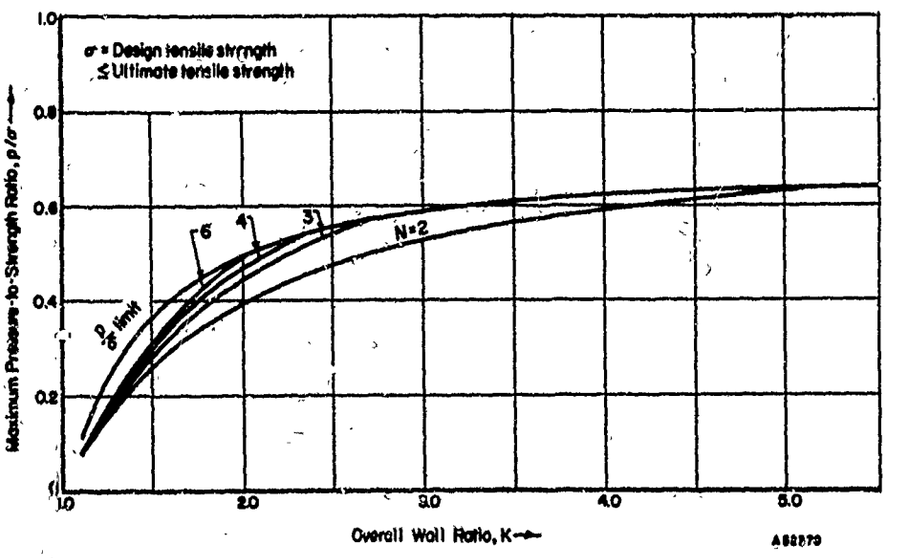

FIGURE 44. MAXIMUM PRESSURE-TO-STRENGTH RATIO, p/σ, IN MULTIRING CONTAINER DESIGNED ON BASIS OF FATIGUE SHEAR STRENGTH

Each ring is assumed to be of the same ductile material.

The stress range parameter α_r depends on the mean stress parameter α_m. The mean stress depends not only on the bore pressure p but on the interface pressures p_1 and q_1 between the liner and the second cylinder. The magnitudes of p_1 and q_1 that are possible depend upon the geometry and strength of the outer cylinders.

The outer rings are assumed to be all made of the same ductile material. Conducting a fatigue-shear-strength analysis of a multiring container having a pressure fluctuating between q_1 and p_1, we find from a method similar to that used in arriving at Equation (39) (using Equation (37) for n = 2, 3, ..., N-1), that in this case also the optimum design has

$$k_2 = k_3 = \ldots = k_n \tag{45}$$

Calculating the mean stress σ_m at the bore of the liner, equating $\alpha_m \sigma_1$ to σ_m from Equation (10b), substituting for q_1 from Equation (32), eliminating σ_1 by use of Equation (44), and solving for p_1, one finds

$$p_1 = \frac{p}{K^2 - 1}\left[\frac{K^2 - k_1^2}{k_1^2} + \frac{(K^2 + 1)}{4}\,\frac{(k_1^2 - 1)}{k_1^2}\,\frac{(\alpha_r - \alpha_m)}{\alpha_r}\right] \tag{46}$$

The other interface pressures p_n, $n \geq 2$ are again given by Equation (38). Eliminating the pressures p_1 and p_n, $n \geq 2$ from Equations (46) and (38), and solving for the pressure-to-strength ratio p/σ, one gets

$$\frac{p}{\sigma} = \frac{2(K^2 - 1)\,(k_n^2 - 1)\,(N-1)\,k_1^2\,\alpha_r}{k_n^2\,[5(K^2 - k_1^2)\alpha_r + (\alpha_r - \alpha_m)\,(K^2 + 1)\,(k_1^2 - 1)]} \tag{47}$$

The k_n, $n \geq 2$ in Equation (47) are equal as shown by Equation (45). Whereas, p/σ_1 depended only upon α_r and K (Equation (44)), p/σ depends on N, k_n, and α_m in addition.

The ratio p/σ can also be limited by the requirement on Relations (7) and (9) that the mean shear stress S_m in Cylinder 2 at r_1 obeys the relation $S_m \geq 0$. $S_m \geq 0$ gives

$$\left(\frac{p}{\sigma}\right)_{\text{limit}} = \frac{2}{3}\,\frac{(K^2 - 1)}{K^2}\,k_1^2 \tag{48}$$

As is evident from the limit curves plotted in Figure 46, the pressure limit for the outer rings can be increased by increasing k_1. This means that the liner has a great effect on p. The strength of the liner, σ_1, influences p in Equation (44). The size of the liner, k_1, limits p in Equation (48).

Whether or not p/σ can be allowed as high as the limit, however, depends on the other factors N, α_r, K, etc., as shown by Equation (47). This dependence is rather complicated. Example curves of p/σ are plotted in Figures 47 and 48 for $\alpha_r = 0.5$ and $\alpha_m = -0.5$. As shown by these curves p/σ increases with N and also increases with k_1 for N = 5, $K \geq 6.5$.

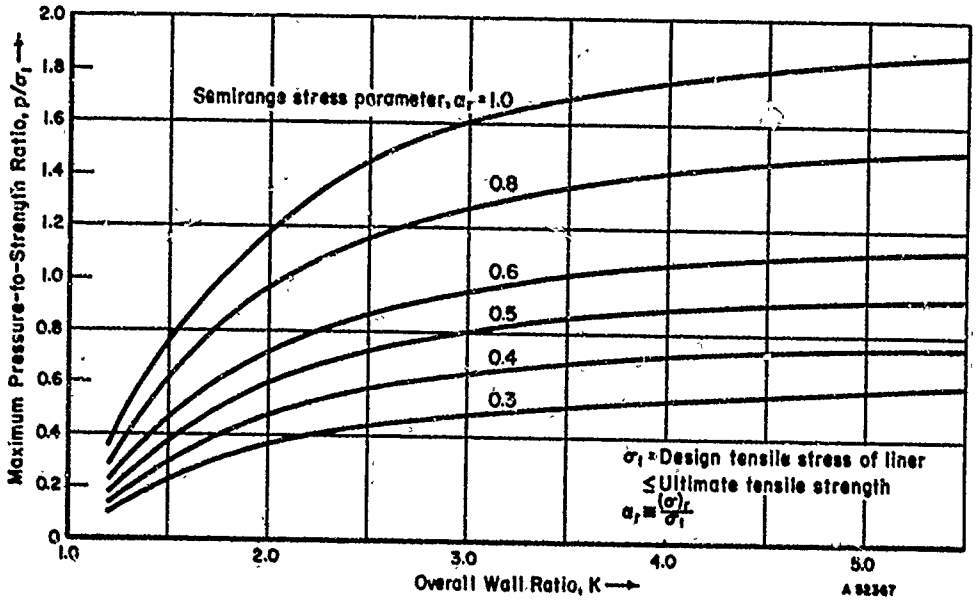

FIGURE 45. MAXIMUM PRESSURE-TO-STRENGTH RATIO, p/σ_1, IN MULTIRING CONTAINER WITH HIGH-STRENGTH LINER BASED ON THE FATIGUE TENSILE STRENGTH OF LINER

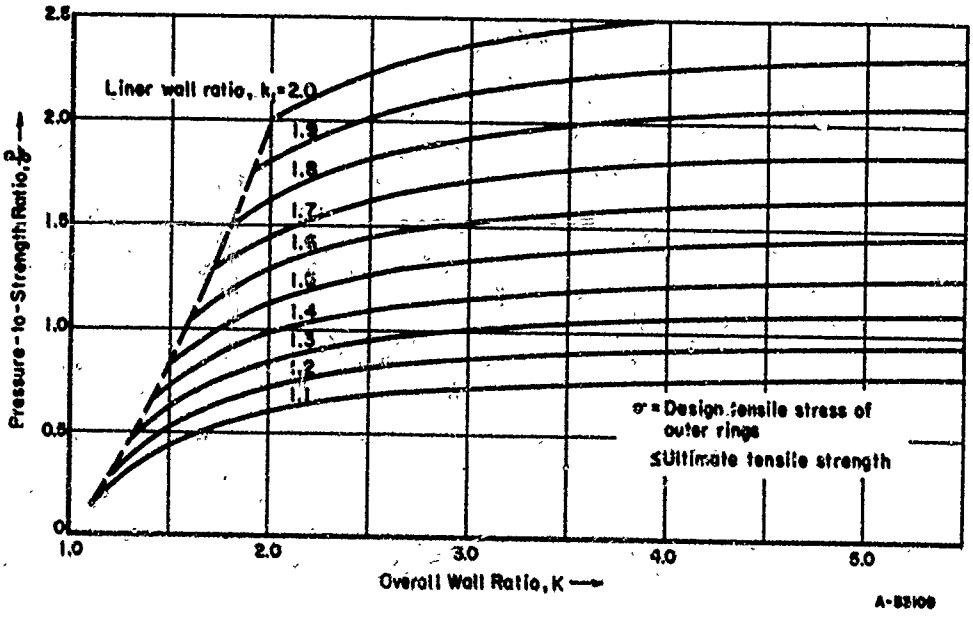

FIGURE 46. LIMIT TO MAXIMUM PRESSURE-TO-STRENGTH RATIO, p/σ, IN MULTIRING CONTAINER WITH HIGH-STRENGTH LINER BASED ON SHEAR FATIGUE STRENGTH OF THE OUTER RINGS

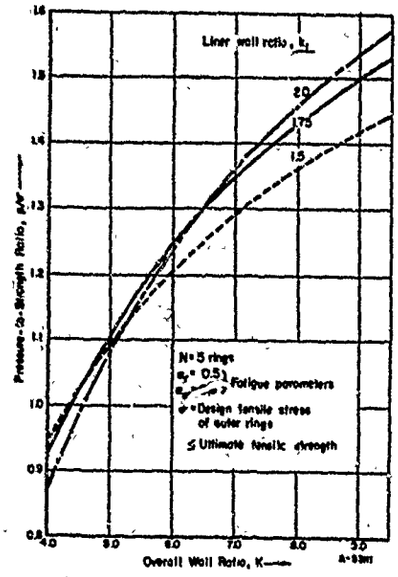

FIGURE 47. INFLUENCE OF NUMBER OF RINGS ON MAXIMUM PRESSURE-TO-STRENGTH RATIO, p/σ, IN MULTIRING CONTAINER WITH HIGH-STRENGTH LINER

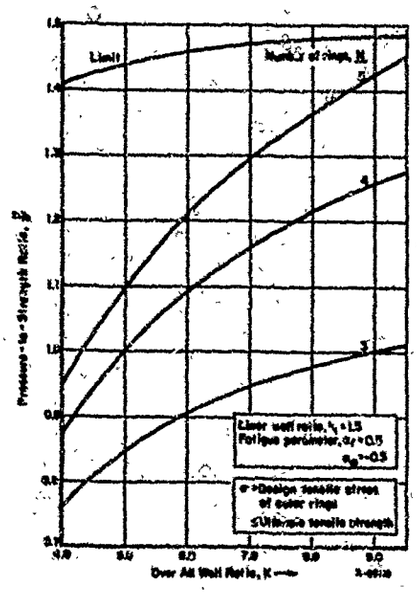

FIGURE 48. INFLUENCE OF LINER SIZE ON MAXIMUM PRESSURE-TO-STRENGTH RATIO, p/σ, IN MULTIRING CONTAINER WITH HIGH-STRENGTH LINER

Suppose p = 300,000 psi as determined from Equation (44) for $\alpha_r = 0.5$ and σ_1 = 300,000 psi. Then from Figure 48, K must be 9.0 for $k_1 = 1.75$ and N = 5 if σ = 210,000. Thus, the multiring cylinder must be quite large in size to support maximum repeated pressures.

The interferences Δ_n and residual pressures q_n have yet to be determined for the multiring container. Since the liner and the outer rings are assumed to be made from two different materials, thermal expansions must be included in the interference calculations. It is assumed that no thermal gradients exist; all components reach the same temperatures uniformly. Therefore, the interference required between the liner and the second cylinder is expressed as

$$\frac{\Delta_1}{r_1} = -\frac{u_1(r_1)}{r_1} + \frac{u_2(r_1)}{r_1} - \alpha_1\Delta T + \alpha_2\Delta T \qquad (49)$$

where

Δ_1 = manufactured interference

$u_1(r_1)$ = radial deformation of liner at r_1 due to residual pressure q_1 at r_1

$u_2(r_1)$ = radial deformation of Cylinder 2 at r_1 due to residual pressures q_1 at r_1 and q_2 at r_2

α = coefficient of thermal expansion at temperature

ΔT = temperature change from room temperature.

The interferences Δ_n required between the outer cylinders is again given by Equation (33) for $n \geq 2$. The residual pressures q_n needed in calculating the Δ_n are found from Equation (32) for p_n given by Equations (46) and (38). In the calculation of the u_n from Equation (14a), the values of the moduli of elasticity, E_n at temperature should be used.

The container designed for use at temperature will have residual pressures q_n^* at room temperature different from the q_n necessary at temperature. The q_n^* are found as follows: the u_n^* are first expressed in terms of q_n^* from Equation (14a) using the values of E_n at room temperature, the Δ_n are expressed in terms of the u_n^* from Equations (49) and (33) for $\Delta T = 0$. This procedure gives the following system of equations in the q_n^*:

$$A_{11}q_1^* + A_{12}q_2^* = E_2\frac{\Delta_1}{r_1}$$

$$A_{nn-1}q_{n-1}^* + A_{nn}q_n^* + A_{nn+1}q_{n+1}^* = E_n\frac{\Delta_n}{r_n},\ n = 2,\ 3,\ \ldots,\ N-1 \qquad (50a, b, \ldots)$$

where

$$A_{11} = \frac{k_2^2 + 1}{k_2^2 - 1} + \nu + \frac{E_2}{E_1}\left(\frac{k_1^2 + 1}{k_1^2 - 1} - \nu\right),\quad A_{nn-1} = \frac{-2}{k_n^2 - 1},\quad A_{12} = \frac{-2k_2^2}{k_2^2 - 1},$$

$$A_{nn} = \frac{k_n^2 + 1}{k_n^2 - 1} + \frac{k_{n+1}^2 + 1}{k_{n+1}^2 - 1} = 2\frac{k_n^2 + 1}{k_n^2 - 1} \qquad A_{nn+1} = \frac{-2k_{n+1}^2}{k_{n+1}^2 - 1} = -2\frac{k_n^2}{k_n^2 - 1}$$

and where Δ_1 and the Δ_n, $n \geq 2$ have been previously calculated for $\Delta T \neq 0$. There are N-1 linear equations (50a,b,...) in N-1 unknowns q_n, $n = 1, 2, \ldots, N-1$ ($Q_N = 0$). These are easily solved by matrix solution on the computer.

Having calculated the residual pressures q_n^* (room temperature the residual stresses can be calculated from Equations (13a-c). These residual stresses can then be checked in order to ensure that they are within tolerated bounds. Examples of such calculations are described later when specific designs are considered. Next, the ring-segment container is considered.

Ring-Segment Container

A ring-segment container has been shown in Figure 39b. For this design, the equilibrium requirement, Equation (21), relates p_1 and p_2. Under shrink-fit it is assumed that the segments just barely contact each other, i.e., the segments carry no hoop stress. (If the segments were in strong contact with each other, they would act like a complete ring, i.e., they would carry compressive hoop stress, and the distinction between a ring-segment container and a multiring container would be lost.) Thus, the same equilibrium requirement applies to the residual pressures q_1 and q_2. This requirement is

$$p = p_1/k_2, \qquad q = q_1/k_2 \tag{51a,b}$$

In order to determine the pressures p_1 and q_1 the following radial deformation equation is formulated:

$$u_2(r_2) - u_2(r_1) + \Delta_{12} + \alpha_2 \Delta T (r_2 - r_1) = u_3(r_2) - u_1(r_1) + \alpha_3 \Delta T r_2 - \alpha_1 \Delta T r_1 \tag{52}$$

where

Δ_{12} = the manufactured interference defined as the amount $(r_2 - r_1)$ of the segments exceeds $(r_2 - r_1)$ of the cylinders

$u_n(r_m)$ = the radial deformation of component n at r_m due to pressure p_n or q_n at r_n and p_{n-1} or q_{n-1} at r_{n-1}

α_n = thermal coefficient of expansion of component n

ΔT = temperature change from room temperature.

If the elasticity solutions, Equations (14a) and (19a)$_r$ for the u_n, and Equation (51a) for p_2 are substituted into Equation (52) and the resulting expression solved for p_1, then there results

$$p_1 = \frac{1}{g}\left\{ \frac{2p}{k_1^2-1} + 2\frac{E_1}{E}\frac{k_2 k_3^2 p_3}{(k_3^2-1)} + \frac{E_1\Delta_{12}}{r_1} - \Delta T E_1\left[k_2(\alpha_3-\alpha_2) + (\alpha_2-\alpha_1)\right]\right\} \quad (53)$$

where

$$g = \frac{k_1^2+1}{k_1^2-1} + \frac{E_1}{E_2}\left[\frac{2(k_2-1)}{k_2+1} + \frac{M_1}{\beta_1}\left(\left(f_3(r_1) - k_2 f_3(r_2)\right)\right)\right]$$
$$+ \frac{E_1}{E_3}\left[\frac{k_3^2+1}{k_3^2-1} + \nu\right] - \nu \quad (54)$$

The E_n are the moduli of elasticity at temperature. The parameters M_1 and β_1 and the function $f_3(r)$ have been defined previously in reference to Equations (19a, b). The procedure for finding q_1 is the same as that for finding p_1 except that $p = 0$ and q_3 replaces p_3, i.e.,

$$q_1 = \frac{1}{g}\left\{ 2\frac{E_1}{E}\frac{k_2 k_3^2 q_3}{(k_3^2-1)} + \frac{E_1\Delta_{12}}{r_1} - \Delta T E_1\left[k_2(\alpha_3-\alpha_2) + (\alpha_2-\alpha_1)\right]\right\} \quad (55)$$

A fatigue analysis of the high-strength liner is now conducted. The range in the hoop stress at the bore is:

$$(\sigma_\theta)_r = \frac{(\sigma_\theta)_{max} - (\sigma_\theta)_{min}}{2} = \frac{p}{2}\frac{(k_1^2+1)}{(k_1^2-1)} - \frac{(p_1-q_1)k_1^2}{k_1^2-1} \quad (56)$$

where Equation (13a) has been used. (p_1-q_1) is given by Equation (55), but an expression for (q_3-p_3) is needed before Equation (56) can be used to solve for p. The expression for (p_3-q_3) is obtained from Equation (32) with (p_2-q_2) replacing p and with $k_3^2 k_4^2 \ldots k_N^2$ replacing K^2 in Equation (31). There results

$$q_n = p_n - \frac{(p_2-q_2)\,(k_{n+1}^2 k_{n+2}^2 \ldots k_N^2 - 1)}{(k_3^2\, k_4^2 \ldots k_N^2 - 1)}, \quad n \geq 3 \quad (57)$$

Substituting for (q_3-p_3) from Equation (57) into (55), then substituting for (p_1-q_1) from Equation (55) into (56), equating $(\sigma_\theta)_r$ and $\alpha_r\sigma_1$ from Definition (10a), and solving for p/σ_1, one obtains

$$\frac{p}{\sigma_1} = \frac{2\alpha_r(k_1^2-1)^2(g-h)}{\left[(g-h)\,(k_1^4+1) - 4k_1^2\right]} \quad (58)$$

where

$$h = \frac{2E_1 k_n^2 (k_n^{2(N-3)}-1)}{E_3 (k_n^{2(N-2)}-1)} \tag{59}$$

($k_3 = k_4 = \ldots = k_n$ for the outer cylinders as shown by Equation (45). Therefore, $k_3^2 k_4^2 \ldots k_N^2 = k_n^{2(N-2)}$ in the expression for h.)

It is easily shown that (g-h) is independent of N, the number of components. Therefore, p/σ_1 given by Equation (58) is independent of N. However, p/σ_1 is dependent upon k_1 whereas for the multiring container it was not as previously shown by Equation (44). This dependence is also shown in Figure 49. From this figure it is evident that the ring-segment container cannot withstand as great a pressure as the multiring container if the overall size is the same. This result is believed due to the fact that the segments do not offer any support to the liner – they are "floating" members between the liner and the third component, another ring. The effect is more pronounced as the segment size is increased. This is shown in Figure 50 where it is seen that the pressure decreases with increasing segment size.

The detrimental effect of insufficient segment support to the liner can be reduced by using a high modulus material, tungsten carbide, for the segment material. This is shown in Figure 51. However, the improvement is not sufficient enough to increase the pressure capability of the ring-segment container to that of the multiring container. This conclusion is based on results for various wall ratios.

The fatigue analysis of the outer ductile cylinders is conducted in the same manner as it was done for the multiring container, except now the component numbers are n = 3, 4, ..., N. The result is

$$\frac{p}{\sigma} = \frac{\alpha_r (k_n^2-1)(N-2)}{k_n^2\left[\frac{(\alpha_r-\alpha_m)}{2}\frac{(k_1^2+1)}{k_2 k_1^2} + \frac{(3\alpha_r+2\alpha_m)}{k_2(k_1^2-1)(g-h)}\right]} \tag{60}$$

This result is plotted in Figure 52, which shows the effect of increasing k_1 and comparison with the multiring container. Although p/σ can be increased by use of segments, the ring-segment container has the limitation of lower p/σ_1 as shown before in Figures 49 and 50.

The effect on p/σ of increasing the segment modulus was also investigated. However, the effects were found to be insignificant.

Ring-Fluid-Segment Container

The ring-fluid-segment container is illustrated in Figure 39c. This container is a combination of a ring-segment container for the inner part and a multiring container for the outer part. All of the equations derived for the multiring container can be used

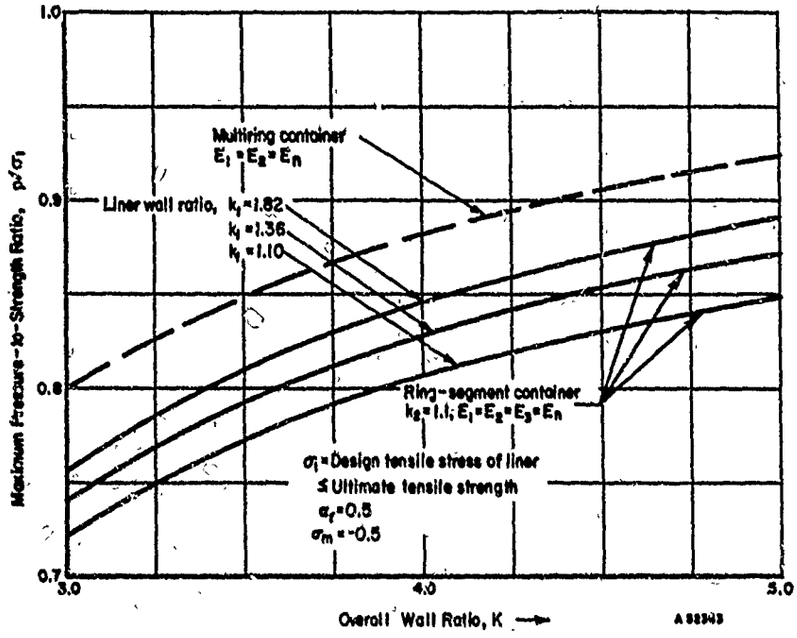

FIGURE 49. COMPARISON OF MULTIRING CONTAINER WITH RING-SEGMENT CONTAINER FOR VARIOUS k_1

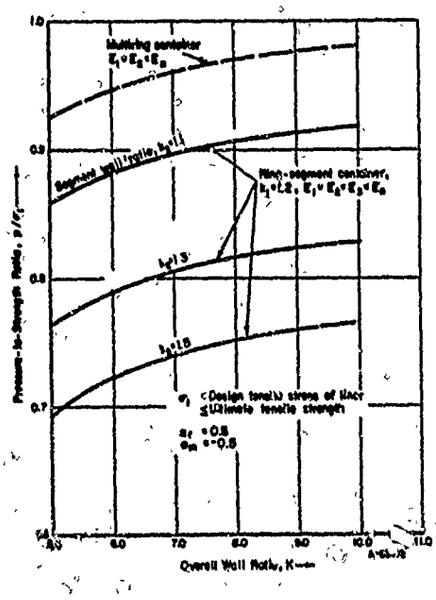

FIGURE 50. COMPARISON OF MULTIRING CONTAINER WITH RING-SEGMENT CONTAINER FOR VARIOUS SEGMENT WALL RATIOS

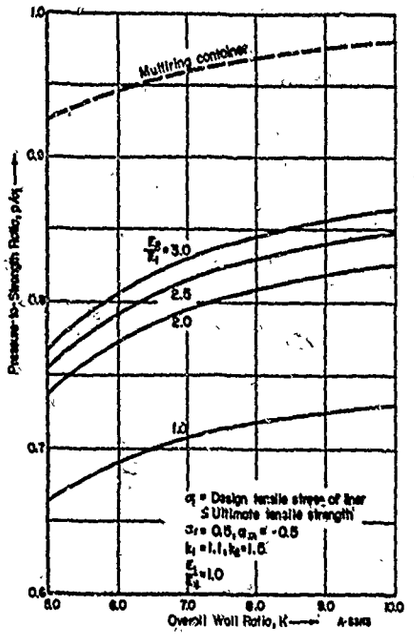

FIGURE 51. EFFECT OF ELASTIC MODULUS OF SEGMENTS ON PRESSURE-TO-STRENGTH RATIO, p/σ_1, FOR THE RING-SEGMENT CONTAINER

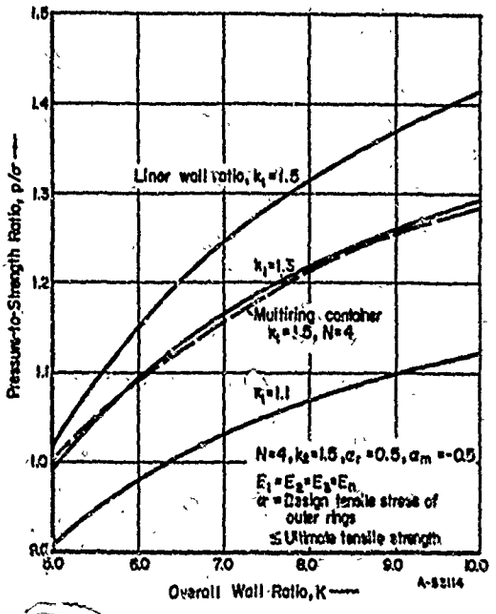

FIGURE 52. EFFECT OF LINER SIZE ON PRESSURE-TO-STRENGTH RATIO, p/σ, FOR RING-SEGMENT CONTAINER

for the outer part. For the inner part, Equations (51a, b), (52), (53), (54), and (55) apply. The latter equation applies with $q_3 = 0$. Equation (56) is valid and can be used to find p/σ_1 for the liner. [Equation (56) is not needed since p_3 is given.] Solving for p/σ_1, one finds

$$\frac{p}{\sigma_1} = \frac{\alpha_r (k_1^2-1)}{\left[\frac{k_1^2+1}{2} - \frac{2}{g}\frac{k_1^2}{(k_1^2-1)} - 2\frac{E_1}{E_3}\frac{p_3}{p}\frac{k_1^2 k_2 k_3^2}{g(k_3^2-1)}\right]} \tag{61}$$

This equation shows that an increase in p_3/p gives an increase in p/σ_1.

Let σ_3 be the ultimate tensile strength of component 3, the outer cylinder of the inner part of the ring-fluid-segment container. If fatigue relation, Equation (9) is used for this cylinder, then there results

$$\sigma_3 = \frac{k_3^2}{k_3^2-1}\left[\frac{5}{2}(p_2 - p_3) - \frac{1}{2}q_2\right] \tag{62}$$

The pressures p_2 and q_2 are related to p_1 and q_1 via Equations (51a, b). p_1 and q_1 are related by Equation (55) with $q_3 \equiv 0$. One other equation involving p_1 and q_1 is needed which is found from the Definition (10b) for the parameter α_m, i.e.,

$$\alpha_m \sigma_1 = \sigma_m = \frac{(\sigma_\theta)_{max} + (\sigma_\theta)_{min}}{2} = \frac{p}{2}\frac{k_1^2+1}{k_1^2-1} - \frac{(p_1+q_1)}{k_1^2-1}k_1^2$$

at r_o.

Solving for p_1 and q_1, finding p_2 and q_2, substituting into Equation (62), and solving for p/σ_3, one obtains

$$\frac{p}{\sigma_3} = \frac{(k_3^2-1)}{k_3^2\left\{\frac{2}{k_2}\frac{q_1}{p} + \frac{5}{g(k_1^2-1)k_2} + \frac{5}{2}\frac{p_3}{p}\left[\frac{2E_1}{gE_2}\frac{k_3^2}{(k_3^2-1)} - 1\right]\right\}} \tag{63}$$

where

$$\frac{q_1}{p} = \frac{(\alpha_r - \alpha_m)}{2}\frac{(k_1^2-1)}{k_1^2}\frac{\sigma_1}{p}$$

The pressure-to-strength ratios p/σ_1 and p/σ_3 are plotted in Figures 53 and 54 as a function of segment size k_2 and wall ratio K' for $k_1 = 1.1$, $p_3/p = 0.2$, $\alpha_r = 0.5$, and $\alpha_m = -0.5$. The pressure-to-strength ratios increase with K' or equivalently with k_3, since $K' = k_1 k_2 k_3$. The behavior shown for $k_1 = 1.1$ is the same as that found previously for the ring-segment container; i.e., p/σ_3 increases with increasing k_2, but p/σ_1 decreases. However, if k_1 is increased to 1.5 from 1.1, then p/σ_1 also increases with

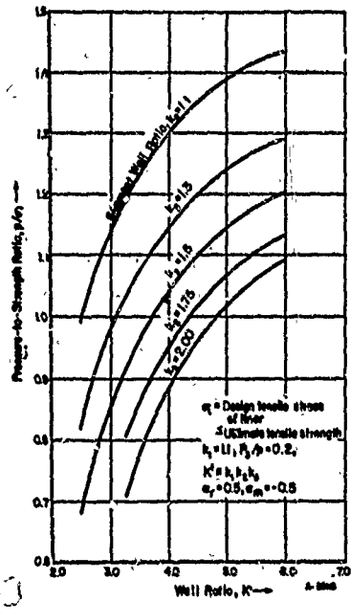

FIGURE 53. EFFECT OF SEGMENT SIZE ON THE PRESSURE-TO-STRENGTH RATIO, p/σ_1, FOR THE RING-FLUID-SEGMENT CONTAINER

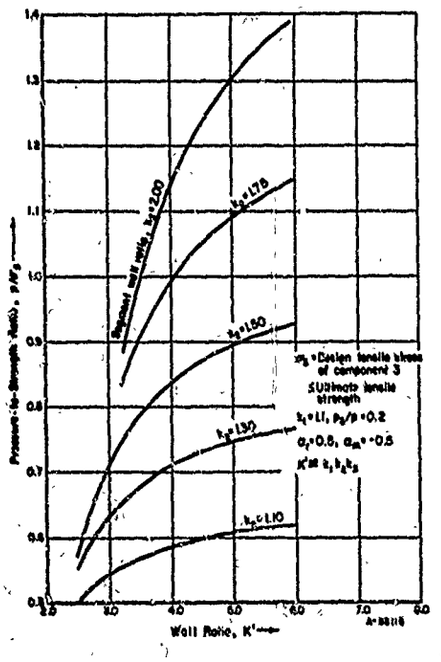

FIGURE 54. EFFECT OF SEGMENT SIZE ON THE PRESSURE-TO-STRENGTH RATIO, p/σ_3, FOR THE RING-FLUID-SEGMENT CONTAINER

k_2 for large K' as shown in Figure 55. p/σ_3 continues to increase with k_2 as shown in Figure 56. Thus, both p/σ_1 and p/σ_3 increase with large K' for $k_2 = 2.0$ and $k_1 = 1.5$. For values of k_2 between 2.0 and 4.0, however, computer calculations show that p/σ_1 and p/σ_3 first continue to increase and then decrease.

The pressure-to-strength ratios can also be increased by increasing the support pressure p_3. This is shown in Figure 57. With the high ratios shown, it is theoretically possible to have bore pressures as high as 1,000,000 psi in ring-fluid-segment container. However, practicable limitations regarding excessive interference and size requirements, which are discussed later, considerably reduce the pressure capability of this design.

The interferences and residual pressures for outer and inner parts of the ring-fluid-segment container can be calculated using the analysis derived previously for the multiring container and the ring-segment container, respectively.

Pin-Segment Container

The analysis of the pin-segment container, shown in Figure 39d, also assumes a high-strength liner. It is also assumed that any manufactured interference is taken up during assembly by slack between pins and holes. Therefore, the residual pressure, q_1, between liner and segments is zero at room temperature and nonzero at temperature only if the coefficient of thermal expansion of the liner, α_1, is greater than that of the segments, α_2. In this analysis, it is assumed that $\alpha_1 \geq \alpha_2$.

The following radial deformation equation must be satisfied:

$$u_1(r_1) + \alpha_1 \Delta T r_1 = u_2(r_1) + \alpha_2 \Delta T r_2 \qquad (64)$$

where

$u_1(r_1)$ = the radial deformation of the liner at r_1 due to p at r_o and p_1 at r_1 when $p \neq 0$, and due to q_1 at r_1 when $p = 0$

$u_2(r_1)$ = the radial deformation of the segments at r_1 due to p_1 or q_1 at r_1 and the pin loading at r_2.

Substituting into Equation (64), Equations (14a) and (23a) for u_1 and u_2, and solving for p_1, one gets

$$p_1 = \frac{1}{g_2}\left[\frac{2p}{k_1^2 - 1} + E_1 \Delta T (\alpha_1 - k_2 \alpha_2)\right] \qquad (65)$$

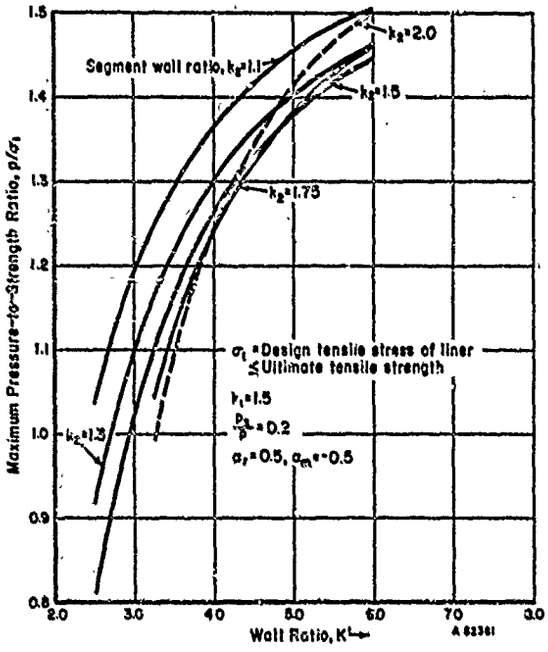

FIGURE 55. EFFECT OF SEGMENT SIZE ON THE PRESSURE-TO-STRENGTH RATIO, p/σ_1, FOR THE RING-FLUID-SEGMENT CONTAINER

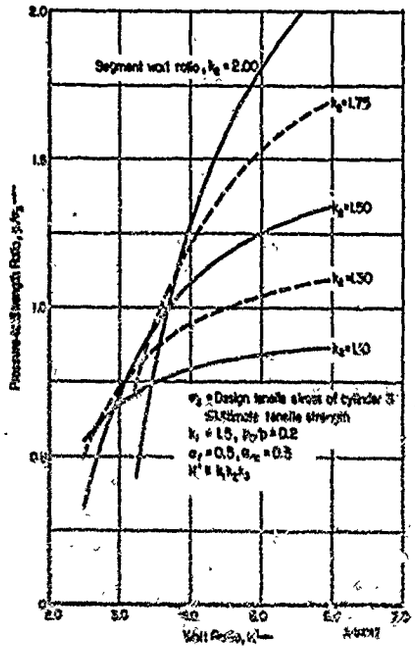

FIGURE 56. EFFECT OF SEGMENT SIZE ON THE PRESSURE-TO-STRENGTH RATIO, p/σ_3, FOR THE RING-FLUID-SEGMENT CONTAINER

where

$$g_2 = \frac{E_1}{E_2}\left[\frac{k_2^2+1}{k_2^2-1} + \nu + \frac{M_2 f_3(r_1)}{\beta_1} + E_2 \frac{G_2}{r_i} + g_{m4}(r_1)\right] + \frac{k_1^2 + 1}{k_1^2 - 1} - \nu \quad . \tag{66}$$

Similarly, q_1 is found if p is taken as zero; i.e.,

$$q_1 = \frac{E_1 \Delta T (\alpha_1 - k_2\alpha_2)}{g_2} \quad . \tag{67}$$

Formulating the range in hoop stress $(\sigma_\theta)_r$ at the bore (Equation (56) and using the definition $\alpha_r \sigma_1 = (\sigma_\theta)_r$, we get the following expression for p/σ_1:

$$\frac{p}{\sigma_1} = \frac{2\alpha_r (k_1^2 - 1)^2 g_2}{\left[g_2 (k_1^4 - 1) - 4k_1^2\right]} \tag{68}$$

[Equation (68) is identical in form to Equation (58).]

The pressure-to-strength ratio p/σ_1 is plotted in Figure 58. Comparing this figure with Figure 45 for the multiring container with $\alpha_r = 0.5$, it is evident that both containers have the same limit $p/\sigma_1 \to 1$ for large wall ratios. However, $\alpha_r = 0.5$ is possible only if $\alpha_m \leq 0$ as shown in Figure 42. Actually, $\alpha_m = +0.5$ is likely in the pin-segment container if $\alpha_r = 0.5$ because any interference is expected to be lost in taking up slack between pins and holes. In this case, then, $\alpha_r = 0.5$ would mean only one cycle life whereas $\alpha_r = 0.5$ means 10^4 to 10^5 cycles life in the multiring container. If this assembly problem could be eliminated by careful machining and selective fitting of pins, then theoretically with sufficient compressive prestress, the p/σ_1 ratio of the pin-segment container could be made to approach that of the multiring container.

Since no prestress has been assumed for the pin-segment container, $\alpha_r = \alpha_m = 0.35$ for 10^4 to 10^5 cycles as shown by Figure 42. For $\alpha_r = 0.35$, it is found that p/σ_1 is limited to 0.7 at best. Therefore, the maximum pressure in the pin-segment container is $p = 0.7\ (300,000) = 210,000$ psi for 10^4 to 10^5 cycles life.

The stresses in the segments have not yet been considered. High stresses develop around the pin holes. These too limit the pressure in the pin-segment container. Analysis of the stresses in the segments is described in Appendix I. For the purpose of estimating stresses in the segments the interface pressure p_1 is needed. Therefore, plots of p_1/p are provided in Figure 59. It is evident that the interface pressure p_1 is appreciably less than the bore pressure p_1 especially for large k_1 and small k_2.

The pins are analyzed in Appendix II. In order to carry the pressure loading p_1, it is found that the pin-to-segment-diameter ratio must be

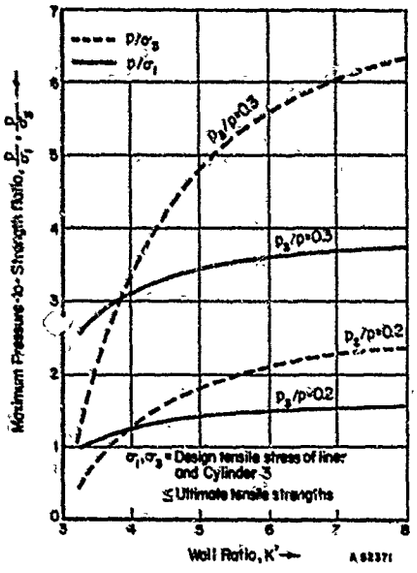

FIGURE 57. EFFECT OF SUPPORT PRESSURE, p_3, ON BORE PRESSURE, p, CAPABILITY FOR THE RING-FLUID-SEGMENT CONTAINER

$\alpha_r = 0.5$, $\alpha_m = -0.5$
$k_1 = 1.5$, $k_2 = 2.0$.

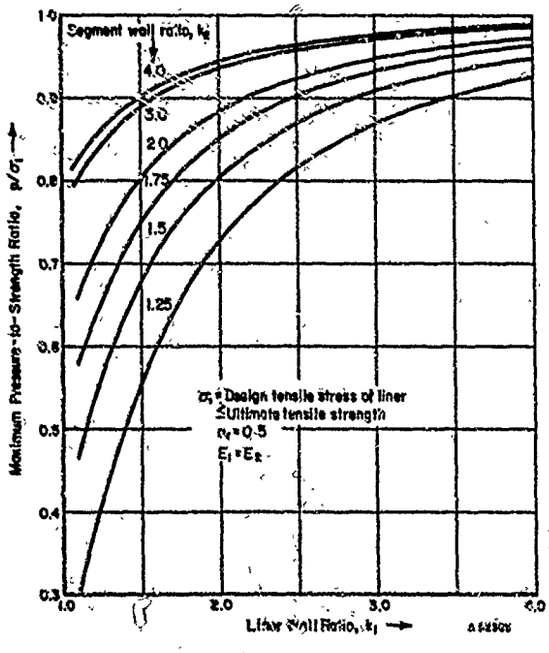

FIGURE 58. MAXIMUM PRESSURE-TO-STRENGTH RATIO, p/σ_1, FOR THE PIN-SEGMENT CONTAINER

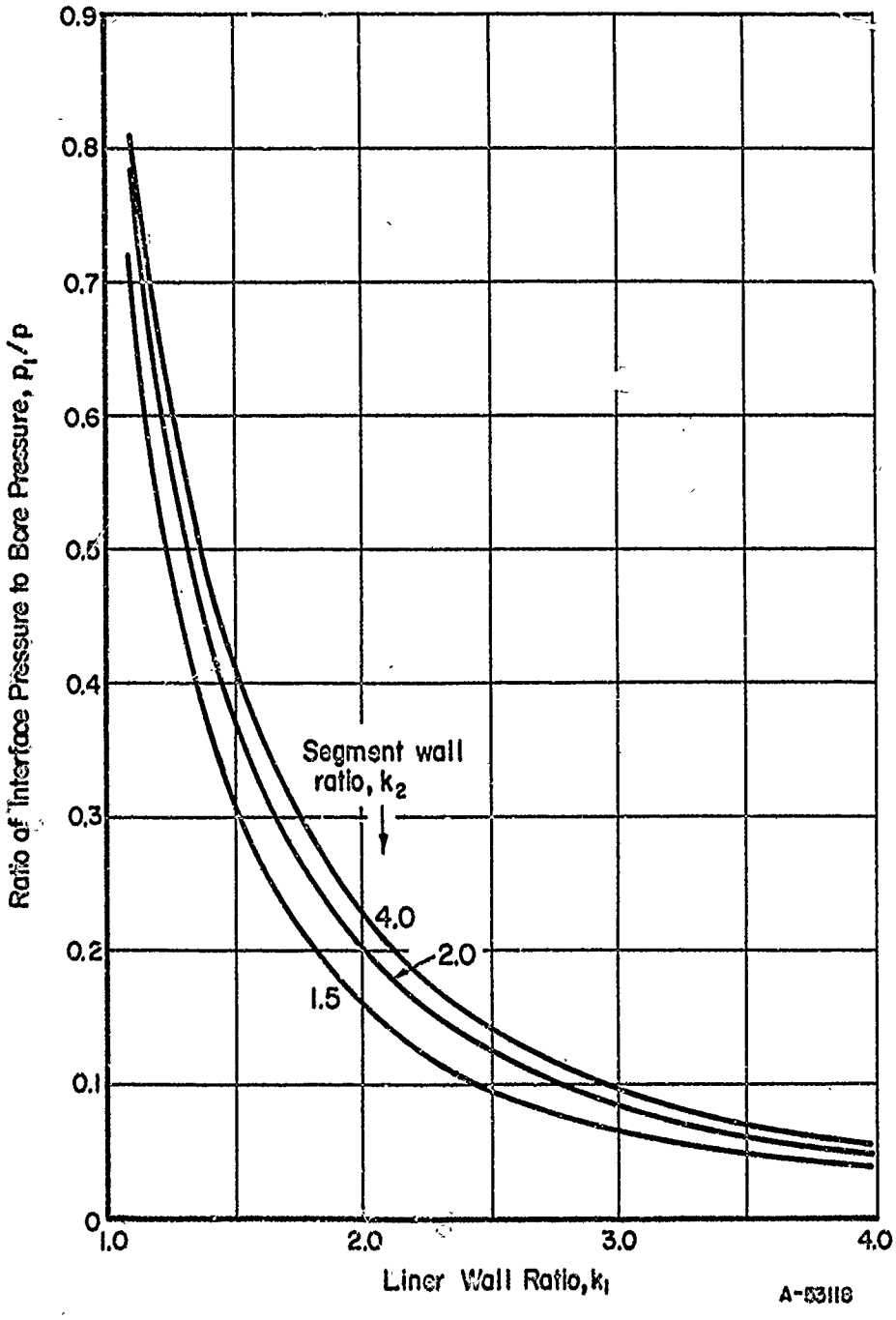

FIGURE 59. RATIO OF INTERFACE PRESSURE BETWEEN SEGMENTS AND LINER TO BORE PRESSURE FOR THE PIN-SEGMENT CONTAINER

$$\frac{d}{2r_1} = \frac{8}{3}\frac{t}{d}\frac{p_1}{\tau} \tag{69}$$

where

d = pin diameter, t = segment thickness,

$2r_1$ = inside segment diameter, τ = maximum shear stress in pin.

Strip-Wound Container

An analysis was not conducted for the strip-wound container, because it is possible to estimate its relative strength based upon the results of the analysis of the multiring container. The strip-wound (wire-wrapped) cylinder uses basically the same principle as the multiring container. It has a cylindrical inner cylinder, the liner, under prestress, but the prestress in the liner is provided by wrapping strips or wire under tension onto the liner.

To estimate the pressure-to-strength ratio of the strip-wound vessel it is assumed that it behaves overall as a thick cylinder under internal pressure after the strip has been wound on. Referring to Equation (44), we see that the pressure-to-strength ratio p/σ_1 depends only on the overall wall ratio K and α_r the stress-range parameter for the liner material. If K for the strip-wound vessel is taken as the ratio of the outside diameter of the last strip layer to the inner bore diameter, then Equation (44) can be used to estimate its pressure capability. Therefore, it may be concluded that the strip-wound container has a maximum pressure equal that of the multiring container. However, unknown local stress concentrations and contact conditions between strips may be detrimental in the strip-wound design. Because of these possible disadvantages and no better pressure capability than the multiring container, detailed analysis of the strip-wound vessel is not warranted. However, the strip-wound design does offer advantages in producibility of large-diameter containers as pointed out later in the "Design Requirements" section of this report.

Controlled Fluid-Fill, Multiring Container

A controlled fluid-fill container, shown in Figure 60, has been proposed by Berman[42]. All the rings are assumed to be made of the same ductile material and a shear-strength criterion applies. Like the ring-segment-fluid container, this container also uses the fluid-pressure support principle. The advantage of this design is that under static applications the residual-stress limitation (the limit curve in Figure 43) can be overcome by controlling the pressures p_n; i.e., the pressures, p_n, can be reduced to zero as the bore pressure, p, is reduced to zero. There are no shrink fits, so there are no residual stresses. Berman's analysis was based upon static strength. A similar analysis is now conducted based on fatigue strength.

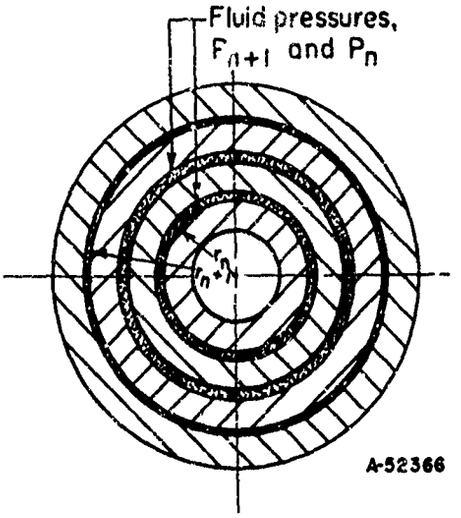

FIGURE 60. CONTROLLED FLUID-FILL CYLINDRICAL-LAYERED CONTAINER [REFERENCE (42)]

In order that each ring may have the same shear stress under static pressure, Berman finds that the same relation, Equation (30) [first found by Manning[5]], applies for the controlled fluid-fill container that also applies for the multiring container designed for static shear strength. If this result is used in a shear fatigue analysis (assuming ductile materials), then Equation (30) can be interpreted as the maximum shear stress developed during a cycle of pressure, i.e.,

$$(S)_{max} = \frac{p}{N} \frac{K^{2/N}}{(K^{2/N}-1)} \tag{70}$$

If the pressures p_n are reduced to zero, then the minimum shear stress during a cycle of pressure is zero. Therefore, the semirange and mean shear stresses are equal,

$$S_m = S_r = \frac{pK^{2/N}}{2N(K^{2/N}-1)} \tag{71a, b}$$

where S_m and S_r are defined in Equations (6a, b).

If Equation (71a, b) are substituted into the fatigue relation, Equation (9), there results

$$\sigma = \frac{5p}{2N} \frac{K^{2/N}}{(K^{2/N}-1)} \tag{72}$$

It is surprising that this result, Equation (72), is the same as Equation (40) plotted in Figure 44, the result of the shrink-fit analysis, except now the limit Equation (42) no

longer applies. Therefore, now p/σ can be made as large as desired simply by increasing N. The only problem is that the required N or K may be too large to be practical. For example, assume σ = 150,000 psi (ultimate strength of a ductile steel), N = 8 and K = 16. Calculating p we find that p = 240,000 psi. Thus, it is concluded that for fatigue applications under high pressure the controlled-fluid-fill, multiring container becomes too large to be practical. Eight rings also means there are seven annuli under fluctuating pressures. (The magnitudes of these pressures are all different and are given by an equation similar to Equation (38).) Design of mechanical apparatus to supply and control all these pressures presents practical difficulties also.

XXX

ANALYSIS OF RING FLUID RING CONTAINERS FOR HIGH PRESSURE

A high-pressure-container design was suggested in Interim Report IV[21] which derives the benefit of both shrink-fit and fluid-pressure support. This design is shown in Figure 40. It is composed of two multiring units and therefore avoids the numerous difficulties encountered in segmented designs. Analyses of this advanced container design are described in this section. The analyses for calculating maximum pressure capability, residual stress, and required shrink-fit interferences were programmed for calculation on Battelle's CDC 3400 and 6400 computers.

Generalized Fatigue Criteria

In the earlier analyses, two fatigue criteria were used for either high-strength liner steels or for ductile outer cylinders. These were a tensile-strength criterion and a shear-strength criterion repectively. These criteria were postulated for pressure-vessel stress conditons. The fatigue data available in the literature were used to determine the criterion for failure. Only uniaxial data could be found on high-strength steels. Some triaxial fatigue data from pulsating fluid-pressure tests were available on low-strength steels.[35]

In a general design of a multiring container, different steels with different fatigue behavior may be used to advantage for each ring. Since no definite fatigue data are available at this time on the biaxial or triaxial fatigue of high-strength steels in particular, generalized fatigue criteria with arbitrary coefficients are formulated here on both a tensile-strength and a shear-strength basis. (For example, it may be that a high-strength brittle steel will fail in a ductile manner when subjected to high bore pressures in a container.) These generalized fatigue relations are as follows:

$$A_n (\sigma_\theta)_r + B_n (\sigma_\theta)_m = \sigma_n \quad ,$$

or (73a, b)

$$A_n S_r + B_n S_m = \sigma_n \quad ,$$

where

A_n, B_n are coefficients describing the material of ring number n,

subscript r denotes the semirange stress component,

subscript m denotes the mean stress component, and

σ_n is the tensile strength of ring number n.

The linear relations (73a, b) can be used to describe in a stepwise manner, nonlinear behavior as illustrated by the semirange, mean-shear-stress plot in Figure 61. (The constant coefficients A_n and B_n in (73a) are related to the variable parameters α_r and α_m defined earlier as follows: $A_n = \frac{1}{\alpha_r}$ for $\alpha_m = 0$, $B_n = \frac{1}{\alpha_m}$ for $\alpha_r = 0$.) The shear fatigue relation

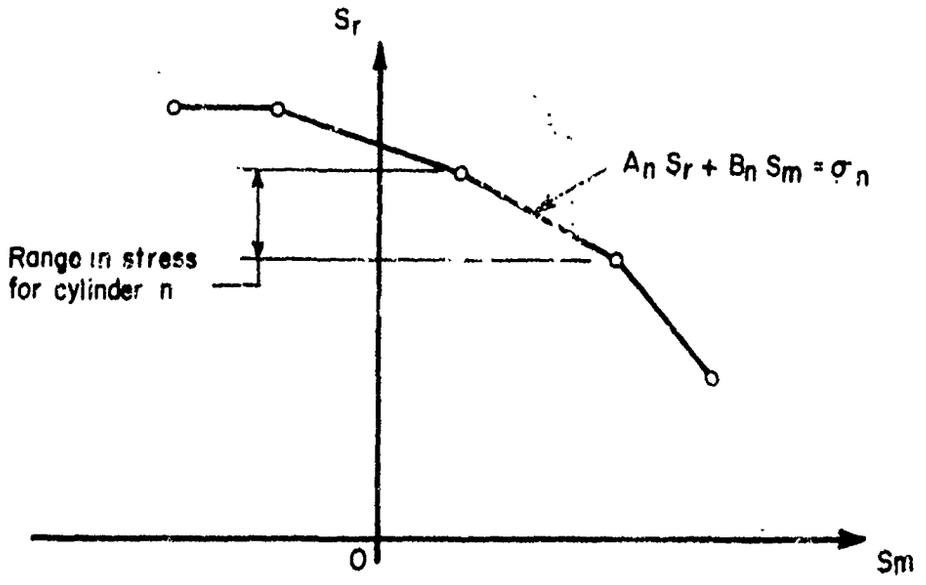

FIGURE 61. GENERALIZED FATIGUE RELATION IN TERMS OF SHEAR STRESSES

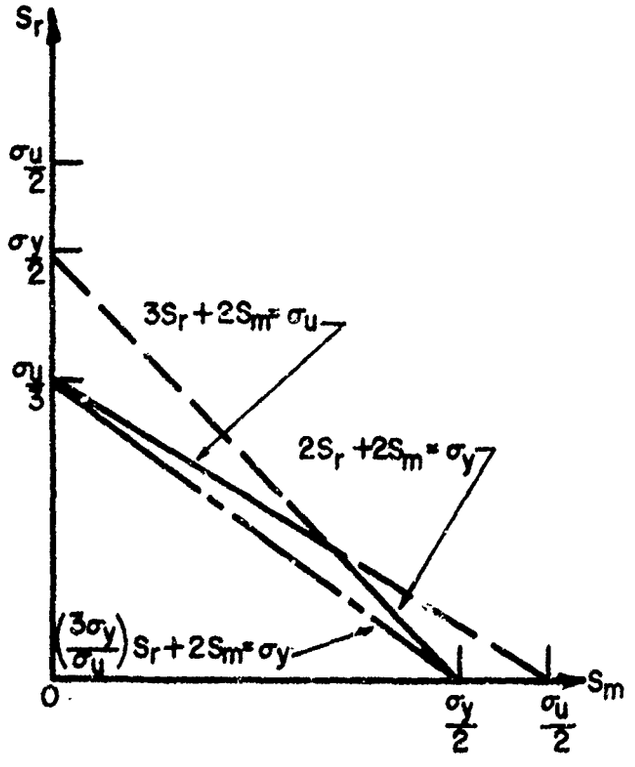

FIGURE 62. SHEAR-YIELD- AND SHEAR-FATIGUE-STRENGTH RELATIONS

$$3S_r + 2S_m = \sigma, \text{ where } \sigma \leq \sigma_u, \text{ for } 10^6 \text{ cycles life} \tag{74}$$

[Equation (9) in the previous analyses], must be limited by the yield strength, σ_y, for large mean stresses as shown in Figure 62, i.e.

$$2S_{max} = 2S_r + 2S_m \leq \sigma_y \tag{75}$$

A conservative shear-fatigue relation is the following:

$$\left(\frac{3\sigma_y}{\sigma_u}\right) S_r + 2S_m = \sigma_y \quad , \quad \text{for } 10^6 \text{ cycles life} \tag{76}$$

Relation (76) is also shown in Figure 62. [The coefficient $A_n = 3$ in Equations (74) and (76) is taken from data in Reference (35) as indicated earlier on page 164.]

The significance of the limit $S_m = 0$ [used in conjunction with Equation (7) on page 163] is now pointed out. S_m at the bore is related to $(\sigma_\theta)_m$ as follows:

$$S_m = \frac{(\sigma_\theta)_m}{2} + \frac{(p_o - q_o)}{4} = \frac{(\sigma_\theta)_m}{2} + \frac{p_o}{4} \text{ for } q_o = 0 \quad .$$

Thus,

$$(\sigma_\theta)_m = -\frac{p_o}{2} \text{ for } S_m = 0 \quad . \tag{77}$$

For a multiwall container it was found that $\left((p_o)_{max} \approx \sigma_u \text{ for } \alpha_r = \frac{(\sigma_\theta)_r}{\sigma_u} = 0.5, \ \alpha_m = \frac{(\sigma_\theta)_m}{\sigma_u} = -0.5 \text{ for } 10^4\text{-}10^5 \text{ cycles life}\right)$. Therefore, the maximum tensile strength fatigue criterion with $\alpha_r = 0.5$, $\alpha_m = -0.5$ is equivalent to $S_m = 0$ for the shear strength criterion.

Coefficients A_n and B_n in Equation (73a) are now calculated for the tensile criterion postulated for high-strength steels ($\sigma_u \geq 250,000$ psi) from the fatigue data given in Table XLII and XLIII. These data are as follows in terms of α_r and α_m:

	Semirange Parameter, α_r	
Fatigue Life, cycles	for $\alpha_m = 0$	for $\alpha_r = \alpha_m$
10^4-10^5	0.50	0.35
10^6-10^7	0.35	0.25

Thus, for $0 \leq \alpha_m \leq \alpha_r$ (zero to a positive mean stress) the coefficients A_n and B_n are calculated to be:

Fatigue Life, cycles	A_n	B_n
10^4-10^5	2.00	0.86
10^6-10^7	2.86	1.14

For, $-\alpha_r \leq \alpha_m \leq 0$, in lieu of actual data, the fatigue relation (73a) is assumed to be horizontal (Figure 61), i.e., $B_n = 0$ with $A_n = 2.00$ and $A_n = 2.86$ for 10^4-10^5 and 10^6-10^7 cycles life, respectively.

General Analysis of Multiring Containers

A multiring container or a multiring unit of a two-unit container such as has been shown in Figure 40, is assumed to have pressures fluctuating between q_o and p_o in the bore and between q_N and p_N on the outside diameter. Minimum stresses during the cycle occur at pressure preloadings q_o and q_N, and maximum stresses occur at operating-pressure loadings of p_o and p_N. (The pressures q_N and p_N are the so called "fluid-support pressures".) The generalized fatigue criteria (73a, b) are used. The elasticity solutions for the stress components in Equations (73a, b) are as follows:

$$(\sigma_\theta)_r = \frac{1}{2(k_n^2 - 1)} \left[(p_{n-1} - q_{n-1})(k_n^2 + 1) - 2(p_n - q_n)k_n^2 \right] , \qquad (78a, b)$$

$$(\sigma_\theta)_m = \frac{1}{2(k_n^2 - 1)} \left[(p_{n-1} + q_{n-1})(k_n^2 + 1) - 2(p_n + q_n)k_n^2 \right] , \qquad (79a, b)$$

$$S_r = \frac{k_n^2}{2(k_n^2 - 1)} \left[(p_{n-1} - p_n) - (q_{n-1} - q_n) \right] .$$

The p_n are related to the q_n as follows:

$$p_n = q_n + (-\sigma_{rn}) \quad , \qquad (80a)$$

where

$$\sigma_{rn} = \frac{(p_o - q_o)}{(K^2 - 1)} (1 - k_{n+1}^2 \; k_{n+2}^2 \; \ldots \; k_N^2) \qquad (80b)$$

$$- \frac{(p_N - q_N)}{(K^2 - 1)} (K^2 - k_{n+1}^2 \; k_{n+2}^2 \; \ldots \; k_N^2) \quad , \; n = 1, 2, \ldots, N-1$$

There are (2N-1) unknowns: N pressures p_n, $(n = 0, 1, \ldots, N-1)$ and N-1 pressure q_n, $n = 1, 2, \ldots, N-1$. (Determining p_o the bore pressure determines the pressure capability.) There are also (2N-1) equations: N equations from Equations (73a) or (79b) for rings $n = 1, 2, \ldots, N$ and (N-1) equations from Equation (80a). Therefore a solution is tractable.

This analysis was programmed into a computer code, Program MULTIR (abbreviation for multiring), for Battelle's 3400 and 6400 CDC computers. Results are given later when specific designs are discussed. First, the influence of "fluid-support pressures" q_N and p_N is studied by considering the example of a fatigue shear strength design.

Shear-Strength Analysis of a Mu'tiring Container

A multiring container is considered which has all rings of the same material, i.e., the same Equation (79b) is assumed valid for all rings, n = 1, 2, . . . , N with $A_1 = A_2 = \ldots A_N$; $B_1 = B_2 = \ldots B_N$; and $\sigma_1 = \sigma_2 = \ldots = \sigma_N = \sigma$. The pressure-to-strength ratio p_o/σ is derived in exactly the same manner as in Equation (42) (for the specific case $A_n = 3$, $B_n = 2$). The result is

$$\frac{p_o}{\sigma} = \frac{p_N}{\sigma} + \frac{2N}{(A_n + B_n)} \frac{K^{2/N} - 1}{K^{2/N}} - \frac{(A_n - B_n)}{(A_n + B_n)} \frac{q_o - q_N}{\sigma} \tag{81}$$

Similarly, a limit is imposed such that the minimum shear stress, S_{min}, at the bore is greater than or equal to the compressive shear strength of the liner, S_c, i.e.

$$S_{min} \geq - S_c = - \frac{\sigma_c}{2} \tag{82}$$

(This limit is believed to be more realistic than the limit $S_{in} = 0$ that was used in the earlier analysis.) Using the definition $S_{min} = - S_r + S_m$, the fatigue relation (73b) and the equation for S_r in the liner,

$$S_r = \frac{K^2}{2(K^2 - 1)} [(p_o - q_o) - (p_N - q_N)] \quad ,$$

in the inequality (82) there results

$$\frac{p_o}{\sigma} \leq \frac{K^2 - 1}{K^2} \frac{B_n}{A_n + B_n} \left(\sigma_c + \frac{2\sigma}{B_n} \right) + (p_n - q_n) + q_o \tag{83}$$

The pressure-to-strength ratio p_o/σ from Equation (82) and the limit (83) are sketched in Figure 63 as functions of p_N, q_N, and q_o. The solid curve for p_o is valid only when it is below the dashed limit curve. The support pressure, p_N, gives the most benefit as shown – both p_o and $(p_o)_{limit}$ increase with p_N. Small amounts of pressure, q_N, are helpful if $p_o \leq (p_o)_{limit}$. A residual bore pressure, q_o, is detrimental – p_o decreases with q_o.

Considering a two-unit, multiring container, it can now be realized that it is best that the fluid support pressure also fluctuates for two reasons:

(1) Too great a residual pressure, q_N, on the inner unit decreases its pressure capability.

(2) The pressure, q_N, on the inner unit corresponds to the pressure, q_o, on the outer unit, which in turn decreases the pressure capability of the outer unit.

The best design in a specific case may not require that $q_N = 0$, but it will require that q_N be sufficiently small.

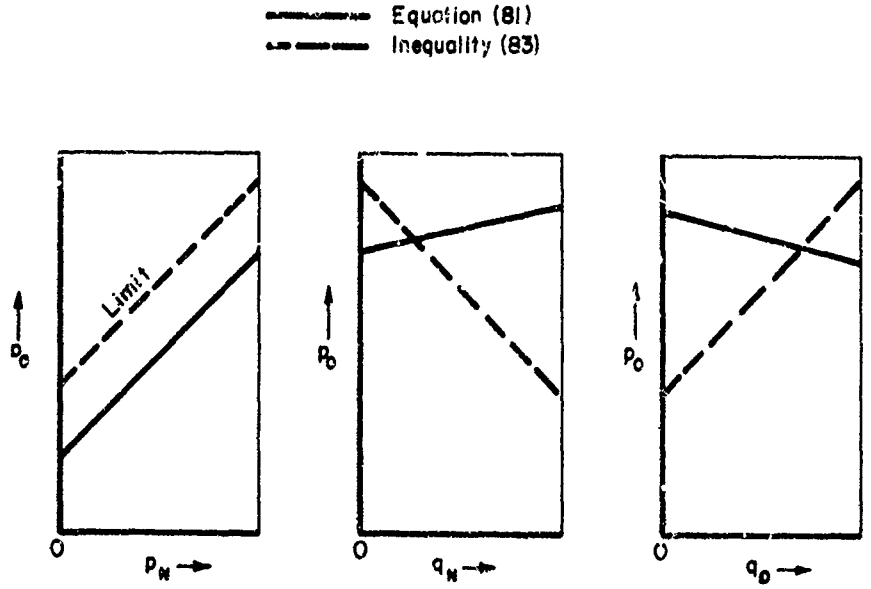

FIGURE 63. INFLUENCE OF PRESSURES p_N, q_N AND q_o ON THE PRESSURE CAPABILITY p_o

Comparison of the Shear and Tensile-Fatigue Criteria

A container designed on the basis of the shear-fatigue criterion will have a predicted pressure capability generally lower than that of a design based upon the tensile fatigue criterion. This is illustrated in Figure 64 for a single-ring (monoblock) container with $p_N = q_o = q_N = 0$. The curves in Figure 64 are plots of the equations

$$p_o/\sigma_u = \frac{2}{(A_n + B_n)} \frac{K^2 - 1}{K^2 + 1} \text{ for the tensile criterion, and} \tag{84}$$

$$p_o/\sigma_u = \frac{2}{(A_n + B_n)} \frac{\sigma_y}{\sigma_u} \frac{K^2 - 1}{K^2} \text{ for the shear criterion} \tag{85}$$

For a large wall ratio (K) the shear criterion predicts lower pressure capability. For thinner walled containers, $K \leq 1.7$, the reverse is true.

For $1.4 \leq K \leq 2.0$ the tensile criterion and the shear criterion both predict about the same pressure capability as shown in Figure 64. This agrees with the conclusion in Reference (46) based upon experimental fatigue data of cylinders with $1.4 \leq K \leq 2.0$ under cyclic internal pressure. However, the shear criterion severely limits the pressure capability for large K. Thick-walled containers, multiring units, are needed to contain the high extrusion pressures and the important question arises, "Which criterion should be used"? The shear criterion curve in Figure 64 is based upon fatigue data from actual pressurized cylinder tests for low-strength ductile steels, having an ultimate tensile strength of $\sigma_u = 126,000$ psi.[35] The tensile criterion curve, however, is based upon rotating-beam and push-pull tests of high-strength steels, $\sigma_u \geq 250,000$ psi. It has been postulated that the tensile criterion holds for the high-strength steel containers under internal pressure. Experimental verification is needed. The successful design of

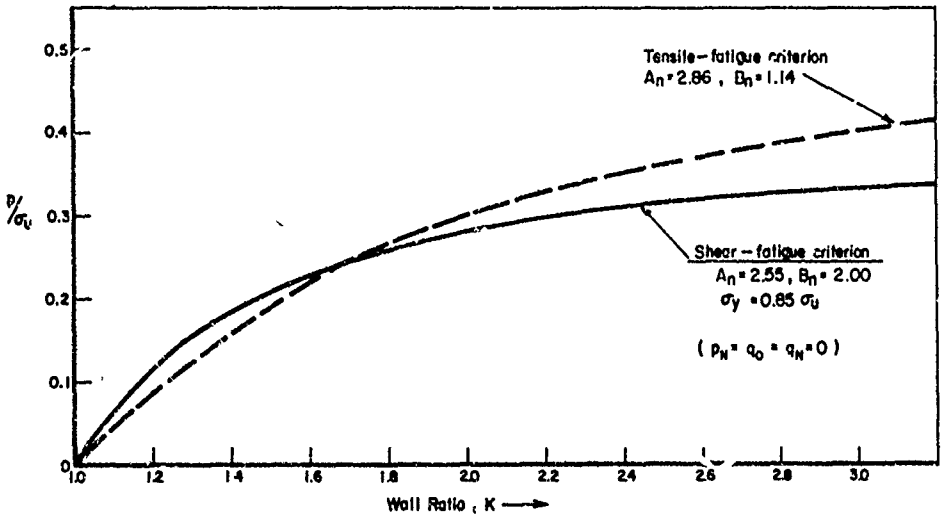

FIGURE 64. PRESSURE-TO-STRENGTH RATIOS FOR SINGLE-RING CONTAINER FOR 10^6-10^7 CYCLES LIFE

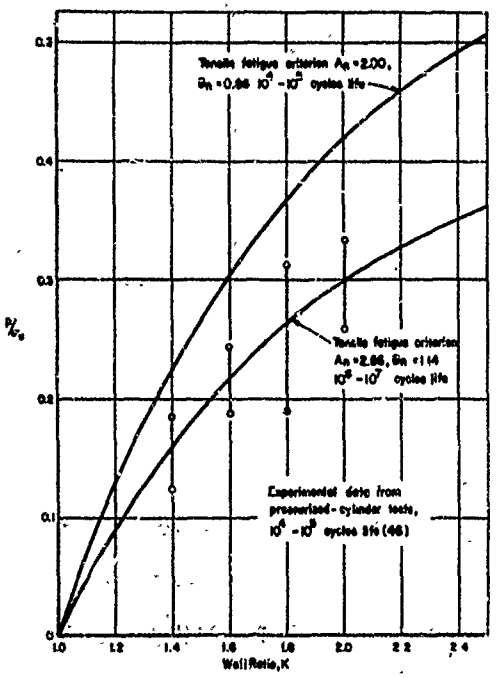

FIGURE 65. COMPARISON OF THEORY AND EXPERIMENT FOR SINGLE-RING CONTAINERS

containers for bore pressures $250,000 \leq p_o \leq 450,000$ psi depends upon the validity of the postulated tensile-fatigue criterion.

In Figure 65 a comparison of the theory based on the tensile criterion is made with experimental data of Reference (46). The data from Reference (46) are for 4340 steel with ultimate tensile strength $\sigma_u = 160,000$ psi. Unfortunately, the experiments were run only for lifetimes up to 10^5 cycles. The comparison, Figure 65 shows that the theory predicts a too high pressure capability in this case. If the theory derived for high-strength steels is valid for the lower strength 4340 steel, then Figure 65 indicates that a cylinder designed for 10^6-10^7 cycles life would actually fail earlier at 10^4-10^5 cycles. This may result from the detrimental effect of fluid entering voids in the materials under pressure. It is expected that large compressive prestresses from shrink-fit in multiring units will prevent this detrimental effect. This expectation needs to be investigated experimentally.

When design pressures are low enough, the more conservative shear criterion should be used. In some cases the tensile criterion can be used for an inner ring and the shear criterion for outer rings as described earlier and in Example Design 2 discussed below.

Example Designs of Containers

The design of the multiring components of the ring-fluid-ring container require not only calculation of required diameters and interferences but also due consideration of the feasibility of manufacture and assembly. Excessive size and interference requirements will render a design impracticable. Calculations are described here, using computer code MULTIR, for two example designs. The diameter and interference requirements are listed so that they may be used as a basis for judging the feasibility of manufacture. Calculations are performed for 6-inch-diameter-bore designs. A larger design, with a 15-inch-bore diameter, is then considered by scaling up the diameter and interference requirements for the smaller design.

Example Design 1

A two-unit, multiring container is analyzed based entirely on the tensile-fatigue-strength criterion. The inner unit consists of only one ring. The data for the inner unit are as follows:

$$\begin{aligned} &\text{wall ratio, } K = 1.5 \\ &\text{inner radius, } r_o = 3.0 \text{ in.} \\ &\text{outer radius, } r_1 = 4.5 \text{ in.} \\ &\text{design tensile strength, } \sigma_1 = 300,000 \text{ psi} \\ &\text{maximum internal bore pressure, } p_o = 450,000 \text{ psi} \\ &\text{minimum internal bore pressure, } q_o = 0 \ . \end{aligned} \tag{86}$$

It is assumed that

$$(\sigma_\theta)_r \cong 1/3\, \sigma_1 \tag{87}$$

(fatigue data from Tables XLII and XLIII for 10^6-10^7 cycles life), under the following conditions:

$$(\sigma_\theta)_{max} = 0, \quad (\sigma_\theta)_{min} \geq -\sigma_1 \tag{88}$$

Equation (84) and the definition

$$(\sigma_\theta)_{min} = (\sigma_\theta)_{max} - 2(\sigma_\theta)_r$$

require from (85) that

$$(\sigma_\theta)_{min} = -2/3\,\sigma_1 \quad . \tag{89}$$

To obtain conditions (87-89) a fluid-support pressure varying between q_1 and p_1 is to be found. Because the inner unit consists of only one ring in this case, calculations on the computer are not necessary as they are easily performed by hand. The analysis proceeds as follows:

$$(\sigma_\theta)_{max} = p_o \frac{K^2 + 1}{K^2 - 1} - 2p_1 \frac{K^2}{K^2 - 1} = 0 \quad ,$$

$$p_1 = \frac{p_o}{2} \frac{K^2 + 1}{K^2} = 325,000 \text{ psi} \quad , \tag{90}$$

$$(\sigma_\theta)_{min} = -2q_1 \frac{K^2}{K^2 - 1} = -2/3\,\sigma_1 \quad ,$$

$$q_1 = \frac{K^2 - 1}{K^2} \frac{\sigma_1}{3} = 55,500 \text{ psi} \quad . \tag{91}$$

Thus, it is found that the outer unit must withstand an internal pressure varying between 55,500 psi and 325,000 psi.

The computer code, MULTIR, is used for the outer-unit calculations. A 1/2-inch gap is allowed between the units for the fluid-support pressure, i.e., $r_o = 4.50 + 0.50 = 5.00$ in. for the outer unit. The assumed data are

wall ratio, $K = 4.0$,

number of rings, $N = 3$,

ring radii, $r_o = 5.0$ in., $r_1 = 7.95$ in., $r_2 = 12.61$ in., $r_3 = 20.0$ in.,

support pressures, $p_N = q_N = 0$,

minimum bore pressure, $q_o = 55,500$ psi,

fatigue coefficients, $A_n = 2.86$, $B_n = 1.14$.

Different calculations, 1A - 1D, are performed for rings made from materials with various strengths. Results are given in Table XLV. All four calculations give results

that satisfy the requirement of maximum bore pressure of p_o = 325,000 psi. The effect of varying the strength of the rings is indicated. Design 1B has the minimum required interference, Δ_1 = 0.0622 in., corresponding to $\frac{\Delta_1}{r_1} = \frac{0.0622}{7.95} = 0.00782$ in. in.

TABLE XLV. RESULTS OF COMPUTER CODE MULTIR FOR EXAMPLE DESIGN 1[a]

Design	Design Tensile Strength of Rings, σ_1, psi			Results: Maximum Bore Pressure for 10^6 Cycles Life	Results: Required Interference[b], in.	
	1	2	3		Δ_1	Δ_2
1A	325,000	325,000	325,000	338,337	0.0670	0.0739
1B	350,000	325,000	300,000	332,699	0.0622	0.0630
1C	375,000	350,000	300,000	345,837	0.0658	0.0578
1D	400,000	350,000	300,000	351,251	0.0625	0.0578

(a) Based entirely on the tensile-fatigue criterion.

(b) Interferences required on the radius. Δ_1 required between rings 1 and 2, and Δ_2 required between 2 and 3.

Example Design 2

In this design the more conservative shear-fatigue-strength criterion is used for the outer (second) ring of the inner unit and for all three rings of the outer unit. The given data are:

Inner Unit

wall ratio, K = 3,

number of rings, N = 2,

radii, r_o = 3.00, r_1 = 5.1960, r_2 = 9.00,

tensile strength of ring 1, σ = 300,000 psi,

yield strength of ring 2, σ_y = 212,500 psi ($\sigma_y = 0.85\,\sigma_u$, σ_u = 250,000 psi),

fatigue coefficients,

A_1 = 2.86 and B_1 = 0. for ring 1,

A_2 = 2.55 and B_2 = 2.0 for ring 2,

minimum bore pressure, q_o = 0,

support pressures, p_2 = 160,000 psi, q_2 = 0.

Outer Unit

wall ratio, K = 4,

radii, r_o = 9.500 in., r_1 = 15.07 in., r_2 = 23.90 in., r_3 = 38.00 in.,

number of rings, N = 3,

yield strength of rings, σ_y = 255,000 psi ($\sigma_y = 0.85\,\sigma_u$, σ_u = 300,000 psi),

fatigue coefficients of rings, A_n = 2.55, B_n = 2.00,

minimum bore pressure, $q_o = 0$,

support pressures, $p_3 = q_3 = 0$.

The support pressure, p_2, on the inner unit was precalculated by an analysis similar to that of Equation (90) to give $(\sigma_\theta)_{max} \approx 0$ at the bore.

The results of computer code MULTIR are

Inner Unit

$p_o = 455,832$, $\Delta_1 = 0.0416$ in.

Outer Unit

$p_o = 202,817$ psi, $\Delta_1 = 0.0772$ in., $\Delta_2 = 0.1220$ in.

The maximum allowable pressure, $p_o = 202,817$ psi, in the outer unit represents a factor of safety of 1.33 over the required pressure of 160,000 psi.

The 6-inch-diameter-bore designs considered would require outside diameters of 40 inches and 76 inches for 325,000 psi and 455,000 psi capacities, respectively. The larger diameter requirement in the second case reflects the conservative shear-strength basis of this design. Containers with 15-inch-diameter bores would require (scaled-up) outside diameters of 100 inches and 190 inches, respectively. Rings of those diameters are considered too large to be practicably manufactured and assembled.

Theoretically, a ring-fluid-ring container can be designed to a maximum pressure capability of $p_{max} \approx 1,000,000$ psi. It would have a multiring inner unit. However, the external-size requirements make such a design impracticable as was the case for the ring-fluid-segment container.

Conclusions and Recommendations

Bore pressures of 450,000 psi corresponding to 10^6 cycles life are found to be theoretically possible in hydrostatic-extrusion containers using the fluid-supported multiring concept. Container designs with 6-inch-diameter bores appear to be practicable to construct. However, outside-diameter requirements of 15-inch-diameter-bore containers appear too large to be practicable at this time.

Theoretical analyses have been based on postulated fatigue behavior of high-strength steels. Experiments to obtain actual fatigue data of high-strength steel cylinders under cyclic pressures up to 450,000 psi is needed before the predictions of theory can be verified. A potential problem in such an experimental fatigue program is foreseen: the fatigue specimens will have to be heavy-walled containers in order to support the high pressures. Therefore, an alternative experimental research program consisting of two steps is recommended:

(1) A preliminary analysis aimed at designing small specimens pressurized and mechanically loaded to simulate the stress condition at the bore of a container, and

(2) Construction and testing of simulated specimens.

XXXI

DESIGN REQUIREMENTS AND LIMITATIONS FOR HIGH-PRESSURE CONTAINERS

As already indicated, the theoretically predicted maximum-pressure capability for the five containers considered in detail in the present study are as follows for 10^4 to 10^5 cycles life:

Container	Maximum Pressure, p, psi
Multiring	~300,000
Ring-segment	~300,000
Ring-fluid-segment ($p_3/p = 0.3$)	~1,000,000
Pin-segment	210,000
Ring-fluid-ring (multiring inner unit)	~1,000,000

These predictions, based on the fatigue strengths of steels with an ultimate tensile strength of 300,000 psi for the liner and 200,000 psi for the outer cylinders or components, apply to any operating temperature provided these are the strengths at that temperature.

For liners with ultimate tensile strengths much greater than 300,000 psi, the theoretical maximum pressure capability of the various designs may be improved appreciably. This is true if it can be assumed that the higher strength materials would exhibit the same fatigue behavior as that shown in Figure 42 for steels with ultimate tensile strength ranging from 250,000-310,000 psi at room temperature. (Tensile strengths of 410,000 psi have been reported for AISI M50 steel. If the previous assumption is correct, then a multiring or ring-segment container with an M50 liner would have a theoretical maximum pressure capability of 410,000 psi. However, these containers may require that some ductile outer cylinders have ultimate tensile strengths greater than 200,000 psi.)

Possible Manufacturing and Assembling Limitations

It is important to note that the theoretical pressures given in the above tabulation may not be achievable for each design because of practicable design limitations. For example, the outside diameters required for designs having 6- and 15-inch bore diameters and maximum pressures up to 450,000 psi are as follows:

Container	Maximum Pressure, p, psi	Outside Diameter, inches	
		6-inch-Bore Design	15-inch-Bore Design
Multiring	300,000	51.0	127.5
Ring-segment	300,000	60.0	150.0
Ring-fluid-segment	450,000	88.0	218.0
Pin-segment	210,000	90.4	180.2
Ring-fluid-ring (Example 2)	450,000	76.0	190.0

It may be impossible to obtain steel cylinders in such large sizes (10- to 50-foot diameters) with ultimate strengths of 200,000 psi, and it may be impossible to machine and transport such large cylinders. Also heat treatment of heavy sections may be a problem. This may not be the case for pin-segment container, however. In this instance, it may be possible to forge the large steel pins (18.2 inches and 45.4 inches in diameter respectively, based on a design shear stress of 50,000 psi in fatigue for the pins) and the segments (thick plates). This indicates an advantage of the pin-segment design for vessels with $p \leqq 210,000$ psi.

A pin-segment arrangement may also be used to advantage as a replacement for the outer cylinder in the other container designs. This would help overcome the difficulties associated with the large steel cylinders. A wire wrap or strip wrap could also be used to this advantage as a replacement to outer cylinders.

The limitations in some of the designs due to large-diameter outer cylinders may also be partially overcome by using the autofrettage process to provide some additional prestress at the liner bore. The process introduces compressive prestresses by plastic deformation of the bore. This approach could reduce the size and number of outer rings that otherwise would be needed to achieve the total prestress by shrink fitting alone. In fact, the autofrettage process could be used to improve the size efficiency of all the design concepts considered. However, if autofretaging is employed, then high-strength steels with appreciable amounts of ductility should be selected for the liner because the process requires plastic deformation of the bore.

In addition to the potential problem of cylinder size, the theoretical pressures may not be possible to achieve because excessive interferences may be required for shrink-fit assembly. The maximum interferences required for the designs are as follows:

Container	Maximum Pressure, p, psi	Maximum Interference Required, inch/inch
Multiring	300,000	$\Delta_1/r_1 = 0.0036$
Ring-segment ($k_2 = 1.1$, $\frac{E_2}{E_1} = 3.0$)	300,000	$\Delta_{12}/r_1 = 0.0028$
Ring-fluid-segment ($k_2 = 2.0$)	450,000	$\Delta_{12}/r_1 = 0.0129$
Pin-segment	210,000	None, except for a small amount to take up slack during assembly
Ring-fluid-ring (Example 2)	450,000	$\Delta_1/r_1 = 0.0080$

For the multiring container, the interference required between the liner and Cylinder 2 as manufactured is $\Delta_1/r_1 = 0.0036$ in./in. This is a reasonable value and it corresponds to a temperature difference of 400 to 500 F for assembly. However, the interference as manufactured is not always the same as the interference as assembled. Suppose that the multiring container is assembled ring by ring from the inside out. Each ring expands as it is shrunk on and the assembly interference progressively increases beyond the manufactured interference. Formulas for the assembly interference can also be derived. Derivations are given in Appendix II.

The interference required for the ring-fluid-segment container is $\Delta_{12}/r_1 = 0.0129$ in./in. This interference requirement is severe, if not impossible, especially when one considers assembling not only the liner and Cylinder 3, but also a number of segments all at the same time. (Δ_{12} is the interference required between the liner, segments, and Cylinder 3. Δ_{12} is also the assembly interference as well as the manufactured interference since the liner, Cylinder 3, and the segments must be assembled simultaneously.) The large magnitude for Δ_{12} is primarily due to large radial elastic deformation of the segments under pressure. This is shown as follows: from Equation (19a) it is found that

$$\frac{E_2 (u_1-u_2)}{r_1 p_1} = 0.69 \text{ for } k_2 = 2 \text{ and } p_2 = p_1/k_2 \quad ,$$

where u_1 and u_2 are the radial displacements of the segment and r_1 and r_2, respectively. From a computer calculation for the ring-fluid-segment container, p_1 at pressure ($\sigma_r = -p_1$ at r_1), is found to be $p_1/\sigma_1 = 2.2$. Thus,

$$\frac{E_2 (u_1-u_2)}{r_1 \sigma_1} = 2.2\,(0.69) = 1.518 \quad .$$

For $p/\sigma_1 = 2.87$ and $p = 450{,}000$ psi, $\sigma_1 = 157{,}000$ psi. Hence, $\frac{u_1-u_2}{r_1} = 0.00795$ in./in.

for $\sigma_1 = 157{,}000$ psi and $E_2 = 30 \times 10^6$ psi, and it is evident that large interference, $\Delta_{12} = 0.0129$ in./in., is required to overcome large deformation of the segments under pressure. This is a disadvantage for the containers having segments in their designs.

Another potential disadvantage of these designs is the possible problem of gouging the liner with the corners of the segments if the components are assembled by pressing. A further factor that must be considered in the design of segments is bending deformation. This is discussed in Appendix I.

The severe interference requirements imposed by the segments are reduced if the segment size (k_2) is reduced and if a higher modulus material is used for the segments. These effects are shown above for the ring-segment container that has a lower interference requirement; i.e., $\Delta_{12} = 0.0028$ in./in. However, selection of a high modulus material must be done with care because tensile stresses do develop in the segments as shown in Appendix I and many high-modulus materials have low tensile strengths.

Thus, it is seen that some theoretical container designs for high pressure may be impossible to fabricate because of the large outside diameters and interferences required. In order to obtain a more realistic evaluation of the various design concepts, predictions of pressure capability are made for more practicable design requirements, i.e., outside diameters limited to 72 inches and the interferences limited to 0.007 in./in. maximum. These predictions are as follows for 10^4-10^5 cycles life:

Container		Bore Diameter, inches	Outside Diameter, inches	Number of Components, N	Maximum Pressure, p, psi
Multiring	$(k_1 = 2.0)$	6	51.0	5	300,000
	$(k_1 = 1.5)$	15	72.0	7	275,000
Ring-segment ($k_2 = 1.1$, $E_2/E_1 = 3.0$)	$(k_1 = 2.0)$	6	60.0	6	290,000
	$(k_1 = 1.5)$	15	72.0	8	265,000
Ring-fluid-segment ($k_1 = 1.5$, $k_2 = 2.0$)	$(p_3/p = 0.3, k_3 = 1.25)$	6	72.0	10	286,000
	$(p_3/p = 0.3, k_3 = 1.20)$	15	72.0	4	160,000
Pin-segment ($k_1 = 1.3$, $k_2 = 2.0$)		6	72.0	3	195,000
		15	(a)	--	--
Ring-fluid-ring[b]	$(k_1 = 2.0)$	6	60.0	8	450,000
	$(k_1 = 1.60)$	15	72.0	4	219,000

(a) OD ≤ 72.0 not possible for 10^4-10^5 cycles life and $\alpha_r = \alpha_m = 0.35$ if no prestress is provided.
(b) One ring inner unit. $p_1/p = (k_1^2 - 1)/(2k_1^2)$.

It is evident that lower maximum pressures are now predicted, particularly for the 15-inch-bore designs. The reduction in pressure capability is due only to the restriction in outside diameter for the multiring, ring-segment, and pin-segment containers. However, both the outside diameter and interference limitations reduce the predicted pressure for the ring-fluid segment container. The reduction for this container is severe and is caused by three effects. The first is excessive deformation of the segments for $k_2 = 2.0$. The other effects are coupled; reducing the outside diameter while maintaining the design pressure increases the interference required, but limiting the interference causes a reduction in maximum pressure because the interference depends upon the pressure.

Residual Stress Limitations

A container designed for a specific cyclic pressure requires certain residual stresses (prestresses) at operating temperature. It is also important, however, to check the residual stresses at room temperature because of differences in thermal expansion.

Calculations of residual stresses are given here for the multiring container as an example. (Residual stresses and operating stresses can be determined for all containers using the computer programs listed in Appendix III.) The specific container design discussed here is the one considered in the foregoing section for a bore diameter of 6 inches. Calculations are performed for design applications at room temperature, 500 F, and 1000 F. The material data assumed are given in Table XLVI. The liner material is assumed to be 18 percent Ni maraging steel, and the outer cylinders are assumed to be made of modified H-11 steel. The differences in thermal expansion for these materials are likely to be the largest expected among the steels that may be used.

TABLE XLVI. ELEVATED-TEMPERATURE DATA FOR 18 PERCENT NICKEL MARAGING STEEL AND H-11 STEEL[a]

	70 F	500 F	1000 F
	Modulus of Elasticity, psi		
18% Ni Maraging	26.5×10^6	23.0×10^6	18.7×10^6
H-11	30.0×10^6	27.4×10^6	22.8×10^6
	Coefficient of Thermal Expansion, in./in./F		
18% Ni Maraging	5.6×10^{-6}	5.6×10^{-6}	5.6×10^{-6}
H-11	7.12×10^{-6}	7.25×10^{-6}	7.37×10^{-6}

(a) Poisson's ratio taken as constant, $\nu = 0.3$ for both materials.

Results are given in Table XLVII. The range and mean stress parameters were $\alpha_r = 0.5$ and $\alpha_m = -0.5$, respectively. The results show that the excessive residual stresses at room temperature occur for the multi-ring container having a required prestress, $\sigma_\theta = -\sigma_1$ at 500 F and 1000 F; i.e., the residual stress $\sigma_\theta < -\sigma_1$ at room temperature, where σ_1 is the design stress and $\sigma_1 \leqq$ ultimate tensile strength. The reason for this is the larger interferences required for elevated-temperature application as shown in Table XLVII. Larger interferences are necessary for high-temperature applications because the outer rings expand more than the liner due to the differences in thermal expansions as shown in Table XLVI. On the other hand, reduction of the temperature from operating temperature to room temperature causes the outer rings to tend to contract more than the liner. The liner resists the contraction and the residual interface pressures are increased, thereby increasing the magnitude of the residual hoop stress at the bore.

If the multiring container is to be used at 500 F and 1000 F with the material properties given in Table XLVI, then the prestress requirement, $\sigma_\theta = -\sigma_1$ at temperature ($\alpha_m = -0.5$) has to be relaxed. Accordingly, calculations of residual stresses and interferences were rerun for $\alpha_m = -0.3$ (prestress $\sigma_\theta = -0.8\,\sigma_1$ at temperature). The results are shown in Table XLVIII. With $\alpha_m = -0.3$, excessive residual stresses at room temperature are avoided for the 500 F design. However, for operation at 1000 F, $\alpha_m > -0.3$ is necessary since $\sigma_\theta < -\sigma_1$ at room temperature for the 1000 F design with $\alpha_m = -0.3$.

Decreasing the interference fit (from those in Table XLVII to those in Table XLVIII), in order to avoid excessive residual stresses at room temperature, increase $(\sigma_\theta)_{max}$ from 0 to positive values. As pointed out in the latter part of the Fatigue Criteria section, zero to small $(\sigma_\theta)_{max}$ is expected to be beneficial in preventing the detrimental effect of fluid pressure from entering voids in the material. Therefore, if excessive residual stresses are to be avoided in containers designed for high temperatures, and if $(\sigma_\theta)_{max}$ is to be kept small, then the thermal coefficients of expansion of the component parts of the container should be more closely matched than those of Table XLVI. Preferably the coefficient of thermal expansion should be larger for the liner than for the outer cylinders; this would cause a reduction rather than an increase in residual stresses upon decreasing the temperature from operating temperature to room temperature.

TABLE XLVII. LINER-BORE STRESSES AND INTERFERENCES FOR A 6-INCH-BORE MULTIRING CONTAINER WITH K = 8.5, N = 5, $k_1 = 2.0$, $k_n = 1.44$, $n \geq 2$, $\alpha_r = 0.5$, AND $\alpha_m = -0.5$[a]

	Stresses at Bore of Liner[b]								
	Residual Stresses at RT			Prestresses at Temperature			Operating Stress at Pressure and Temperature		
	σ_r/σ_1	σ_θ/σ_1	S/σ_1	σ_r/σ_1	σ_θ/σ_1	S/σ_1	σ_r/σ_1	σ_θ/σ_1	S/σ_1
RT Design	0	-1.000	-0.5000	0	-1.0000	-0.5000	-0.9727	0	0.4863
500 F Design	0	-1.1230	-0.5615	0	-1.0000	-0.5000	-0.9727	0	0.4863
1000 F Design	0	-1.2998	-0.6499	0	-1.0000	-0.5000	-0.9727	0	0.4863

	Dimensionless Interference Required as Manufactured[c]	
	Between Cylinders 1 and 2 for p = 300,000 psi[d], $E\Delta_1/r_{1p}$	Between Outer Cylinders n and n + 1 $E\Delta_n/r_{np}$
RT Design	0.358	0.343
500 F Design	0.454	0.343
1000 F Design	0.533	0.343

(a) The k_n, K, α_r, and α_m are defined in the list of symbols. Material data are given in Table XLVI. The liner is 18% Ni steel and the outer cylinders are H-11 steel.1
(b) σ_r is the radial stress, σ_θ the hoop stress, S the shear stress ($S = (\sigma_\theta - \sigma_r)/2$), and σ_i is the design strength – less than or equal to the ultimate tensile strength of the liner.
(c) E is the modulus of elasticity of the outer cylinders. Δ_n is interference in inches between cylinders n and n + 1. r_n is the outer radius of cylinder n.
(d) $E\Delta_1/r_1p$, at elevated temperatures, depends on p. $\sigma_1 = 310,000$ psi is required, ($p = 0.9727\sigma_1$).

TABLE XLVIII. LINER-BORE STRESSES AND INTERFERENCES FOR A 6-INCH-BORE MULTIRING CONTAINER WITH K = 8.5, N = 5, k_1 = 2.0, k_n = 1.44, n = 2, α_r = 0.5, AND α_m = -0.3[a]

	Stresses at Bore of Liner[b]								
	Residual Stresses at RT			Prestresses at Temperature			Operating Stress at Pressure and Temperature		
	σ_r/σ_1	σ_θ/σ_1	S/σ_1	σ_r/σ_1	σ_θ/σ_1	S/σ_1	σ_r/σ_1	σ_θ/σ_1	S/σ_1
RT Design	0	-0.8000	-0.4000	0	-0.8000	-0.4000	-0.9727	0.2000	0.5863
500 F Design	0	-0.9054	-0.4527	0	-0.8000	-0.4000	-0.9727	0.2000	0.5863
1000 F Design	0	-1.0505	-0.5253	0	-0.8000	-0.4000	-0.9727	0.2000	0.5863

	Dimensionless Interference Required as Manufactured[c]	
	Between Cylinders 1 and 2 for p = 300,000 psi[d], $E\Delta_1/r_1p$	Between Outer Cylinders n and n + 1 $E\Delta_n/r_np$
RT Design	0.217	0.304
500 F Design	0.309	0.304
1000 F Design	0.383	0.304

(a) The k_n, K, α_r, and α_m are defined in the list of symbols. Material data are given in Table XLVI. The liner is 18% Ni steel and the outer cylinders are H-11 steel.

(b) σ_r is the radial stress, σ_θ the hoop stress, S the shear stress ($S = (\sigma_\theta - \sigma_r)/2$), and σ_1 is the design strength - less than or equal to the ultimate tensile strength of the liner.

(c) E is the modulus of elasticity of the outer cylinder. Δ_n is interference in inches between cylinders n and n + 1. r_n is the outer radius of cylinder n.

(d) $E\Delta_1/r_{1p}$, at elevated temperatures, depends on p. σ_1 = 310,000 psi is required (p = 0.9727 σ_1).

Other Possible Material Limitations

It has been postulated that a maximum-tensile-stress fatigue criterion applies to the high-strength liner. Accordingly, fatigue data from uniaxial tension and rotating-beam bending tests were used to evaluate fatigue behavior of liners for high-pressure containers. However, the state of stress in an open-end hydrostatic extrusion container is biaxial and in a closed-end container a triaxial state of stress exists. (A triaxial state of stress may also occur in a shrink-fit open-end container where axial stresses may be produced by interface friction between shrink-fitted rings.) The effect of combined stresses on the fatigue strength of high-strength steels is unknown. It is pointed out, however, that the analyses performed in this study allow for arbitrary material behavior; i.e., the fatigue parameters, α_r and α_m, used in the analyses are left arbitrary in the equations and could be determined from combined-stress fatigue experiments.

It has also been postulated that a compressive mean stress may benefit material fatigue strength under cyclic fluid pressure. However, biaxial and triaxial fatigue behavior under compressive mean stress is unknown. Even fatigue data in the uniaxial case are lacking for conditions of compressive mean stress.

Also unknown is the possible fracture of high-strength steels under large compressive stresses. Pugh and Green[43] and Crossland and Dearden[44] found for cast iron that the fracture strain and ductility (and the maximum shear stress at fracture) are increased by superimposing hydrostatic pressure. Bridgman[45] found similiar but less conclusive results for steel. These are favorable results for the effect of true hydrostatic pressure, but the possibility of similiar behavior when only one principal stress (the radial stress in a container) is highly compressive is unknown and should be investigated. This is a particularly important factor because the difference between the hoop stress and the high compressive radial stress represents an extremely large shear stress.

The effect of a brittle-ductile transition in high-strength steels on the fatigue behavior near and above the transition temperature is another factor which may need to be considered.

SECTION 4

HYDROSTATIC EXTRUSION CONTAINERS DESIGNED AND CONSTRUCTED IN THE PROGRAM

SECTION 4

HYDROSTATIC EXTRUSION CONTAINERS DESIGNED AND CONSTRUCTED IN THE PROGRAM

XXXII

SUMMARY OF SECTION 4

The history of container design during the course of this program essentially follows the developments described in Section 3. An early container of 3-ring construction, designed on the maximum-shear-strength failure criterion failed due to low-cycle fatigue. The liner was replaced by two shrink-fit rings to obtain a higher prestress in the bore. This container was used in the remainder of the program. Stress analyses are presented for both of those containers. In addition, this section describes the design and the construction of a container that was intended for stand-by use in the event of another fatigue failure. This container was designed on the basis of fatigue design described in Section 3.

XXXIII

ANALYSIS OF THREE CONTAINERS DESIGN

The configuration of the three hydrostatic-extrusion containers described herein was basically as shown in Figure 66. The boundary conditions fo. the designs were:

(1) Maximum operating internal pressure on bore = 250,000 psi

(2) Maximum operating temperature = 500 F

(3) Pressure vessel ID = 2.375 inches

(4) Pressure vessel OD = 22.000 inches

(5) Axial load on vessel is negligible.

For reference purposes, the containers will be designated Containers I, II, and III in order of historical development. The design of Container I commenced in June, 1961, and was modified in January, 1965, to be redesignated Container II. As a result of the liner fatigue failure experienced with Container I, Container III was designed on the basis of a fatigue-failure criterion with the aim of obtaining a fatigue life in the order of 10^4 to 10^5 cycles. Container III was completed toward the end of the program but was not used in the hydrostatic-extrusion studies described in Sections 1 and 2.

Container I

Container I, which was designed and constructed in the previous program[47], was used in the early stages of this program. A detailed analysis of its design has been published.[47] In view of the more sophisticated analysis made in Section 3, it would be irrevelant to detail the design steps taken. However, the failure criterion used and the design interferences obtained will provide a useful background to the development of container designs.

Selection of Failure Criterion

Initially, failure of the design for Container I was interpreted as that condition where the diameter of the bore increased due to plastic yielding of the bore surface. Such a condition would have caused leakage by the previously close fitting stem that would result in an inability to compress the fluid adequately. With this in mind, three commonly applied failure criterion were examined to determine which was the most applicable.

The Rankine or maximum-normal-stress theory teaches that failure will occur when any one of the principal stresses reaches the level of the yield strength in uniaxial tension. Thus, it neglects the effects of the other two principal stresses. The Tresca or maximum-shearing-stress theory predicts yielding will occur when the difference between the maximum and minimum principal stresses reaches a level of the yield strength in simple tension. Experimental evidence suggested that this theory was on the

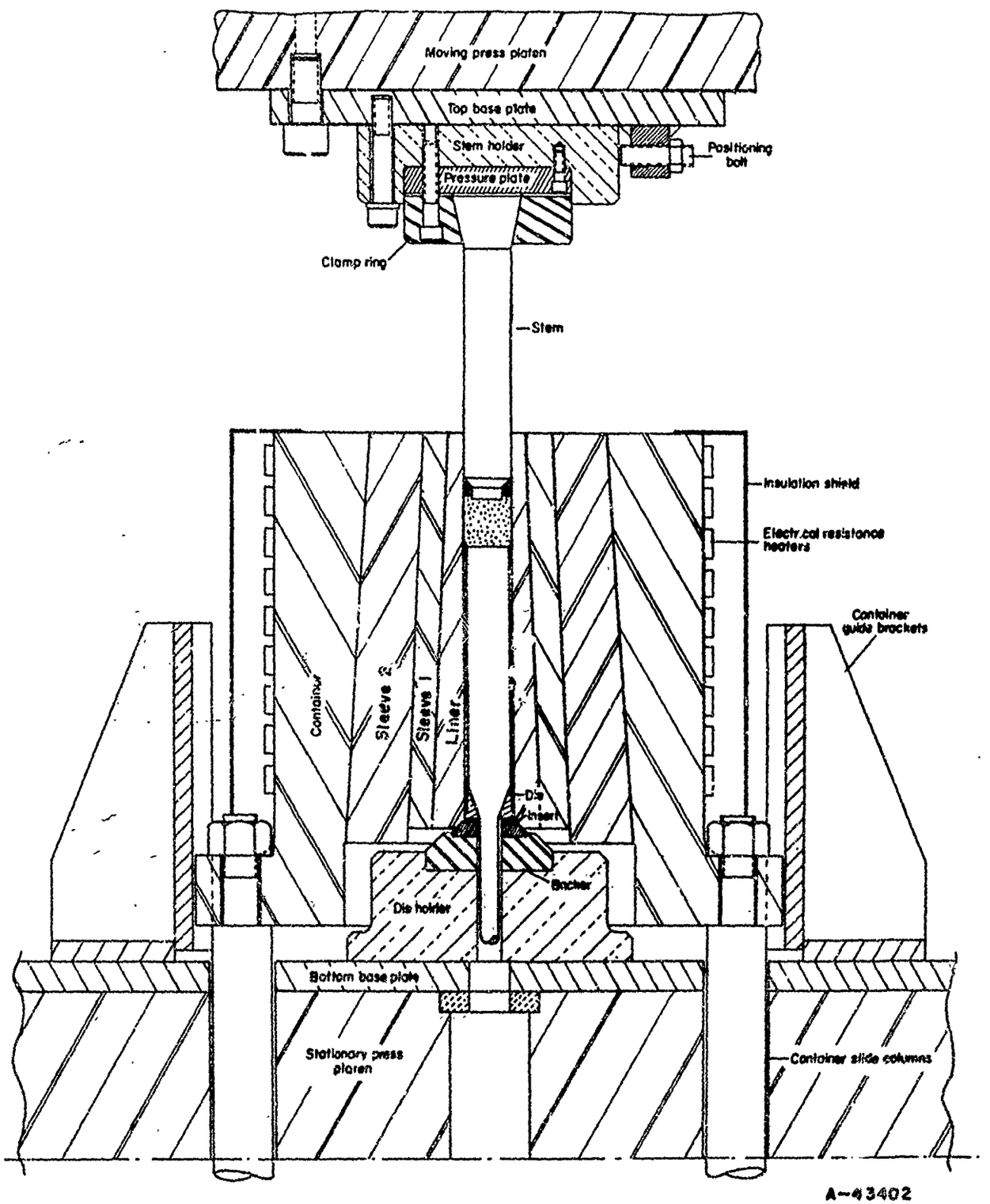

FIGURE 66. CROSS-SECTIONAL VIEW OF HYDROSTATIC-EXTRUSION TOOLING

conservative side for predicting stresses that would produce yielding in shear. Therefore, it was decided to base the container design on the Hencky-Von Mises or maximum-distortion-energy criterion.

The Hencky-Von Mises theory holds that a material subjected to a three-dimensional stress system will yield when

$$(\sigma_1 - \sigma_2)^2 + (\sigma_2 - \sigma_3)^2 + (\sigma_3 - \sigma_1)^2 = 2\,\sigma_y^2 = 6\,K^2 \quad ,$$

where

σ_1, σ_2, σ_3 = principal stresses

σ_y = yield stress as determined in uniaxial tensile or compressive tests

K = yield stress in pure shear.

In this case, for a container assembly, the stresses are considered to be biaxial because there is no axial load on the vessel. The hoop stresses are usually tensile and the radial stresses are always compressive. These two stresses will be the principal stresses because there are not externally applied shear stresses in the system. High resulting shear stresses can be expected when the system consists of two principal stresses of opposing sign.

Under biaxial conditions the Mises yield criterion becomes:

$$\sigma_1^2 - (\sigma_1\sigma_3) + \sigma_3^2 = \sigma_y^2 = 3\,K^2 \quad .$$

This equation predicts that yielding will occur when the stress in pure shear becomes equal to 0.577 Y. This value is equivalent to the maximum-shear-stress criterion provided that the yield stresses in pure tension or compression are multiplied by $2/\sqrt{3}$. With that modification of the Tresca criterion, solutions determined by either relationship agree within approximately two to six percent.

Therefore, it was decided that the container would not be expected to deform plastically, and the design would be acceptable, if the stressed metal in the vessel met either of the following equivalent limiting conditions:

Von Mises $$\frac{(\sigma_1^2 - \sigma_1\,\sigma_3 + \sigma_3^2)^{0.5}}{\sqrt{3}} < 0.577\ Y$$

Modified Tresca $$\frac{\sigma_1 - \sigma_3}{2} < 0.577\ Y$$

where

σ_1 = hoop stress at the inside of the liner

σ_3 = radial stress at the inside of the liner.

Stress Analysis of Container Assembly

To keep the tensile hoop stress on the liner bore to an acceptable minimum, the maximum shrink fit considered feasible was used between the sleeve and the liner. The shrink fit was limited by the temperature to which the sleeve could be heated without softening. This temperature was 1000 F for the alloy steel used for the sleeve. Since the liner was kept at room temperature during assembly, the maximum permissible shrink fit was 0.007 inch per inch. Although this is an extraordinarily large shrink fit for the size of the components involved, it was achieved with no apparent adverse effects. The shrink fit of the container on the sleeve was 0.0025 inch per inch. Figure 67 shows the arrangement of the rings and indicates interferences between them.

For the component dimensions, the effects of the shrink fits were as indicated in Table XLIX. These values were computed in a straight-forward manner by applying Lamé's equations for thick-walled pressure vessels. The elastic modulus was taken to be 30×10^6 psi at 80 F and 25×10^6 psi at 500 F. A step-by-step procedure was used to determine each component stress in the assembly. The resulting prestresses at various conditions of interest were then determined by super-position of the component stresses.

TABLE XLIX. PRESTRESSES DEVELOPED IN THE CONTAINER ASSEMBLY AT 80 F AND 500 F

Component	Nominal Diameter, inches	Taper, degrees	Diametral Interference, inch	Resulting Prestress at 80 F, psi		Resulting Prestress at 500 F, psi	
				Radial	Hoop	Radial	Hoop
Liner, Inside	2.375	0	--	0	-200,000	0	-166,650
Outside	7.437	2	--	-88,800	-110,200	-74,700	-91,850
			0.052				
Sleeve, Inside	7.437	2	--	-88,800	+102,000	-74,700	+85,000
Outside	13.375	3	--	-23,200	+35,750	-19,700	+29,300
			0.033				
Container, Inside	13.375	3	--	-23,200	+51,175	-19,700	+42,650
Outside	22.0	0	--	0	+27,625	0	+23,000

The hoop and radial components of the stresses developed in the container assembly solely by internal pressure, or independent of prestress, were also calculated. The values are given in Table L. The stresses resulting from the combined effects of the shrink fits and internal pressure are equal, of course, to the algebraic sums of the appropriate values in Tables XLIX and L. The resultant stresses, at various locations, are indicated on Figures 68 and 69.

TABLE L. STRESSES RESULTING SOLELY FROM AN INTERNAL PRESSURE OF 250,000 PSI

Component	Stress, psi	
	Radial	Hoop
Liner, Inside	-250,000	+255,900
Outside	-23,900	+28,750
Sleeve, Inside	-23,900	+28,750
Outside	-8,000	+10,900
Container, Inside	-8,000	+10,900
Outside	0	+5,775

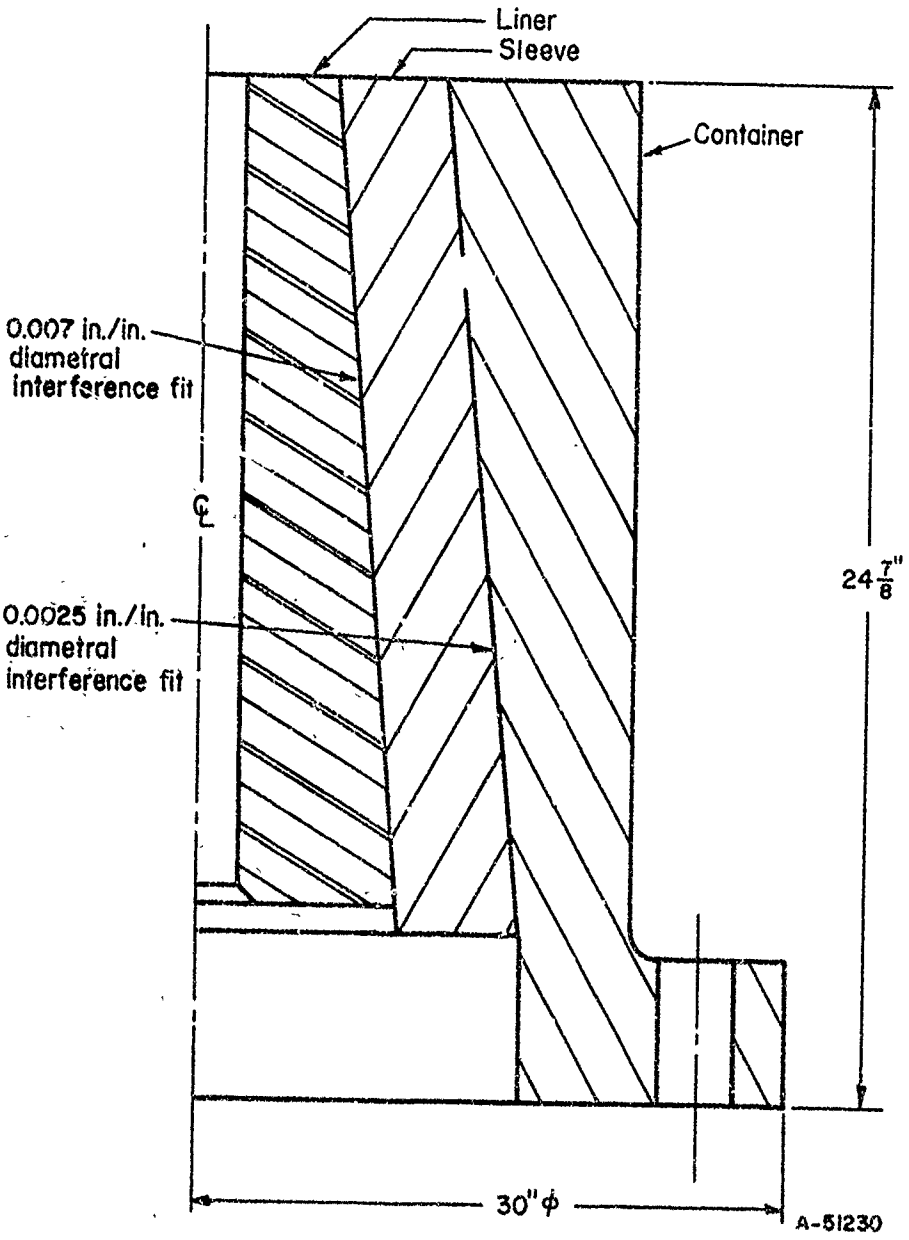

FIGURE 67. CROSS-SECTIONAL VIEW OF CONTAINER I

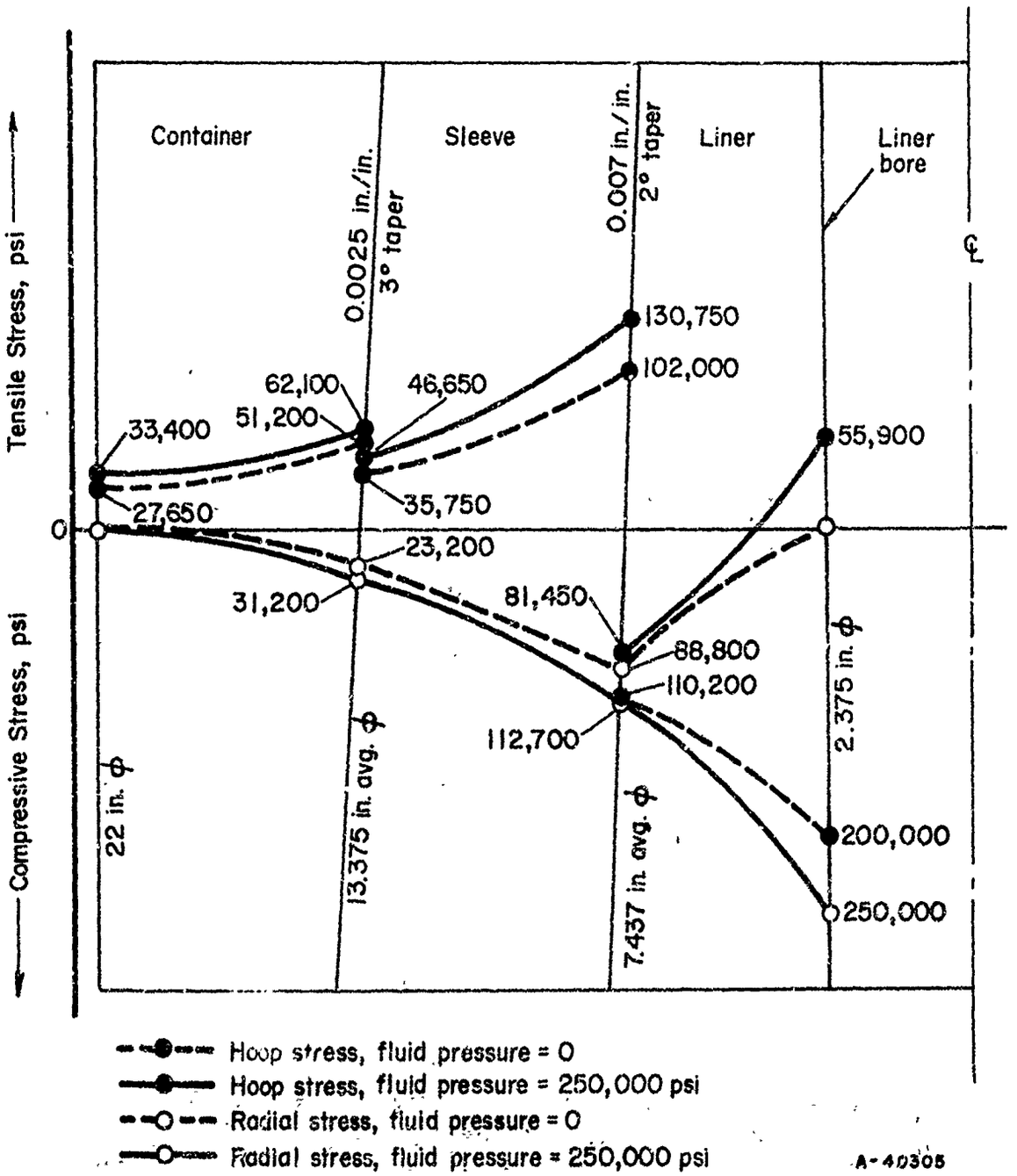

FIGURE 68. STRESS PATTERN IN CONTAINER I AT ROOM TEMPERATURE

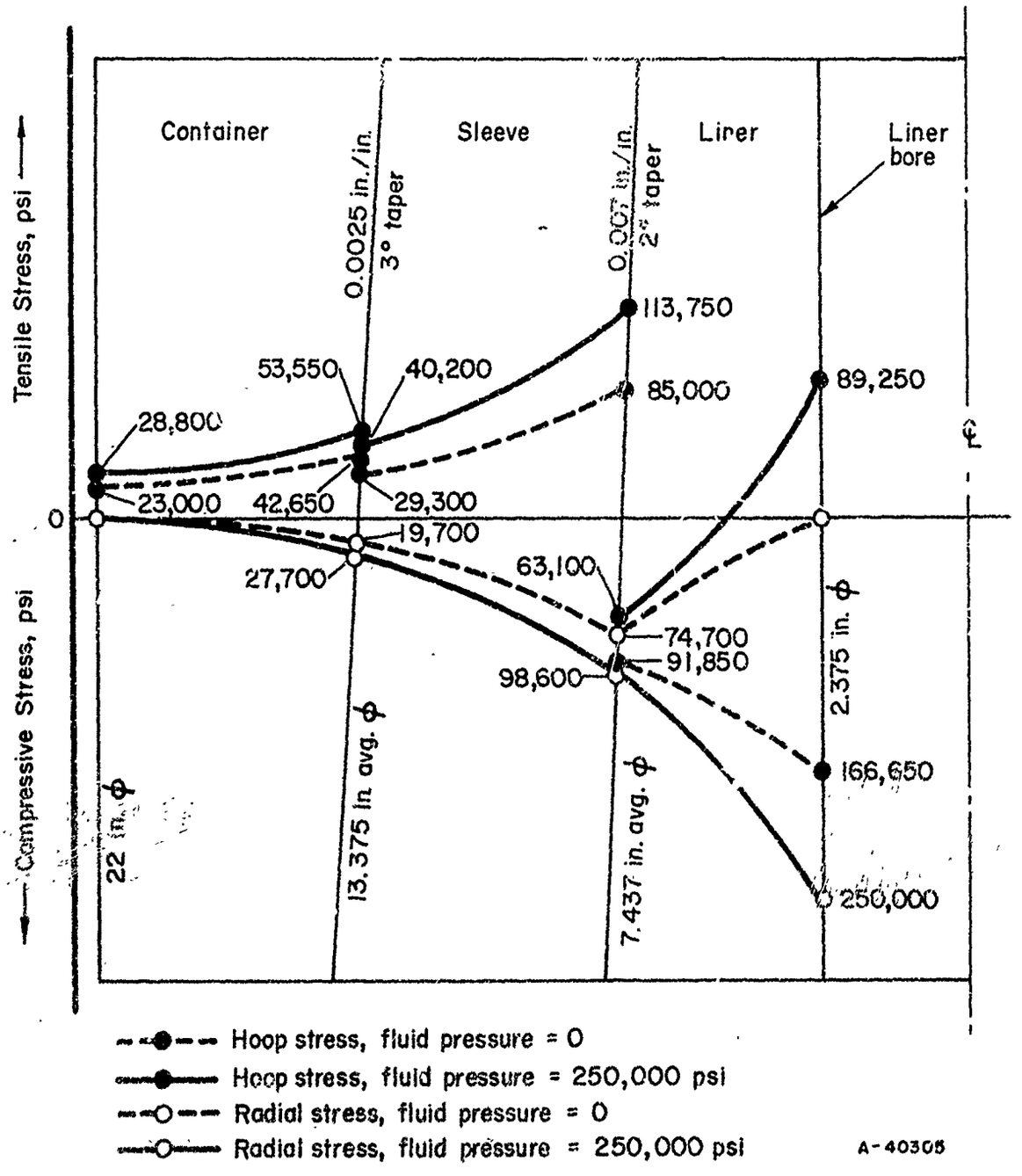

FIGURE 69. STRESS PATTERN IN CONTAINER I AT 500 F

The fact that the elastic modulus of the liner, sleeve, and container materials would be less at 500 F than at 80 F, lower estimates of interfacial pressures and prestresses were obtained.

The combined effect of the liner-sleeve and sleeve-container shrink fits caused a hoop prestress of -200,000 psi, at 80 F, on the liner bore. Figure 68 shows that, for this amount of precompression, an internal pressure of 250,000 psi produces a tensile hoop stress on the bore of only 55,900 psi. As shown in Figure 69, a similar internal pressure at 500 F would produce a tensile hoop stress of 89,250 psi at the bore.

In spite of these relatively low hoop stresses, obtained by using the heavy shrink fits, the effective stresses at the bore are extremely severe. For example, the effective shear stress at 500 F, where $\sigma_1 = +89,250$ psi and $\sigma_3 = -250,000$ psi, is approximately 175,500 psi. This means that the uniaxial yield strength of the liner material at 500 F would have to be about 304,000 psi to avoid yielding. Obviously, this is a difficult requirement for most liner materials to meet.

The types of steel ordinarily used for hot-working tools do not have sufficient strength for the application. Some of the high-speed-type tool steels which will develop adequate strength levels are lacking in ductility. Although tungsten carbide has an extremely high compressive strength, the cost of such a large component would be prohibitive.

The compositions of the steels selected for the three parts of the container assembly are given in Table LI. The steel selected for the liner appeared to have the most suitable combination of strength and ductility of materials available in suitable sections. It was less expensive than some of the other materials considered such as tungsten carbide. Both the liner and sleeve were made from steel produced by consumable-electrode vacuum-melting practices. It was expected that this melting process would minimize alloy segregation and inclusion contents. The heat treatments given the components, and the resulting hardnesses, are also given in Table LI.

The components were subjected to ultrasonic inspection at different stages of manufacture. One forging intended for the container ring was scrapped in the rough-machined condition on the basis of the inspection.

The mating surfaces of the components were finished to a surface roughness of 65 μ-in., rms. The inside surface of the liner was ground to a surface finish of 4 μ-in., rms. The smoother surface minimizes the possibility of fluid leaking past the seals at high pressures.

Operational Capabilities Predicted by Theory

Despite the high stresses on the liner and sleeve, stress analyses indicated that the container assembly would meet or closely approach the operational requirements. Table LII presents the results of the stress analyses of greatest interest. The safety factors listed were based on reasonable estimates of the tensile yield strengths and the effective stresses computed by the Hencky-Von Mises relationship. They indicated the container assembly was capable of operating at an internal pressure up to 250,000 psi at room temperature and up to 230,000 psi at 500 F.

TABLE LI. COMPOSITIONS, HEAT TREATMENTS, AND HARDNESSES OF THE COMPONENTS USED FOR CONTAINER I

	Liner AISI M50	Sleeve AISI H11	Container AISI 4340
Composition, percent			
Carbon	0.80	0.41	0.35
Chromium	3.96	5.10	0.97
Molybdenum	4.05	1.23	0.41
Vanadium	1.10	0.50	0.11
Nickel	0.06	--	2.39
Manganese	0.23	0.27	0.70
Silicon	0.20	0.94	0.28
Phosphorus	0.01	0.002	0.012
Sulfur	0.007	0.003	0.011
Cobalt	0.02	--	--
Copper	0.06	--	--
Tungsten	0.03	--	--
Heat Treatment			
Preheat	1500 F for 1-1/2 hour		
Austenitize	2000 F for 1/4 hour	1850 F for 1-1/2 hours	1570 F for 6 hours
Quench	1050 F for 5 min. in salt bath. air cool	Air cool	Oil bath
Temper	1000 F for 6 hours 1000 F for 6 hours	1000 F for 4 hours 1025 F for 4 hours 1025 F for 4 hours	900 F for 12 hours
Hardness			
Rockwell "C"	63	57/58	43

TABLE LII. SAFETY FACTORS ESTIMATED FOR THE COMPONENTS OF CONTAINER I FOR VARIOUS OPERATING CONDITIONS

Component	Type of Steel	Tensile Temperature, F	Tensile Yield Strength(a), psi	Shear Yield Strength(b), psi	Internal Pressure, psi	Effective Stress on Component(c), psi	Safety Factor(d)
Liner (ID)	AISI M50	80	330,000	190,000	250,000	162,250	1.17
		500	290,000	167,000	250,000	173,500	0.95
		80	330,000	190,000	230,000	144,000	1.32
		500	290,000	167,000	230,000	156,500	1.07
Sleeve (ID)	AISI H11	80	240,000	138,500	250,000	121,000	1.14
		500	215,000	124,000	250,000	106,250	1.17
		80	240,000	138,500	230,000	117,000	1.18
		500	215,000	124,000	230,000	104,250	1.19
Container (ID)	AISI 4340	80	180,000	92,300	250,000	47,250	1.95
		500	125,000	72,100	250,000	41,250	1.75
		500	125,000	72,100	230,000	40,750	1.77

(a) Estimated from measured hardnesses.
(b) Estimated as being 0.577 of tensile yield strength.
(c) Stress computed by Hencky-Von Mises relationship; shear stress by Tresca relationship would be approximately 2 to 6 percent lower.
(d) Based on ratio of shear yield strength to effective stress.

During the experimental research program the container assembly was operated approximately 12 times at 500 F and pressures up to 250,000 psi on the ram or stem. Based on experience at room temperature, the internal fluid pressures in those experiments are believed to have reached about 225,000 psi at the inside surface of the liner. The container was operated in approximately 350 experiments at room temperature. Fluid pressures inside the container ranged up to 265,000 psi. However, early in this program, the liner failed after holding at a fluid pressure of 246,000 psi (at 80 F) for 2-3/4 minutes. The failure consisted of a longitudinal crack that ran from the bottom of the liner to about 3-1/2 inches from the top and terminated in a transverse crack. At the time of failure, the stem was inserted about 4 inches into the liner bore. The longitudinal crack did not extend much beyond this point, evidently because of the high compressive prestresses on the bore above the stem seals.

The liner had been made from consumable, vacuum-melted AISI-M50 tool steel. Examination of the fractured surfaces of the liner by several techniques indicates that the failure resulted from low-cycle fatigue. The failure appears to have initiated at a point near the middle of the longitudinal crack. A photomacrograph at 25X of the fractured surface at the suspected point of initiation is shown in Figure 70. It is noted that radial markings appear to emanate from a small round void indicated by an arrow. This void is approximately 0.005 inch in diameter and is located about 0.008 inch beneath the liner bore surface. The mating fractured surface contains a protrusion which appears to match the void in size, shape, and location.

The precise nature of the protrusion is not known. It is suspected that it is an inclusion, although it is unusually large for consumable, vacuum-melted materials in which inclusions generally are no larger than about 0.0005 inch. This was found to be

25X 25674

FIGURE 70. FRACTOGRAPH OF FRACTURED SURFACE OF LINER OF CONTAINER I

ow points to void located about 0.008 inch beneath the linet bore surface.

the case on metallographic examination of other specimens taken close to the origin of failure. In spite of the relatively large size of the suspected defect, however, it is still far below the sensitivity range (3/64 inch) of the ultrasonic equipment used to inspect the liner during fabrication. Detection would have been made even more difficult, of course, if the protrusion had filled the void completely at the time of testing.

Electron microscopic fractography was employed to determine the mode of crack propagation in the vicinity of the origin. A standard two-stage plastic carbon replication technique was used to obtain replicas of an area approximately 0.1 $inch^2$ containing the above described void. Examination at a magnification of 12,200X revealed the fractured surface to be generally flat and featureless with localized regions containing very fine fatigue striations. The fatigue striations are indicated by the arrows in the electron microscopic fractograph shown in Figure 71. The small spacing of the striations suggests that crack growth may not have been due to the extrusion pressure cycles alone, but also to a vibration or pulsation superimposed on the high pressure. An obvious source of this vibration is the hydraulic pump of the press which can transmit pulsations to the liner by way of the stem and hydrostatic fluid. The extent to which such vibrations may have contributed to the rate of crack growth is not known.

Another feature of significance is evident in the fractograph shown in Figure 72. This is the typical cleavage-type fracture (fan-like striations indicated by arrow) of undissolved carbides. This observation indicates that these particles would have accelerated growth of the fatigue crack by fracturing in a brittle manner on a single cycle of load over a distance much larger than the crack growth per cycle indicated by the very fine striations noted earlier.

Metallographic examination of an area adjacent to the void revealed interdendritic networks of undissolved carbide particles.

Container II

Revised Container-Assembly Design

Tooling components that are made from low-ductility materials and operate in service at low safety factors are prone to failure by low-cycle fatigue.[23, 48] The liner component is a case in point. To minimize possible problems with low-cycle fatigue, it was felt at the time that the service stresses should be held below the elastic limit, rather than below the 0.2 percent offset yield strength of the material. One of the problems, however, was the lack of adequate and reliable data on elastic limit and yield strength of AISI-M50 steel (liner material) in the hardness range of R_C 61 to 63. In the absence of such data, a minimum safety factor of 1.25 (based on best estimates of yield strength) was selected for the revised design to reduce the possibility of stressing the component above the elastic limit.

Changes in the container assembly design aimed at increasing the safety factor were necessarily limited to those which would keep fabrication costs to a minimum. Thus, possible design changes were narrowed to two options, both of which included use of the present sleeve and container components. In one design, use of a tungsten carbide liner was considered because of its high compressive yield strength. However, this design was eliminated because the difference in thermal-expansion coefficients between steel and carbide (6.5×10^{-6} versus 2.5×10^{-6} inch/inch/F) would cause the

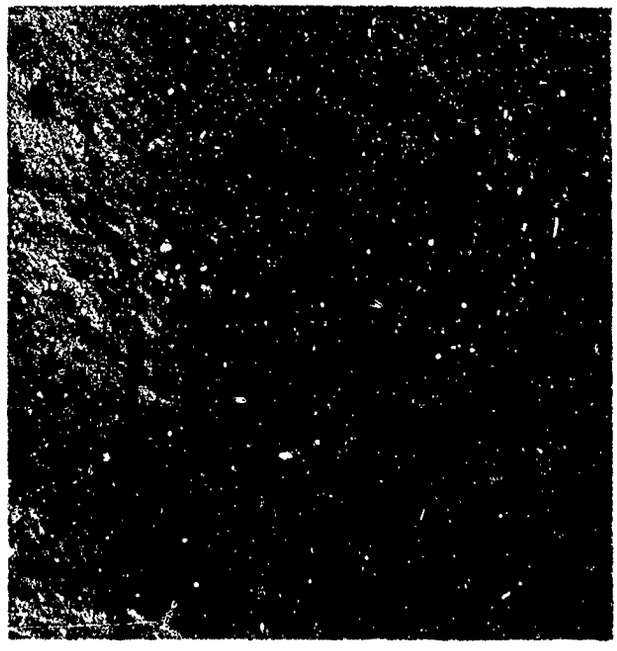

12,200X E1646A

FIGURE 71. ELECTRON MICROSCOPIC FRACTOGRAPH SHOWING FINE FATIGUE STRIATIONS IN LINER OF CONTAINER I

6,200X E1646E

FIGURE 72. ELECTRON MICROSCOPIC FRACTOGRAPH SHOWING CLEAVAGE FRACTURE OF UNDISSOLVED CARBIDES IN LINER OF CONTAINER I

required interference fit between the liner and sleeve to be lost during operation at 500 F.

The second design consisted of replacing the liner component with two rings which occupy the same volume as did the liner component. This design was used because calculations indicated that the safety factor could be increased to a minimum of about 1.25 without resorting to any larger interference fits than were used in the present container assembly.

The final revised container assembly design is illustrated in Figure 73. To avoid possible confusion, the designations for the component rings have been changed as follows:

Container I (Figure 67)	Container II (Figure 73)
Liner	Liner
(None)	Sleeve 1
Sleeve	Sleeve 2
Container	Container

In other words, Sleeve 1 was a new addition to the old design, but Sleeve 2 is the same component as the "sleeve" in the old design.

Stress Analysis

Referring to Figure 73, it can be seen that the liner was assembled with the same manufactured* interference fit of 0.007 in./in. as that in the previous container. However, because the liner in Container II had a thinner wall such an interference would generate a higher hoop prestress on assembly than was obtained in Container I providing the "assembly" interferences were also of the same order. To achieve the same "assembly" interference between the liner and Sleeve 1 shown in Figure 73 as that obtained in Container I, it was found necessary to manufacture an interference of 0.0048 in./in. between Sleeve 1 and Sleeve 2. Measurements of the liner bore before and after assembly were used to determine the actual stress distribution achieved in the assembly. Equations 13 and 14 in Section 3 were used in these calculations.

The stress patterns calculated for both room temperature and 500 F are presented in Figures 74 and 75. Each figure shows both the hoop and radial stresses developed at the ring interfaces under internal fluid pressures of 0 and 250,000 psi.

The combined interference fits of 0.0071 and 0.0048 inch per inch on the Sleeve 1-liner and Sleeve 2-Sleeve 1 interfaces, respectively, place the liner bore in precompression with a stress of 260,650 psi at room temperature. With this amount of precompression, it can be seen in Figure 4-8 that an internal pressure of 250,000 psi at room temperature produces a tensile hoop stress on the liner bore of only 5,600 psi. At 500 F, the precompression is reduced from 260,650 to 217,250 psi (Figure 75) because of the decrease in elastic moduli of the rings at this temperature. In this case, the tensile stress on the liner bore at maximum internal pressure is increased from 5,600 to 49,000 psi.

*The "manufactured" interference is that which is obtained before assembly and represents the difference in size between each mating diameter. The "assembled" interference is greater than the "manufactured" interference before assembly by an amount proportional to the extent that each ring changes dimensions elastically as the rings are assembled.

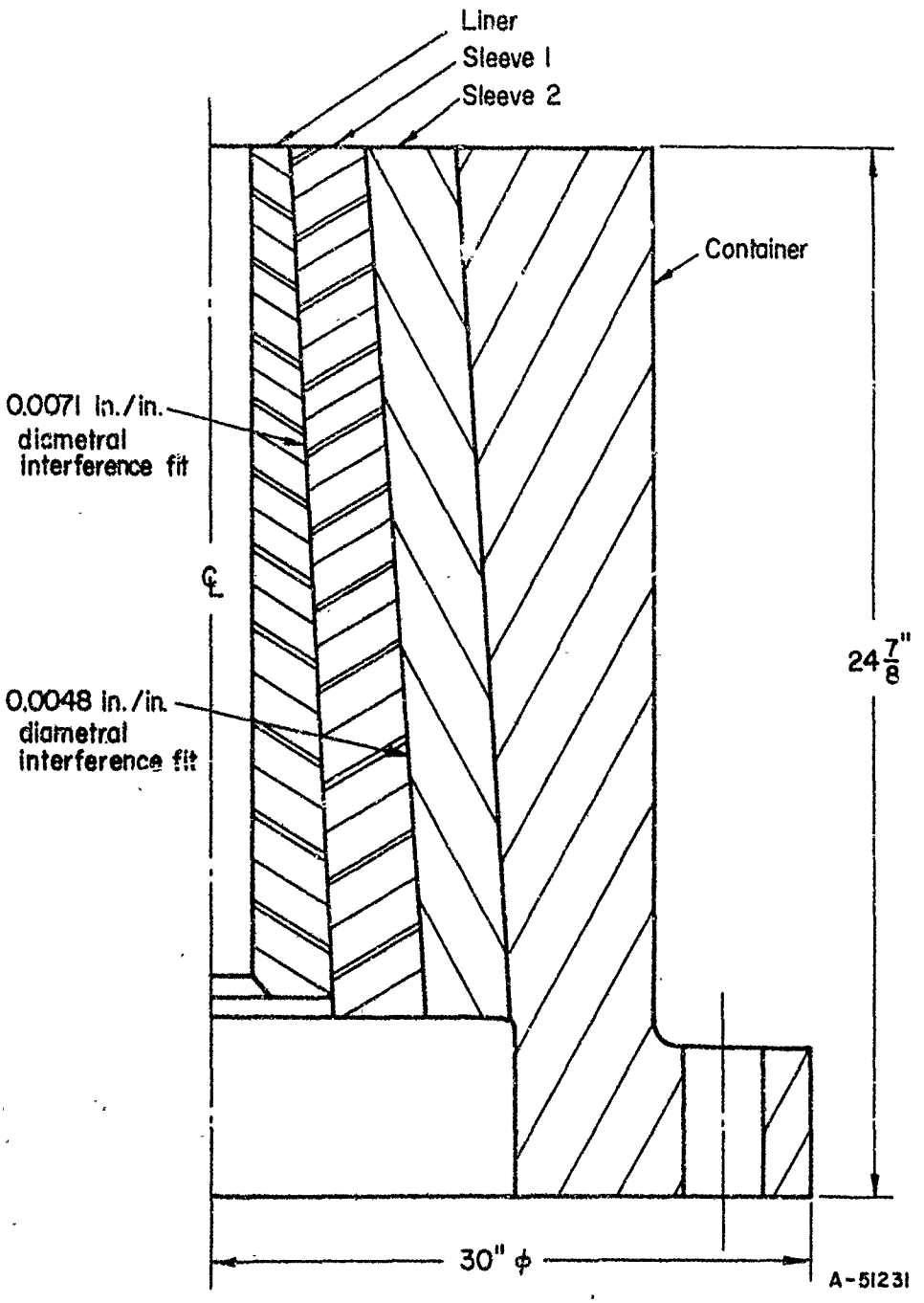

FIGURE 73. CROSS-SECTIONAL VIEW OF CONTAINER II

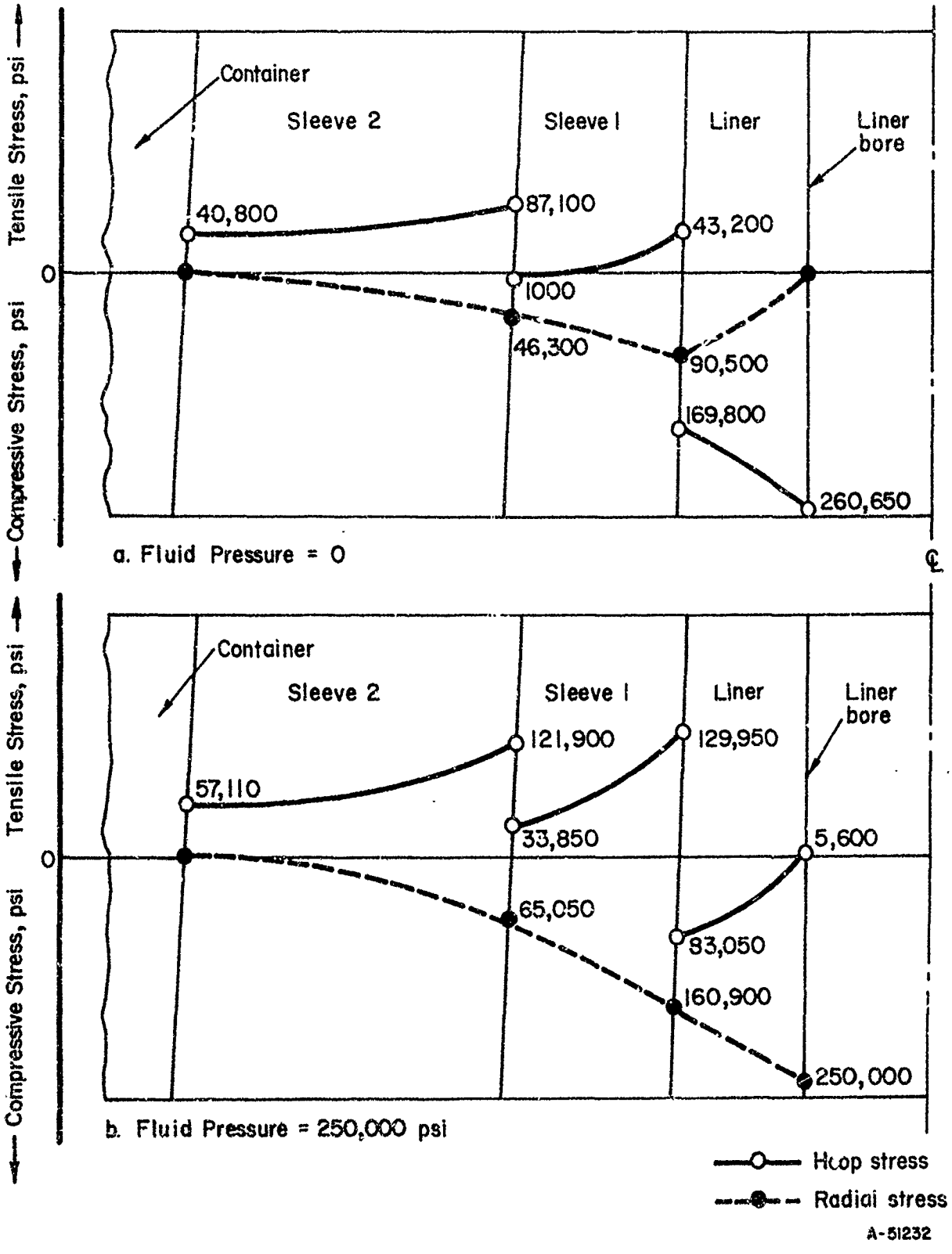

FIGURE 74. STRESS PATTERN IN CONTAINER II AT ROOM TEMPERATURE

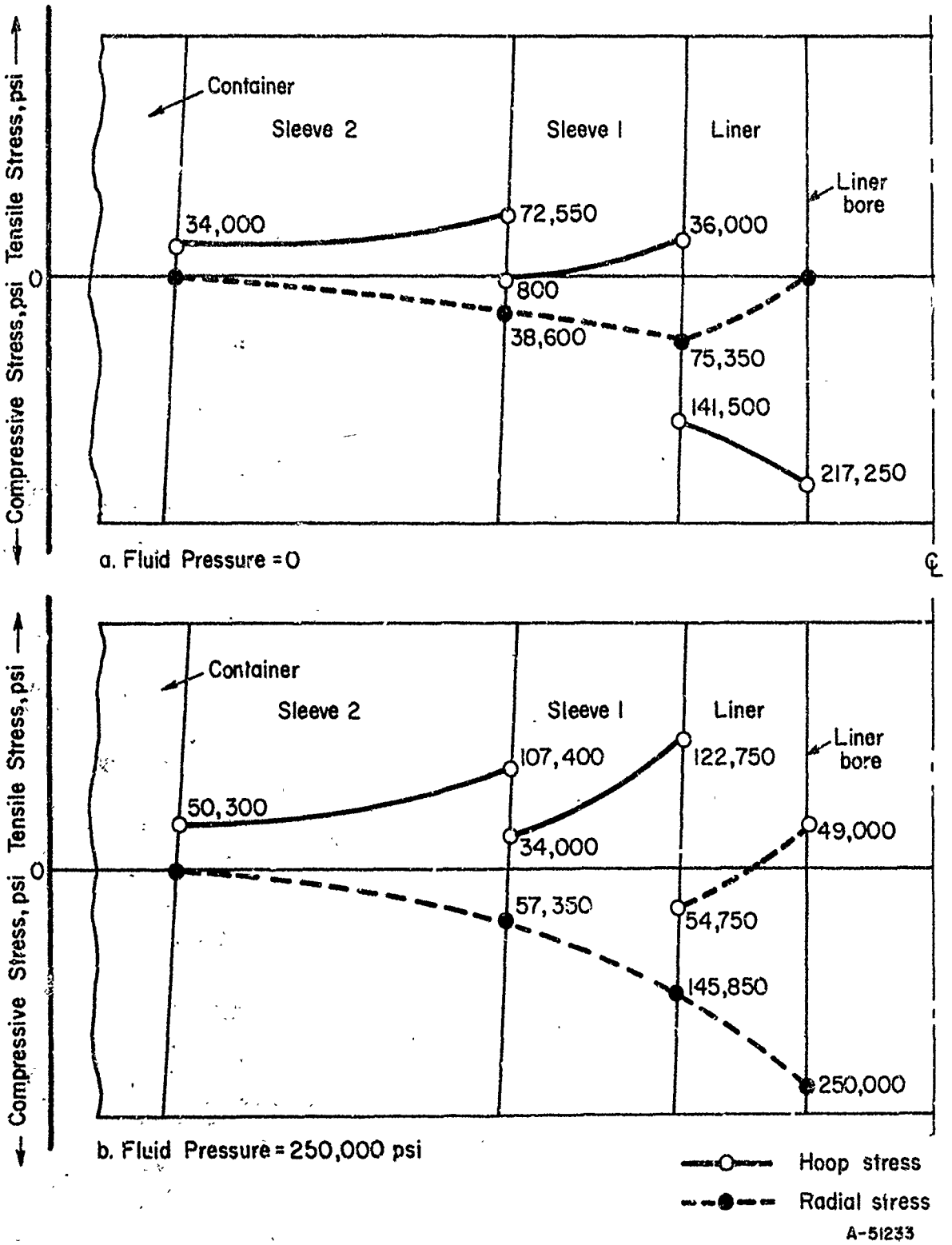

FIGURE 75. STRESS PATTERN IN CONTAINER II AT 500 F

Component Ring Materials

Consumable-electrode vacuum-melted AISI-M50 tool steel was selected for the liner and Sleeve 1 rings. This tool steel, which had been used in the original liner, was selected over other candidate steels (such as AISI-M1 or M10) because it possessed the most suitable combination of strength and ductility. Each component was hardened to R_C 61 to 63.

Sleeve 2 and the container ring were made of AISI-H11 (R_C 57) and 4340 (R_C 43) steels, respectively.

Operational Capabilities

Safety factors were calculated for internal fluid pressures of 250,000 and 230,000 psi at both room temperature and 500 F. They were also calculated for a fluid pressure of 220,000 psi at 500 F. The results of the calculations are given in Table LIII. It can be seen that the safety factors for the liner and Sleeve 1 are 1.29 and 1.30, respectively, for operation at fluid pressures of 250,000 psi at room temperature. At 500 F, the safety factors fall below the minimum of 1.25. Thus, the fluid pressure must be reduced for 500 F operation to minimize the possibility of low-cycle fatigue. At 230,000 psi, the safety factor for Sleeve 1 is 1.37 but only 1.18 for the liner. In view of this, it is recommended that fluid pressures at 500 F do not exceed about 220,000 psi. At this pressure level, the safety factors are 1.27 for the liner and 1.33 for Sleeve 1.

TABLE LIII. SAFETY FACTORS ESTIMATED FOR LINER, SLEEVE 1 AND SLEEVE 2 OF CONTAINER II FOR VARIOUS OPERATING CONDITIONS

Component	Type of Steel	Tensile Temperature, F	Tensile Yield Strength, psi	Shear Yield Strength[a], psi	Internal Pressure, psi	Effective Stress on Component[b], psi	Safety Factor[c]
Liner (ID)	AISI-M50	80	330,000	190,000	250,000	146,250	1.29
		500	290,000	167,000	250,000	160,500	1.04
		80	330,000	190,000	230,000	137,000	1.48
		500	290,000	167,000	230,000	141,500	1.18
		500	290,000	167,000	220,000	132,250	1.27
Sleeve 1 (ID)	AISI-M50	80	330,000	190,000	250,000	145,500	1.30
		500	290,000	167,000	250,000	134,500	1.24
		80	330,000	196,000	230,000	135,000	1.49
		500	290,000	167,000	230,000	128,000	1.31
		500	290,000	167,000	220,000	130,000	1.29
Sleeve 2 (ID)	AISI-H11	80	240,000	138,500	250,000	95,000	1.46
		500	215,000	124,000	250,000	83,500	1.48
		500	215,000	124,000	230,000	81,500	1.52

(a) Estimated as being 0.577 of tensile yield strength.
(b) Stress computed by Hencky-Von Mises relationship.
(c) Based on ratio of shear yield strength to effective stress.

It should be noted that the stress analysis of the revised container assembly does not include any supporting contribution from the container component. This assumption was used because it is not known whether the original interference-fit of 0.0025 inch per inch between the container and Sleeve 2 could be maintained while removing and replacing the failed liner. Therefore, the stress analysis assumed that only a metal-to-metal fit existed at this interface and that the container ring was not a load-bearing component. However, if any interference-fit did exist and the container ring did bear a portion of the load, the safety factors of the revised container assembly would be slightly higher than those shown in Table LIII.

Container III

As a result of the liner fatigue failure in Container I, it was considered desirable to have a standby container which would ensure continuity in hydrostatic-extrusion research if further failures occurred. At the same time, construction of such a container presented a unique opportunity to use the up-to-date stress analysis and design for a four-ring unit based on a fatigue-life criterion.

The Design of Container III

It was decided to construct Container III with materials whose fatigue properties were known. On the basis of the data given in Tables XLI, XLII and XLIII, AISI H11 tool steel was considered to be a good candidate material. Calculations showed that a fatigue life of 10^5 - 10^6 cycles could be achieved with AISI H11 within the 250,000 psi pressure limit.

A four-ring container, similar in dimensions to those of Container II, Figure 67, was chosen for analysis. The liner was considered to be of high-strength steel surrounded by lower strength, ductile outer rings. The analysis of residual stresses (prestresses) and the required shrink-fit interferences were programmed for calculation of the Battelle computer. The computer codes developed at Battelle for this container design were:

PROGRAM COMPHS1 - Calculation of maximum pressure-to-strength ratio for container having an ultrahigh-strength liner.

PROGRAM COMPHS2 - Calculation of operating stresses, prestresses at operating temperature, and interferences required for shrink fit assembly.

The hoop and radial components of the design prestresses and operating stresses at room temperature are plotted at their various locations in the assembly in Figure 76. The combined effect of the multiple shrink fits was to cause a compressive hoop stress of 256,000 psi on liner bore. Under an internal fluid pressure of 250,000 psi the figure shows that the design tensile hoop stress produced on the bore is zero.

The high interface and hoop stresses, bore pressures of both zero and 250,000 psi, were considered to be out of the realm of the capabilities of an alloy such as AISI 4340, which was used previously as an outer ring material. Consequently, AISI H11 tool steel in a softer condition than the liner, was chosen for the outer rings. The composition, heat treatment and hardnesses of the H11 steel produced by consumable-

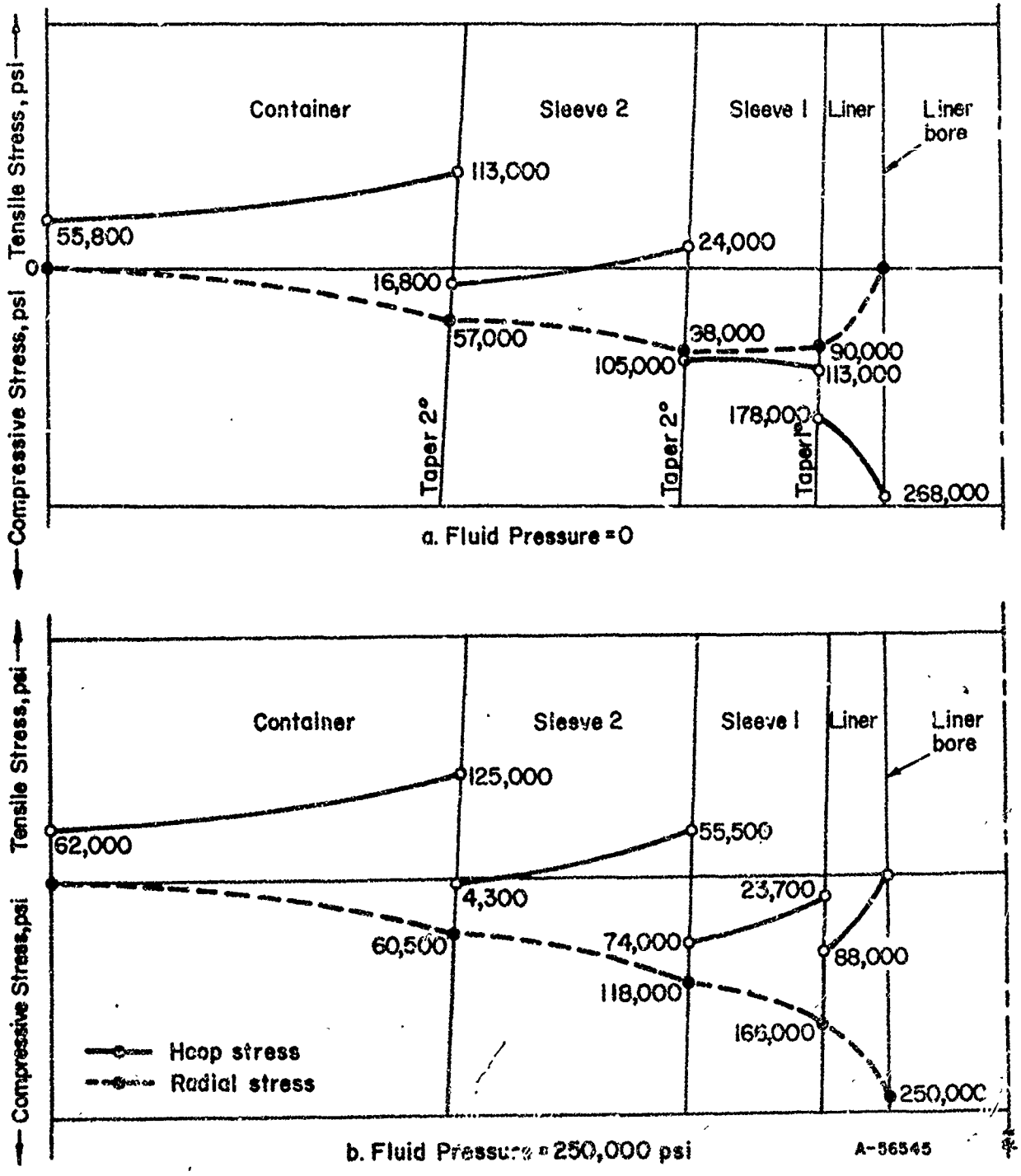

FIGURE 76. DESIGN STRESS PATTERN IN CONTAINER III AT ROOM TEMPERATURE

electrode vacuum-melting practices, used for constructing the container are given in Table LIV. A thorough ultrasonic inspection of each ring revealed no measurable defects.

TABLE LIV. COMPOSITION, HEAT TREATMENT, AND HARDNESSES OF THE COMPONENTS USED FOR THE FOUR-RING ASSEMBLY OF CONTAINER III

AISI-H11, Nominal Composition, percent - (All rings)				
0.41 Carbon	5.1 Chromium	1.23 Molybdenum		
0.5 Vanadium	0.27 Manganese	1.0 Silicon		
		Heat Treatment		
Austenitize		1850 F for 1-1/2 hr	All rings	
Quench		Air cool		
Temper, liner		950 for 2 hr		
		1000 for 2 hr		
		1000 for 2 hr		Hardness - R_C 54/56
Temper, outer three rings		1090 for 4 hr		
		1100 for 4 hr		
		1110 for 4 hr		Hardness - R_C 44/46

Because the whole container unit was made from the same material, the coefficient of thermal expansion in each ring under temperature was the same. (It was not expected that differences in hardness levels of the rings would markedly affect the coefficient of thermal expansion.) Therefore, the stress distribution pattern for the rings at 500 F would be the same as those shown in Figure 76b. However, the pressure capability at 500 F is limited to 225,000 psi by the effect of temperature on strength. Therefore, the interface stresses predicted in Figure 76b would be less proportionately to the bore stresses, in service at 500 F. The same pressure limit, 225,000 psi at 500 F was also imposed on Containers I and II.

It is pertinent at this stage to compare the residual stress patterns in Container II, Figure 74a, with those predicted for Container III. It is seen that the design hoop prestress of 268,000 psi in the H-11 liner of Container III is about 3 percent higher than that for the harder AISI-M50 liner in Container II. In view of the lack of knowledge of the fatigue properties of AISI-M50 it is not possible to determine what the predicted fatigue life of Container II would be. However, rotating-beam fatigue data obtained on a similar type of material AISI M2 at a hardness of R_C 62, suggests that the fatigue limit at 10^6 cycles for AISI-M50 might be about 140,000 psi whereas for AISI H11 the corresponding figure is 150,000 psi.[49]

Container Assembly

The four rings, which were slightly tapered for press fitting, were assembled by a hydraulic press from the outer ring inwards. A lubricant was applied to the interfaces of the rings to ease assembly. The calculated press loads required for assembly

ars given below with the associated manufactured interferences. The press loads were estimated by assuming an interface coefficient of friction of 0.1.

Ring	Load, tons	Manufactured Interference, inch/inch
Sleeve 2 into container housing	1500	0.00208
Sleeve 1 into assembly	1040	0.00443
Liner into assembly	1130	0.00443

It is important to note that all the interferences given above are as manufactured and not as generated during assembly. The assembly interference achieved in pressing the liner into position was 0.0092 inch/inch. It was not possible to determine the actual press loads required because in each case, the rings were pressed home in a continuous stroke up to the press capacity of 2200 tons.

By measuring the liner bore diameter before and after its assembly, the actual surface hoop prestress was calculated to be -255,000 psi. This is lower than the design prestress of -268,000 psi. While the maximum pressure capability of the container remains at 250,000 psi, the effect of the reduction in prestress obtained is expected to marginally reduce the fatigue life (10^6 cycles) compared to the design value.

APPENDIX I

ELASTICITY SOLUTION FOR A RING SEGMENT

A ring segment is shown in Figure 77. Its geometry is defined by the radii r_1 and r_2 and the angle α. The loading of the segment is a pressure p_1 at r_1 and p_2 at r_2. For equilibrium, p_2 is related to p_1 by Equation (21) in the text; i.e.,

$$p_2 = \frac{p_1}{k_2} \tag{92}$$

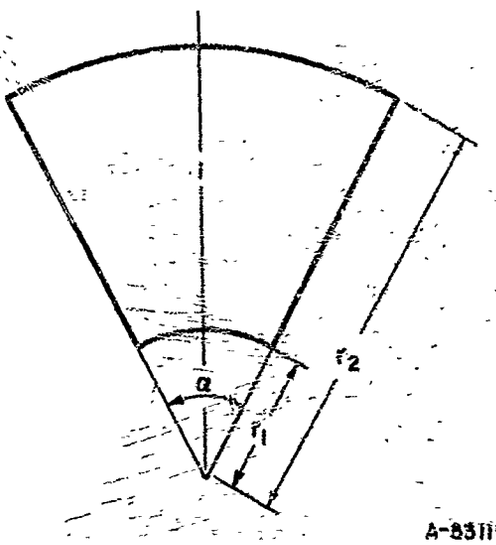

FIGURE 77. GEOMETRY OF RING SEGMENT

The solution for the stresses within the segment is found by superposition of two solutions: The Lamé solution for a cylinder, Equations (13a-c) and (14a, b) in the text, plus a bending solution, Equations (48) and (53) in Reference (41). The bending solution removes the moment from the sides of the segment that exists in the Lamé solution. The latter equations for the bending solution are written as

$$(\sigma_r)_b = \frac{4M_1 p_1}{\beta_1} f_1(r), \quad (\sigma_\theta)_b = \frac{4M_1 p_1}{\beta_1} f_2(r), \quad (\tau_{r\theta})_b = 0 \tag{93a-c}$$

and

$$\left(\frac{u}{r}\right)_b = \frac{M_1 p_1}{E_2 \beta_1} f_3(r) + \frac{G_1 p_1}{r} \cos\theta$$

$$\left(\frac{v}{r}\right)_b = \frac{8M_1 p_1}{E_2 \beta_1} (k_2^2 - 1)\theta - \frac{G_1 p_1}{r} \sin\theta \qquad (94a\text{-}c)$$

where $f_1(r)$, $f_2(r)$, and $f_3(r)$ are defined by Equations (20a-c) in the text and where

$$\beta_1 \equiv (k_2^2 - 1)^2 - 4k_2^2 (\log k_2)^2 \qquad (95)$$

The moment $M = M_1 p_1 r_1^2$ is found by integrating the negative of the Lamé hoop stress $(\sigma_\theta)_c$ for a cylinder given by Equation (13b) in the text over the side of the segment; i.e.,

$$M = -\int_{r_1}^{r_2} (\sigma_\theta)_c \, r \, dr \ ,$$

hence,

$$M_1 = \frac{\pi l}{p_1 r_1^2} \int_{r_1}^{r_2} \left\{ \frac{(p_1 - p_2 k_2^2)}{k_2^2 - 1} - \frac{(p_2 - p_1) k_2^2}{k_2^2 - 1} \left(\frac{r_1}{r}\right)^2 \right\} r \, dr$$

$$M_1 = -\frac{1}{2}\left(1 - \frac{p_2}{p_1} k_2^2\right) + \left(\frac{p_2}{p_1} - 1\right) \frac{k_2^2}{k_2^2 - 1} \log k_2 \qquad (96)$$

G_1 is found by taking a reference point for the radial deflection u. If the point $r_0 = \frac{r_1 + r_2}{2}$, $\theta = 0$ is fixed,

then

$$G_1 = -\frac{M_1 r_0}{E_2 \beta_1} \left\{ -4(1+\nu) k_2^2 \left(\frac{r_1}{r_0}\right)^2 \log k_2 + 4(1-\nu) \left[k_2^2 \log\left(\frac{r_0}{r_1}\right) - \log \frac{r_0}{r_1} \right] - 4(k_2^2 - 1) \right\} \qquad (97)$$

The equations for the total stresses and displacements in ring segments were programmed on the computer and some calculations carried out. Example results are given in Table LV for $k_2 = 2.0$ and $\alpha = 60$ degrees. It is noted that a small residual stress σ_θ remains on the side of the segments. To be more accurate, i.e., to achieve sides entirely free of stress, the residual σ_θ could be removed by using a "dipole" solution in addition to the bending solution. However, the self-equilibrating residual stress that would be removed ha. a local edge effect according to the principle of St. Venant. Therefore, the σ_θ stresses in Table LVI are believed to be indicative of the actual magnitude of hoop stresses in segments at the center.

TABLE LV. STRESSES AND DEFLECTIONS IN A RING SEGMENT, $k_2 = 2.0$, $\alpha = 60°$, $\nu = 0.3$

r/r_1	σ_r/p_1	σ_θ/p_1	$\frac{Eu}{p_1}$ at $\theta = 0°$	$\frac{Ev}{rp_1}$ at $\theta = 30°$
1.0	-1.0000	0.0394	0.6324	-0.1301
1	-0.9068	0.0123	0.4877	-0.0853
1.2	-0.8310	-0.0033	0.3747	-0.0480
1.3	-0.7676	-0.0112	0.2846	-0.0164
1.4	-0.7137	-0.0137	0.2117	0.0107
1.5	-0.6670	-0.0126	0.1519	0.0341
1.6	-0.6260	-0.0089	0.1022	0.0547
1.7	-0.5896	-0.0033	0.0606	0.0728
1.8	-0.5568	0.0035	0.0254	0.0890
1.9	-0.5271	0.0113	-0.0046	0.1034
2.0	-0.5000	0.0197	-0.0303	0.1163

Appreciable bending, displacement v, is also noted. The bending increases with segment size and angle α as shown in Table LVI. This bending would tend to cause the segments to dig into the liner as shown in Figure 78. Therefore, it is recommended that segments be designed with radii larger than the radii of mating cylinders in order to compensate for the change in radii due to bending. This is illustrated in Figure 78.

Note that the deflection u in Table LV can have an arbitrary translational component; i.e., the segment is free to move radially a constant amount. In calculating interferences, the difference in deflection $u(r_1) - u(r_2)$ at $\theta = 0°$ is used and the constant amount drops out.

ELASTICITY SOLUTION FOR A PIN SEGMENT

A pin segment is shown in Figure 79. Its geometry is defined by the radii r_1 and r_2 and the angle α. r_2 is taken to the inside of the pin holes as indicated. The loading of the pin segment is more complicated than that of the ring segment as shown in Figure 80. A constant pressure p_1 is assumed to act at the inside. A variable pressure is assumed to act at the outside, i.e.,

$$\sigma_r = -p_1, \text{ at } r_1$$
$$\sigma_r = -p_2 (1 + \cos m\theta), \text{ at } r_2 \qquad (98a,b)$$

In addition, a shear acts at r_2:

$$\tau_{r\theta} = -\tau \sin m\theta, \text{ at } r_2 \qquad (98c)$$

TABLE LVI. DEFLECTIONS IN RING SEGMENTS, $\nu = 0.3$

(a) $\alpha = 60°$

k_2	$\frac{Eu}{rp_1}$ at $\theta = 0°$		$\frac{Ev}{rp_1}$ at $\theta = \alpha$	
	$r = r_1$	$r = r_2$	$r = r_1$	$r = r_2$
1.1	0.3463	0.2291	-0.0008	0.0447
1.2	0.3899	0.1730	-0.0221	0.0612
1.3	0.4287	0.1494	-0.0408	0.0652
1.4	0.4642	0.1153	-0.0576	0.0743
1.5	0.4970	0.0611	-0.0726	0.0931
2.0	0.6324	-0.0303	-0.1301	0.1163
3.0	0.8251	-0.0905	-0.2013	0.1243

(b) $k_2 = 2.0$

α	$\frac{Eu}{rp_1}$ at $\theta = 0°$		$\frac{Ev}{rp_1}$ at $\theta = \alpha/2$	
	$r = r_1$	$r = r_2$	$r = r_1$	$r = r_2$
45°	0.6324	-0.0303	-0.1052	0.0835
60°	0.6324	-0.0303	-0.1301	0.1163
90°	0.6324	-0.0303	-0.1529	0.1957

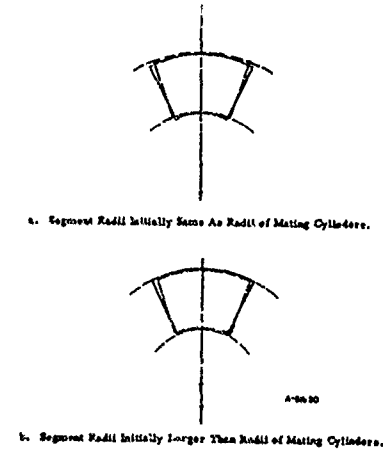

FIGURE 78. BENDING DEFORMATION OF RING SEGMENTS

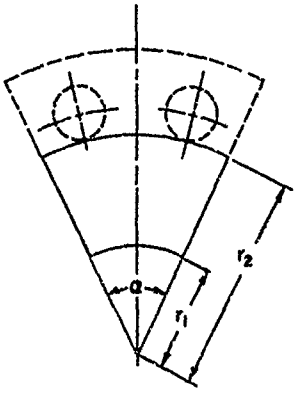

FIGURE 79. GEOMETRY OF PIN SEGMENT

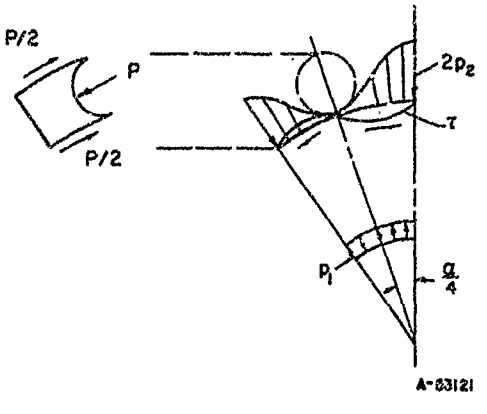

FIGURE 80. LOADING OF PIN SEGMENT

where

$$m = 4\pi/\alpha \tag{99}$$

If N_s is the number of segments then $m = 2N_s$.

The shear force $\tau_{r\theta}$ must balance the pin force P shown in Figures 80 and 81. From Figure 80, it is seen for equilibrium of P, that it is required

$$t\int_{\alpha/4}^{\alpha/2} \tau_{r\theta} \cos\left(\theta - \frac{\alpha}{4}\right) r_2 d\theta = P/2$$

where t is the segment thickness. Substitution of (98c) into this integral and integration gives

$$\tau = \frac{(m^2 - 1)\,P}{2mtr_2\,(1 + \cos \pi/m)} \tag{100}$$

where P must be in equilibrium with p_1 as shown in Figure 81, i.e.,

$$P = p_1 r_1 t \ . \tag{101}$$

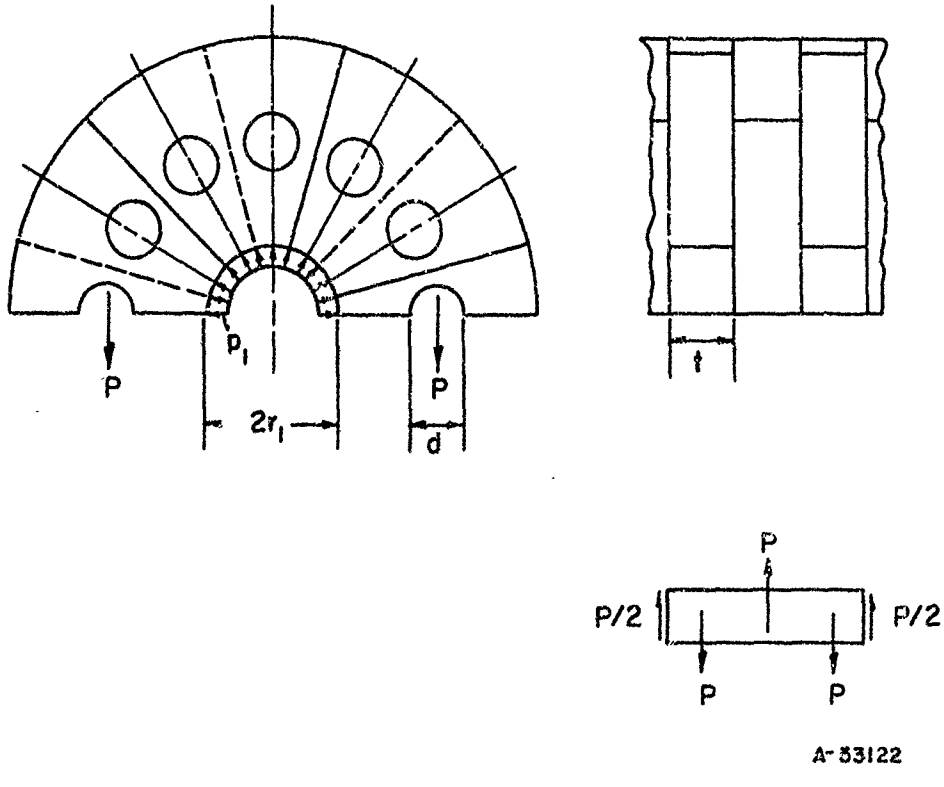

FIGURE 81. LOADING OF PINS

For radial equilibrium of the loadings shown in Figure 80, p_2 can be found by integration, i.e.,

$$2\int_0^{\alpha/2} [\tau_{r\theta}\sin\theta - \sigma_r \cos\theta]\, r_2 d\theta \,\Big|_{r_2} = 2p_1 r_1 \sin\frac{\alpha}{2} \quad .$$

Substitution for $\tau_{r\theta}$ and σ_r from (98b, c) and integration gives

$$p_2 = \frac{1}{(m^2-2)} \left[(m^2-1)\frac{p_1}{k_2} - m\tau\right] \quad . \tag{102}$$

The stresses in a pin segment are found by superposition of three solutions: the Lamé solution for constant pressures p_1 and p_2 at the r_1 and r_2 respectively, a sinusoidal solution for the variable σ_r loading $-p_2 \cos m\theta$ at r_2, and a bending solution to remove the hoop stress of the first two solutions from the sides of the segments. The Lamé solution is given by Equations (13a-c) and (14a, b) in the text. The sinusoidal solution, taken from the cos $m\theta$ part of Equation (81) in Timoshenko and Goodier[41], is

$$\begin{aligned}
\sigma_r &= \Big[m(1-m)\, a_m \rho^{m-2} + (2-m)(1+m)\, b_m \rho^m \\
&\quad - m(m+1)\, c_m \rho^{m-2} + (2+m)(1-m)\, d_m \rho^{-m}\Big] \cos m\theta \\
\sigma_\theta &= \Big[m(m-1)\, a_m \rho^{m-2} + (m+2)(m+1)\, b_m \rho^m \\
&\quad + m(m+1)\, c_m \rho^{-m-2} + (m-2)(m-1)\, d_m \rho^{-m}\Big] \cos m\theta \qquad (103a\text{-}c) \\
\tau_{r\theta} &= m\Big[(m-1)\, a_m \rho^{m-2} + (m+1)\, b_m \rho^m - (m+1)\, c_m \rho^{-m-2} \\
&\quad + (-m+1)\, d_m \rho^{-m}\Big] \sin m\theta
\end{aligned}$$

where

$$\rho \equiv r/r_2 \quad . \tag{104}$$

From the boundary conditions $\sigma_r = 0$, $\tau_{r\theta} = 0$ at r_1 and $\sigma_r = -p_2 \cos m\theta$, $\tau_{r\theta} = -\tau \sin m\theta$ at r_2 for the sinusoidal solution, the constants a_m, b_m, c_m, and d_m are found to be

$$a_m = \left(\frac{-p_2}{2} + \frac{\tau}{2}\right)\left[\frac{m^2 + (1-m^2)\, k_2^2 - k_2^{2m+2}}{\beta_2 (m-1)}\right]$$

$$+\left(\frac{-p_2}{2} - \frac{\tau}{2}\right) \frac{k_2^2 (1 - k_2^{2m})}{\beta_2}$$

$$b_m = \left(\frac{-p_2}{2} + \frac{\tau}{2}\right) \frac{mk_2^2}{\beta_2} (k_2^2 - 1)$$
$$-\left(\frac{-p_2}{2} - \frac{\tau}{2}\right) \frac{m(k_2^2 - k_2^{2m+2})}{(m+1)\beta_2}$$

$$c_m = -\left(\frac{-p_2}{2} + \frac{\tau}{2}\right) \frac{k_2^2 (1 - k_2^{-2m})}{\beta_2}$$
$$+\left(\frac{-p_2}{2} - \frac{\tau}{2}\right)\left[\frac{(1-m^2) k_2^2 - k_2^{-2m+2} + m^2}{\beta_2 (m+1)}\right] \qquad (105)$$

$$d_m = \left(\frac{-p_2}{2} + \frac{\tau}{2}\right) \frac{mk_2^2 (k_2^2 - k_2^{-2m})}{\beta_2 (m-1)}$$
$$+\left(\frac{-p_2}{2} - \frac{\tau}{2}\right) \frac{m}{\beta_2} k_2^2 (k_2^2 - 1)$$

where

$$\beta_2 \equiv m\left[-m^2 k_2^4 + 2(m^2 - 1) k_2^2 + k_2^{2-2m} + k_2^{2m+2} - m^2\right] \qquad (106)$$

The bending solution is found in a similar manner to the method used previously for the ring segment. The resulting total stresses and displacements for the pin segment are given in Equations (22a-c) and (23a, b) in the text. The functions $g_{m1}(r)$, $g_{m2}(r)$, and $g_{m3}(r)$ in Equations (22a-c) are recognized as the coefficients of cos $m\theta$ and sin $m\theta$ in Equations (103a-c). $g_{m4}(r)$ and $g_{m5}(r)$ in Equations (23a, b) are defined as:

$$g_{m4} \equiv -m(1+\nu) a_m \rho^{m-2} + \left[2(1-\nu) - m(1+\nu)\right] b_m \rho^m$$
$$+m(1+\nu) c_m \rho^{-m-2} + \left[2(1-\nu) + m(1+\nu)\right] d_m \rho^{-m}$$

$$g_{m5} \equiv m(1+\nu) a_m \rho^{m-2} + m\left[\frac{m+4}{m} + \nu\right] b_m \rho^m \qquad (107a, b)$$
$$+m(1+\nu) c_m \rho^{-m-2} + m\left[\frac{m-4}{m} + \nu\right] d_m \rho^{-m}$$

and G_2 is defined as

$$G_2 \equiv \frac{r_o}{E}\left\{ m(1+\nu) a_m \left(\frac{r_o}{r_2}\right)^{m-2} - \left[2(1-\nu) - m(1+\nu)\right] g_m \left(\frac{r_o}{r_2}\right)^m \right.$$
$$\left. -m(1+\nu) c_m \left(\frac{r_o}{r_2}\right)^{m-2} - \left[2(1-\nu) + m(1+\nu)\right] d_m \left(\frac{r_o}{r_2}\right)^{-m} \right\} \qquad (107c)$$

where

$$r_o = \frac{r_1 + r_2}{2} .$$

The bending moment is $M_2 p_1 r_i^2$ where

$$M_2 = \frac{1}{k_2^2 - 1}\left[\frac{k_2^2 - 1}{2} + k_2^2 \log k_2\right] + p_2\left[\frac{k_2^2}{2} + \frac{k_2^2 \log k_2}{k_2^2 - 1}\right]$$

$$+ \frac{1}{p_1}\left\{ - (m - 1)\, a_m\, k_2^{-m+2}\left[k_2^m - 1\right] - (m + 1)\, b_m\, k_2^{-m}\left[k_2^{m+2} - 1\right]\right.$$

$$\left. + (m + 1)\, c_m\, k_2^{m+2}\left[k_2^{-m} - 1\right] - (m - 1)\, d_m\, k_2^{m}\left[k_2^{-m+2} - 1\right]\right\} \qquad (108)$$

β_1 was defined previously by Equation (95).

The equations for stresses and deflections in pin segments were programmed on the computer and some calculations were carried out. Table LVII gives some results for $k_2 = 4.0$ and $\alpha = 60°$. At $\theta = \alpha/4 = 15°$ and $r/r_1 = 4$, edge of pin hole, it is noted that $\sigma_\theta/p_1 = 2.01$. This indicates the stress concentration effect of the hole. At $\theta = \alpha/2 = 30°$ appreciable σ_θ stress remains. The edge of the segment should be free of stress. Therefore, the results must be considered approximate. However, the residual σ_θ stress on the edge is self equilibrating and its removal would be expected to cause only a local effect near the edge according to the St. Venant principle.

Bending of the pin segment again is evident as shown by the v displacement. The variation of displacements and of the maximum σ_θ stress at the hole with segment geometry are shown in Table LVIII. Larger u displacements and smaller hoop stresses are found for larger k_2 and α. The bending displacement v increases with α but decreases with k_2.

The bending of pin segments would cause the inside corners to dig into the liner just as in the ring segments (Figure 78a). Therefore, an inside diameter of the segments larger than the outside diameter of the liner would again be recommended to counteract the bending effect.

SOLUTION FOR SHEAR STRESSES IN PINS

The pins of the pin-segment container are subject to shear and bending as shown in Figure 81. The shear stress is larger than the bending stress and will be used as the critical stress in the pins. The maximum shear stress in a circular pin is given by

$$\tau_{max} = \frac{4}{3A}(P/2)$$

TABLE LVII. STRESSES AND DEFLECTIONS IN A PIN SEGMENT, $k_2 = 4.0$, $\alpha = 60°$, $\nu = 0.3$

RESULTS AT THETA = 0.00 DEGREES

R/R1	SIGMA R/P1	SIGMA THETA/P1	TAU RTHETA/P1	FU/RP1	EV/RP1
1.000	-1.0000	-0.2009	0.0000	1.1739	0.0000
1.250	-0.8356	-0.1524	0.0000	0.7673	0.0000
1.500	-0.7174	-0.0967	0.0000	0.5167	0.0000
1.750	-0.6256	-0.0415	0.0000	0.3502	0.0000
2.000	-0.5522	0.0122	0.0000	0.2335	0.0000
2.250	-0.4946	0.0657	0.0000	0.1482	0.0000
2.500	-0.4555	0.1221	0.0000	0.0833	0.0000
2.750	-0.4409	0.1841	0.0000	0.0310	0.0000
3.000	-0.4598	0.2472	0.0000	-0.0143	0.0000
3.250	-0.5169	0.2840	0.0000	-0.0567	0.0000
3.500	-0.5954	0.2088	0.0000	-0.0986	0.0000
3.750	-0.6186	-0.1929	-0.0000	-0.1336	0.0000
4.000	-0.3755	-1.3937	-0.0000	-0.1456	0.0000

RESULTS AT THETA = 15.00 DEGREES

R/R1	SIGMA R/P1	SIGMA THETA/P1	TAU RTHETA/P1	FU/RP1	EV/RP1
1.000	-1.0000	-0.2009	0.0000	1.1048	-0.2753
1.250	-0.8355	-0.1525	0.0000	0.7120	-0.1703
1.500	-0.7169	-0.0972	0.0000	0.4707	-0.1003
1.750	-0.6236	-0.0433	0.0000	0.3109	-0.0503
2.000	-0.5449	0.0058	0.0000	0.1998	-0.0128
2.250	-0.4731	0.0478	0.0000	0.1202	0.0164
2.500	-0.3997	0.0797	0.0000	0.0625	0.0397
2.750	-0.3145	0.0998	0.0000	0.0218	0.0588
3.000	-0.2058	0.1129	0.0000	-0.0046	0.0747
3.250	-0.0670	0.1471	0.0000	-0.0178	0.0882
3.500	0.0863	0.2888	0.0000	-0.0202	0.0997
3.750	0.1788	0.7530	-0.0000	-0.0188	0.1097
4.000	-0.0000	2.0126	-0.0000	-0.0339	0.1185

TABLE LVII. (Continued)

RESULTS AT THETA = 22.50 DEGREES

R/R1	SIGMA R/P1	SIGMA THETA/P1	TAU RTHETA/P1	EU/RP1	EV/RP1
1.000	-1.0000	-0.2009	-0.0000	1.0195	-0.4018
1.250	-0.8356	-0.1524	-0.0000	0.6437	-0.2465
1.500	-0.7171	-0.0970	-0.0002	0.4138	-0.1430
1.750	-0.6246	-0.0424	-0.0010	0.2620	-0.0691
2.000	-0.5486	0.0090	-0.0034	0.1567	-0.0139
2.250	-0.4839	0.0567	-0.0099	0.0809	0.0285
2.500	-0.4276	0.1009	-0.0245	0.0249	0.0613
2.750	-0.3777	0.1419	-0.0527	-0.0172	0.0866
3.000	-0.3328	0.1800	-0.0971	-0.0494	0.1057
3.250	-0.2920	0.2156	-0.1467	-0.0742	0.1219
3.500	-0.2545	0.2488	-0.1504	-0.0933	0.1436
3.750	-0.2199	0.2800	0.0371	-0.1082	0.1915
4.000	-0.1877	0.3094	0.7577	-0.1197	0.3124

RESULTS AT THETA = 30.00 DEGREES

R/R1	SIGMA R/P1	SIGMA THETA/P1	TAU RTHETA/P1	EU/RP1	EV/RP1
1.000	-1.0000	-0.2009	-0.0000	0.9021	-0.5149
1.250	-0.8356	-0.1524	-0.0000	0.5498	-0.3120
1.500	-0.7174	-0.0967	-0.0000	0.3355	-0.1768
1.750	-0.6256	-0.0415	-0.0000	0.1948	-0.0801
2.000	-0.5522	0.0122	-0.0000	0.0976	-0.0177
2.250	-0.4948	0.0657	-0.0000	0.0274	0.0487
2.500	-0.4555	0.1221	-0.0000	-0.0255	0.0938
2.750	-0.4409	0.1841	-0.0000	-0.0678	0.1307
3.000	-0.4598	0.2472	-0.0000	-0.1049	0.1614
3.250	-0.5169	0.2840	-0.0000	-0.1404	0.1874
3.500	-0.5954	0.2088	-0.0000	-0.1757	0.2097
3.750	-0.6986	-0.1929	0.0000	-0.2061	0.2290
4.000	-0.3755	-1.3937	0.0000	-0.2135	0.2459

TABLE LVIII. DISPLACEMENTS AND MAXIMUM HOOP STRESSES IN FIN SEGMENTS, $\nu = 0.3$

k_2	σ_θ / p_1 at $\theta = \alpha/4$, $r = r_2$	$\frac{Eu}{rp_1}$ at $\theta = 0$		$\frac{Ev}{rp_1}$ at $\theta = \alpha/2$	
		$r = r_1$	$r = r_2$	$r = r_1$	$r = r_2$
		(a) $\alpha = 60°$			
2.0	4.3266	1.0174	-0.0151	-0.6387	0.5367
3.0	2.7247	1.0681	-0.1303	-0.5313	0.3202
4.0	2.0126	1.1739	-0.1456	-0.5149	0.2459
5.0	1.6019	1.2865	-0.1397	-0.4068	0.2554
		(b) $k_2 = 3.0$			
α					
45°	3.3815	1.0516	-0.1281	-0.4082	0.2336
60°	2.7247	1.0681	-0.1303	-0.5313	0.3202
90°	2.0820	1.1137	-0.1305	-0.7382	0.5195

where A is the area of the pin and F/2 is the shear force shown in Figure 81. For $A = \frac{\pi d^2}{4}$ (d is pin diameter) and P given by Equation (101), the maximum shear stress becomes

$$\tau_{max} = \frac{16}{3} \frac{p_1 r_1 t}{\pi d^2} \tag{109}$$

This equation is the basis of Equation (69) in the text.

APPENDIX II

DERIVATIONS OF FORMULAS FOR ASSEMBLY INTERFERENCES

The interferences Δ_n calculated in the text are the interferences required on the component parts as manufactured. However, the manufactured interference is not equal to the interference as assembled. The multiring container is taken as an example. It is assumed the rings are shrink-fit assembled one-by-one from the inside. The outer rings expand as they are shrunk on and the assembly interference for the next ring to be fitted is increased beyond the manufactured interference. The assembly interference between cylinders n and n + 1 is denoted by δ_n. It has dimensions of inches.

For assembly of cylinder n + 1 onto the other cylinders, δ_n is expressed as

$$\frac{\delta_n}{r_n} = \frac{\Delta_n}{r_n} + \frac{u'_n(r_n)}{r_n} \tag{110}$$

where

$u'_n(r_n)$ = radial displacement at r_n of cylinder n due to residual pressure q'_{n-1} at r_{n-1}.

q'_{n-1} = residual pressure at r_{n-1} due to assembly of cylinder n of wall ratio k_n onto a compound cylinder of wall ratio $k_1 k_2 \cdots k_{n-1}$ with an interference δ_{n-1}.

q'_{n-1} is calculated as follows:

$$\frac{\delta_{n-1}}{r_{n-1}} = \frac{u_n(r_{n-1}) - u_{n-1}(r_{n-1})}{r_{n-1}}$$

Substitution for u_n and u_{n-1} from Equation (14a) gives

$$\frac{\delta_{n-1}}{r_{n-1}} = \frac{1}{E_n(k_n^2-1)}\left[(1-\nu)\, q'_{n-1} + (1+\nu)\, q'_{n-1}\, k_n^2\right]$$

$$- \frac{1}{E_{n-1}(k_{n-1}^2\, k_{n-2}^2 \cdots k_1^2 - 1)}\left[-(1-\nu)\, q'_{n-1}\, k_{n-1}^2\, k_{n-2}^2 \cdots k_1^2 - (1+\nu)\, q'_{n-1}\right]$$

$$= \frac{q'_{n-1}}{E}\left[\frac{k_n^2+1}{k_n^2-1} + \frac{k_{n-1}^2\, k_{n-2}^2 \cdots k_1^2 + 1}{k_{n-1}^2\, k_{n-2}^2 \cdots k_1^2 - 1}\right]$$

where $E_n = E_{n-1} = E$ is assumed.

$$\text{Hence, } q'_{n-1} = E\left(\frac{\delta_{n-1}}{r_{n-1}}\right)\frac{\left(k_n^2-1\right)\left(k_{n-1}^2 k_{n-2}^2 \cdots k_1^2-1\right)}{2\left(k_n^2 k_{n-1}^2 k_{n-2}^2 \cdots k_1^2 - 1\right)} \tag{111}$$

Since

$$\frac{u'_n(r_n)}{r_n} = \frac{2q'_{n-1}}{E\left(k_n^2-1\right)} \tag{112}$$

Substitution of (111) and (112) into (110) gives

$$\frac{\delta_n}{r_n} = \frac{\Delta_n}{r_n} + \frac{\delta_{n-1}}{r_{n-1}}\frac{\left(k_{n-1}^2 k_{n-2}^2 \cdots k_1^2 - 1\right)}{\left(k_n^2 k_{n-1}^2 k_{n-2}^2 \cdots k_1^2 - 1\right)} \tag{113}$$

Now the $\frac{\delta_n}{r_n}$ can be calculated in sequence; i.e.,

$$\frac{\delta_1}{r_1} = \frac{\Delta_1}{r_1}$$

$$\frac{\delta_2}{r_2} = \frac{\Delta_2}{r_2} + \frac{\delta_1}{r_1}\frac{\left(k_1^2 - 1\right)}{\left(k_1^2 k_2^2 - 1\right)} \quad \text{, etc.}$$

Equation (113) applies if the rings are assembled from the inside out. If the rings are assembled one by one from the outside in, then the assembly interference for assembly of cylinder n-1 into the other cylinders is

$$\frac{\delta_n}{r_n} = \frac{\Delta_n}{r_n} + \frac{\delta_{n+1}}{r_{n+1}}\frac{k_n^2 + 1\quad\left(k_{n+1}^2 k_{n+2}^2 \cdots k_N^2 - 1\right)}{\left(k_{n+1}^2 k_{n+2}^2 \cdots k_N^2 - 1\right)} \tag{114}$$

Equation (114) was found by an analogous procedure to that used in deriving (113).

The method used to determine assembly interferences δ_n for the multiring container can also be used to determine assembly interferences for the other container designs. It is important to determine assembly interferences because they are larger than the manufactured interferences and excessive interference requirements may make a design impracticable.

APPENDIX III

COMPUTER PROGRAMS

The analyses described in the text were programmed in the FORTRAN IV alogarithmic language for calculation on Battelle's CDC 3400 and 6400 computers.* The following is a list of programs which includes a brief description of each:

PROGRAM COMPST1 – Analysis of compound (multi-ring) cylinder based upon static shear strength. Calculation of pressure-to-strength ratio p/2S in Figure 43 in the text.

PROGRAM COMPFG1 – Analysis of compound cylinder based upon shear fatigue strength. Calculation of pressure-to-strength ratio p/σ shown in Figure 44.

PROGRAM SEGMENT1 – Analysis of ring segment under radial pressures. Some results given in Appendix 1.

PROGRAM SEGM2N – Analysis of pin segment under radial pressures and shear. Some results given in Appendix I.

PROGRAM COMPHS1 – Analysis of compound cylinder with high-strength liner. Calculations of pressure-to-strength ratios p/σ_1 and p/σ shown in Figures 45, 46, 47, and 48.

PROGRAM COMPHS2 – Analysis of compound cylinder with high-strength liner. Calculation of shrink-fit interferences, operating stresses, and prestresses.

PROGRAM PLTR1 – Analysis of Poulter (ring-segment) cylinder with high-strength liner. Calculation of pressure-to-strength ratios p/σ_1 and p/σ shown in Figures 49, 50, 51, and 52.

PROGRAM PLTR2 – Analysis of Poulter cylinder or pressure support cylinder (inner part of ring-fluid-segment container). Calculation of interferences, operating stresses, and prestress.

PROGRAM PSCYL1 – Analysis of pressure support cylinder (inner part of ring-fluid-segment container). Calculation of pressure-to-strength ratios p/σ_1 and p/σ_3 shown in Figures 53, 54, 55, 56, and 57.

PROGRAM PGSPNCYL – Analysis of segmented shear-pin (pin-segment) cylinder with high-strength liner. Calculation of pressure-to-strength ratio p/σ_1 and p_1/p shown in Figures 58 and 59.

PROGRAM MULTIR – General analysis of compound (multiring) cylinder based on fatigue-strength criterion. The program may be used interchangeably for the ring-fluid-ring design concept.

*Since writing the early programs, the CDC 3400 computer has been superceded by the more versatile CDC 6400 computer. The codes have been modified accordingly.

REFERENCES FOR VOLUME II

(20) Fiorentino, R. J., Abramowitz, P. H., Sabroff, A. M., and Boulger, F. W., "Development of the Manufacturing Capabilities of the Hydrostatic Extrusion Process", Interim Engineering Progress Report No. IR-8-198 (III), Contract No. AF 33(615)-1390 (August, 1965).

(21) Fiorentino, R. J., Gerdeen, J. C., Hansen, W. R., Sabroff, A. M., and Boulger, F. W., "Development of the Manufacturing Capabilities of the Hydrostatic Extrusion Process", Interim Engineering Progress Report No. IR-8-198 (IV), Contract No. AF 33(615)-1390 (December, 1965).

(22) Fiorentino, R. J., Gerdeen, J. C., Hansen, W. R., Sabroff, A. M., and Boulger, F. W., "Development of the Manufacturing Capabilities of the Hydrostatic Extrusion Process", Interim Engineering Progress Report No. IR-8-198 (V), Contract No. AF 33(615)-1390 (March, 1966).

(23) Manning, W. R. D., "High Pressure Engineering", University of Nottingham, Bulleid Memorial Lectures, Vol II, Lecture II, Chapter 4 (1965).

(24) Manning, W. R. D., "The Design of Compound Cylinders for High Pressure Service", Engineering, pp 349-352 (May 2, 1947).

(25) Manning, W. R. D., "Residual Contact Stresses in Built-Up Cylinders", Engineering, p 464 (December 8, 1950).

(26) Poulter, T. C., "High Pressure Apparatus", U. S. Patent No. 2,554,499 (May 9, 1951), Code No. P67.35, Annotated Bibliography on High Pressure Technology, ASME, Butterworths (May, 1964).

(27) Ballhausen, C., German Patent No. 1,142,341 (January 17, 1963).

(28) Gerard, G., and Brayman J., "Hydrostatic Press for an Elongated Object", Barogenics, Inc., U. S. Patent No. 3,091,804 (June 4, 1963).

(29) Fuchs, F. J., Jr., "Production Metal Forming With Hydrostatic Pressures", Western Electric Company, ASME Publication No. 65-PROD-17 (June 1965).

(30) Zeitlin, Alexander, Brayman, J., and Boggio, F. George, "Isostatic and Hydrostatic Equipment for Industrial Applications of Very High Pressure", ASME Paper No. 64-WA/PT-14.

(31) Meissner, M., "Hydrostatic Pressure Device", U. S. Patent No. 3,224,042, Filed October 23, 1963, Patented December 21, 1965.

(32) Lengyel, B., and Alexander, J. M., "Pressure Vessels for Hydrostatic Extrusion", The Chartered Mechanical Engineer, pp 405-406 (September, 1966).

(33) Lengyel, B., Burns, D. J., and Prasad, L. V., "Design of Containers for a Semi-Continuous Hydrostatic Extrusion Production Machine", Preprint of paper presented at 7th Int. M.T.D.R. Conference, Univ. of Birmingham, 12th-16th September, 1966.

(34) Manson, S. S. and Hirschberg, M. H., "Fatigue Behavior in Strain Cycling in the Low and Intermediate Cycle Range", 10th Sagamore Army Materials Research Conference, Sagamore, New York (August 13-16, 1963).

(35) Morrison, J. L. M., Crossland, B., and Parry, J. C. S., "The Strength of Thick Cylinders Subjected to Repeated Internal Pressure", J. of Engineering for Industry, Trans. ASME, Series B, Vol 82, pp 143-153 (1960).

(36) Aerospace Structural Materials Handbook, Vol I, Table 3.051.

(37) Gilewicz, E. P., Fragetta, W. A., Mehra, V., and Krohn, R., "Research on the Binary Iron-Nickel Alloys With 20-25% Ni", ASD-TDR-62-996, Fig. 107 (June, 1964).

(38) Lunn, J. A., Sampson, H. B., Federico, A. M., and Macaulay, J. R., "Nickel Maraging Steels, Preliminary Investigation of 250 and 300 Bar", North American Aviation Report No. NA63H-202, pp 22-27 (March 15, 1963).

(39) Booth, E. T., Brodrick, R. F., Friesecke, B. P., and Schofield, B. H., "Fatigue and Dynamic Creep of High Strength Steels", ASD-TDR-62-480 (August, 1962).

(40) O'Connor, H. C. and Morrison, J. L. M., "The Effect of Mean Stress on the Push-Pull Fatigue Properties of an Alloy Steel", Int. Conf. on the Fatigue of Metals, Inst. of Mech. Engineers, London (September, 1956).

(41) Timoshenko, S. and Goodier, J. N., "Theory of Elasticity", 2nd Edition, McGraw-Hill, pp 58-59, 66-67 (1951).

(42) Berman, I., "Design and Analysis of Commercial Pressure Vessels to 500,000 psi", ASME Paper No. 65-WA/PT-1, to be published in Trans. ASME, J. Basic Engineering.

(43) Pugh, H. Ll. D., and Green, D., "The Effect of Hydrostatic Pressure on the Plastic Flow and Fracture of Metals", Proc. Instn. Mech. Engrs., Vol. 179, Pt. 1, No. 12, 1964-65, pp 415-437.

(44) Crossland, B., and Dearden, W. H., "The Plastic Flow and Fracture of a "Brittle" Material (Gray Cast Iron) With Particular Reference to the Effect of Fluid Pressure", Proc. Instn. Mech. Engrs. Vol. 182 (1958) p 805.

(45) Bridgman, P. W., "Studies in Large Plastic Flow and Fracture", McGraw-Hill, New York (1952).

(46) Davidson, T. E., Eisenstadt, R., and Reiner, A. N., "Fatigue Characteristics of Open-End Thick-Walled Cylinders Under Cyclic Internal Pressure", Watervliet Arsenal Technical Report WVT-RI-6216 (August, 1962).

(47) Fiorentino, R. J., Sabroff, A. M., and Boulger, F. W., "Investigation of Hydrostatic Extrusion". Final Technical Documentary Report No. AFWL-TD-64-372, Contract No. AF 33(600)-43328 (January, 1965).

(48) Coffin, L. F., Jr., "Thermal Stress and Thermal Stress Fatigue", Proceedings of the Society of the Experimental Stress Analysis, 15 (2), 117-130 (1958).

(49) Sachs, G., Sell, R., Brown, W. F., "Tension, Compression and Fatigue Properties of Several Steels for Aircraft Bearing Applications", Proc. ASMT, 59, 635 (1959).

UNCLASSIFIED

Security Classification

DOCUMENT CONTROL DATA - R & D

(Security classification of title, body of abstract and indexing annotation must be entered when the overall report is classified)

1. ORIGINATING ACTIVITY (Corporate author)	2a. REPORT SECURITY CLASSIFICATION
Battelle Memorial Institute Columbus Laboratories Columbus, Ohio 43201	Unclassified
	2b GROUP

3 REPORT TITLE

DEVELOPMENT OF THE MANUFACTURING CAPABILITIES OF THE HYDROSTATIC EXTRUSION
VOL. I AND II

4. DESCRIPTIVE NOTES *(Type of report and inclusive dates)*

TECHNICAL REPORT (FINAL) December 1964 - October 1967

5. AUTHOR(S) *(First name, middle initial, last name)*

Vol. I - Robert J. Fiorentino, Barry D. Richardson, George E. Meyer, Alvin M. Sabroff, Francis W. Boulger
Vol. II - Robert J. Fiorentino, James C. Gerdeen, Barry D. Richardson, Alvin M. Sabroff, Francis W. Boulger

6. REPORT DATE	7a. TOTAL NO. OF PAGES	7b. NO. OF REFS
October 1967	258	49

8a. CONTRACT OR GRANT NO.	9a. ORIGINATOR'S REPORT NUMBER(S)
AF 33(615)-1390	AFML-TR-67-327
b. PROJECT NO. 8-198	
c.	9b. OTHER REPORT NO(S) *(Any other numbers that may be assigned this report)*
d.	--

10. DISTRIBUTION STATEMENT This document is subject to special export controls and each transmittal to foreign governments or foreign nationals may be made only with prior approval of the Manufacturing Technology Division of the Air Force Materials Laboratory, Wright-Patterson Air Force Base, Ohio 45433.

11. SUPPLEMENTARY NOTES	12. SPONSORING MILITARY ACTIVITY
	Air Force Materials Laboratory Research and Technology Division, Air Force Systems Command, Wright-Patterson Air Force Base, Ohio

13. ABSTRACT

The effects of critical process variables on product quality and pressure requirements were investigated for wrought and powder material; 7075-0 aluminum, AISI 4340 steel, Ti-6Al-4V alloy, beryllium, TZM molybdenum alloy, S.A.P., Alloy 718, A286, Cb752. Products investigated were rounds, shapes, tubing and wire.

A study of general high pressure container designs has led to a better understanding of the design parameters to be applied for specific applications. A description of containers designed and constructed in this program is given.

This document is subject to special export controls and each transmittal to foreign governments or foreign nationals may be made only with prior approval of the Manufacturing Technology Division of the Air Force Materials Laboratory, Wright-Patterson Air Force Base, Ohio 45433.

DD FORM 1 NOV 65 1473

UNCLASSIFIED

14. KEY WORDS	LINK A		LINK B		LINK C	
	ROLE	WT	ROLE	WT	ROLE	WT
Hydrostatic extrusion						
Hydrostatic extrusion - Drawing						
Processing parameters						
Rounds, shapes and wire						
80 and 500 F						
AISI 4340 steel						
7075-0 aluminum						
Ti- Al-4V alloy						
TZM molybdenum alloy						
Beryllium						
Alloy 718						
A286						
Sintered Aluminum Product (SAP)						
Hydrostatic extrusion containers						
Design						
Construction						
Evaluation						